ULTRASONIC SYSTEM FOR FRACTURE DETECTION IN ROCK FACES

by Thiann-Ruey Yu B.Sc.

ABSTRACT

An ultrasonic system utilizing the pulse reflection technique has been constructed for the detection of fractures in rock faces.

The apparatus sends out a train of modulated ultrasonic pulses into the rock. If a fracture exists in the rock, a part of the pulse energy is reflected from the fracture plane. The reflected pulses are displayed on the screen of a cathode ray oscilloscope. A number of reflected pulses observed on the oscilloscope indicates multiple fractures while the travel time of the reflected pulse determines the position of each fracture.

The above equipment was used to measure the velocity of longitudinal ultrasonic waves and the attenuation of ultrasonic waves in various solid materials.

By employing a technique similar to that used in seismic methods the direction of the fracture plane could be determined.

Detection of fractures was made on samples of epoxy resin, paraffin and rock masses.

It was observed that although the apparatus using high frequency ultrasonic waves is very suitable for detecting flaws in metals, its applicability is limited in detecting fractures in rocks.

ULTRASONIC SYSTEM FOR FRACTURE DETECTION IN ROCK FACES

by

THIANN-RUEY YU B.Sc.

A thesis submitted to the Faculty of Graduate Studies and Research in partial fulfillment of the requirements for the degree of Master of Engineering

Department of Mining Engineering
and Applied Geophysics
McGill University
Montreal

August 1967.

ACKNOWLEDGMENT

The author wishes to express his sincere thanks to Dr. W. M. Telford, Director of this Research Project, for his guidance and suggestions.

The author is indebted to Professor R. G. K. Morrison and Dr. D. F. Coats of this department for their encouragement and interest in this work. Thanks are also due to Mr. B. Sharma and Mr. B. B. Dhar, my colleagues in this department for their valuable assistance from time to time.

TABLE OF CONTENTS

Chapter Page

LIST OF TABLES

LIST OF FIGURES

CHAPTER I

INTRODUCTION

1.1. General Principles

All sound waves with frequencies corresponding to a normally audible sound are generally referred to as audio or sonic waves. The usual frequency of the sound wave in the audio range is from 15 to 20,000 c.p.s., and waves with frequencies above this audio range are normally called ultrasonic or supersonic waves.

For the past 20 years or more, there has been a considerable development in the technical application of sound waves, chiefly because of the rapid development of electronics in recent years. Some important applications of sound waves, in particular ultrasonic waves, are to be found in industrial testing, signaling, medicine, and other branches of science and technology.

There are a number of ways in which ultrasonic waves can be generated. These methods can roughly be divided into two types. One is the mechanical vibration type, such as power-driven whistles or tuning forks. At present, this method of generating ultrasonic waves is rarely used. The other method of generating ultrasonic waves is by electronic vibration. This type of ultrasonic waves is produced by the use of magnetostriction or crystal transducers, and this is by far the most common and the simplest method of producing ultrasonic waves.

Depending upon their propagation characteristics, sound waves can be divided into several groups. Waves in which the oscillations of the particles in a medium are along the direction of wave propagation are defined as longitudinal or compressional waves. If the movement of the particles in the medium is at right angles to the direction of wave propagation, the waves are known as shear or transverse waves. In addition to these two principal types of waves, there are also other waves, such as Rayleigh waves and Love waves. These travel along the surface of a medium, and therefore, are called surface waves.

In the technical application of sound waves to the detection of cracks in materials, the use of longitudinal waves is by far the most common.

In 1793, Lazzaro Spallazani was fascinated to observe that blinded bats could navigate perfectly. This eventually led him to discover the marvellous ultrasonic radar system of the bat. Later, scientists applied the principle and developed various equipment using light, acoustic and electromagnetic waves for various purposes, such as underwater signaling, aircraft location, flaw detection in metals, concretes, rocks etc..

The first application of ultrasonic waves for the detection of fractures in rocks was made in 1959 by A. Lutsch(1) of South Africa. After Lutsch's work, however, no further application of ultrasonic waves for the detection of fractures in rocks has been reported. The first commercial apparatus(2) for measuring

cracks in rocks, called the "ultrasonic reflectometer", has recently appeared on the market. However information on this equipment is not available.

1.2. Previous Work

The study of the propagation of elastic waves in solid materials, such as ground rock, concrete, metals, etc., is of great interest in all branches of earth sciences and material technology.

In exploration geophysics, artificial seismic waves have long been used in oil prospecting for underground reconnaissance. In industrial technology, ultrasonic waves produced by magnetostriction or piezo-electric effect have been employed as a means of non-destructive flaw detection in metals and in inspection of concrete structures.

In mining engineering, the first application of sonic waves was the detection of fractures in rocks in connection with the study of rock bursts, first used in 1958 by M.E.Spendrei and J.P.A.Lochner(3) of South Africa. In their work, they developed an equipment similar to a portable refraction seismograph used in shallow subsurface exploration. The equipment measures the travel time of a sonic pulse, produced by a special hammer, over known distances in the rock. Using this equipment one can measure the depths to fracture zones by using two different means, the so called "time delay along a surface" and the "time delay in depth" methods. Both are based on the assumption that there

exists a fracture zone behind the rock surface, and the degree of fracture affects the travel time of sonic waves.

The "time delay along a surface" method is the one used in seismic refraction. By measuring the travel time of the refracted waves, the depth to the fractured zone can be determined. The "time delay in depth" method measures the travel time from the surface to various depths in a hole drilled perpendicular to the surface. By plotting the time-depth curve, the depth beyond which the slope becomes constant represents the depth of the fractured layer.

Szendrei and Lochner's methods, though sound, face many difficulties in their practical applications. One big problem, encountered in studying the fracture pattern in rocks, is the uncertain velocity of sound waves in an inhomogeneous rock. This makes the determination of the thickness of the fracture zone and the degree of fracture quite unreliable. In addition to the above, rock faces usually are fractured and uneven. These conditions do not permit the application of the "time delay along a surface" method.

In 1959, A. Lutsch of South Africa, taking into account the limitation in Szendrei and Lochner's apparatus, constructed an ultrasonic pulse reflection system. This system was based on the phenomenon that short waves, transmitted through a medium, are reflected back from the fracture plane. A single transducer was employed for both transmitting and receiving ultrasonic waves, which was pushed into a drill hole to a depth where no fractures were

expected, and then gradually withdrawn to the surface. From the number of reflected pulses observed on the screen of the cathode ray oscilloscope, the degree of fracture could be assessed.

Charles E. Mongan,Jr. and Thomas C. Miller (4) of U.S.A. built a sonic non-destructive testing apparatus in 1960, in an attempt to obtain data for preventing fatal accidents due to roof collapse in coal mines. They hoped to obtain information on the roof composition, the thicknesses of various layers, and the locations of fractures.

In principle, the equipment was almost the same as that constructed by Lutsch except that sonic waves were used instead of ultrasonic waves, and two transducers were employed for transmitting and receiving signals. Measurements were made by placing two probes on the surface of the roof. The reflected waves were displayed on the screen of the oscilloscope. From the travel time, the depth of the various layers could be obtained. It has been reported that the apparatus worked well; however many unmentioned problems still remained, and a safe, compact and portable unit is still desirable for use in underground workings.

In 1965, G.E.Larocque (5) of Canada developed a portable system to measure sonic velocity in underground openings. The system was also based on the principle that the presence of fracture or discontinuities affects the velocity of propagation of sonic waves. An apparent reduction in the average velocity resulting from the lower velocity across air gaps or from the more circuitous transmission paths around air gaps, indicates that the rock is

incompetent.

Measurements were made by inserting the transmitting and receiving units into two boreholes to selected depths by means of extension rods. The boreholes were drilled so that they were perpendicular to the surface and parallel to each other. The units, after placement, were secured in the required positions by means of hydraulic expansion of the side pistons. The sonic waves are produced by hammering a solid steel stud connected to the extension rods of the transmitting unit. The transit time was read from the oscilloscope. The results indicated that the velocity of sonic waves in the fracture zone is not reduced significantly. As mentioned earlier, Szendrei and Loshner encountered the same difficulty with their system. Besides, the equipment was not free from background noise. This made reliable measurements almost impossible. It seems, therefore, that the basic approach to the problem by Larocque as well as the equipment he built, need some improvements.

This brief description of background work indicates that many attempts have been made, using various techniques, to detect fractures in rocks. However, dependable, portable equipment is still not available.

Recently the first commercial apparatus, measuring cracks in rocks, called the "ultrasonic reflectometer", has been developed by Standard Telephones and Cables, Boksburg, South Africa, in conjunction with the South Africa Council for Scientific & Industrial Research. However, no further information on this apparatus is available.

1.3. Object and Scope of this Work

As mentioned earlier, after Lutsch's work in 1959, no further progress in the development of ultrasonic equipment for detecting fractures in rocks is reported. The present work was initiated primarily to study the applicability of ultrasonic waves to the detection of fractures in rocks. Subsequently, an attempt was also made to use this ultrasonic equipment for laboratory studies of some properties of wave propagation by means of seismic model studies.

This thesis presents the principle and the methods employed in constructing the ultrasonic equipment, and the various experimental results.

The experimental work covers:

(1) the measurement of velocity of compressional ultrasonic waves in solids.

(2) the measurement of attenuation of ultrasonic waves in solids.

(3) the detection of fractures in specimens of epoxy resin, paraffin and rock masses.

(4) a model study to determine the direction of fracture planes by means of seismic reflection techniques.

CHAPTER II

DESCRIPTION OF ULTRASONIC FRACTURE DETECTING SYSTEM

2.1. General Principles

The ultrasonic system described here is an application of the radar principle in which ultrasonic waves are sent through the specimen to be tested. As the transmitted ultrasonic waves travelling through one material impinge on an interface between it and a second medium of different acoustic impedance from the first, part of the energy travels forward into the second medium while part of it is reflected back into the first medium, usually accompanied by a phase change.

The amplitude of the reflected wave is determined by the relative specific acoustic impedances of the two layers. The ratio of amplitudes in the reflected, A_r, and the incident, A_i, waves for normal angle of indidence is given by

$$\left[\frac{A_r}{A_i}\right]_{i=0} = \frac{\rho_1 V_1 - \rho_2 V_2}{\rho_1 V_1 + \rho_2 V_2} \qquad (2.1)$$

where

ρ_1, ρ_2 = density of material in the first and the second medium

V_1, V_2 = ultrasonic p-wave velocity in the first and the second medium

The product of density and velocity, ρV, is called the "specific acoustic impedance" or the "specific acoustic resistance"

of the medium.

Since the energy is proportional to the square of the amplitude, the ratio of reflected to incident energy at a boundary between two media for normal incidence, called the "reflection coefficient", is given by

$$\left[\frac{E_r}{E_i}\right]_{i=0} = \left[\frac{A_r}{A_i}\right]^2_{i=0} = \left[\frac{\rho_1 V_1 - \rho_2 V_2}{\rho_1 V_1 + \rho_2 V_2}\right]^2 \qquad (2.2)$$

where

E_r = reflected energy

E_i = incident energy

As an example, to calculate the reflection coefficient from the above equation, we take the case of an interface formed by the rock, say norite, on one side and air on the other. The specific impedance of norite is approximately 17.5×10^5 g/sec-cm^2 and of air, 0.000413×10^5 g/sec-cm^2. Then the ratio of reflected to incident energy is $\left(\frac{17.5 - 0.000413}{17.5 + 0.000413}\right)^2 \times 100 \cong 100\%$. Thus, theoretically almost 100% of the energy is reflected back into the first medium.

The above calculations are based on the assumptions that there is no attenuation in the medium, and the energy is not scattered. In all practical situations, however, energy is dissipated in the medium in various ways.

Equation (2.2) is valid only for the interface formed by two media which are both quite thick. If, in a homogeneous medium there is a thin film of different acoustic impedance

from the medium itself, then the ratio of the reflected and the incident energy at the interface between the two media will depend upon several factors, such as, the difference in the acoustic impedance between the two media, the thickness of the film and the wavelength of the wave travelling in the film. For this case, Rayleigh (6) has given the following formula for the energy ratio:

$$\frac{\text{reflected energy}}{\text{incident energy}} = \left(\frac{Z_1}{Z_2} - \frac{Z_2}{Z_1}\right)^2 \Big/ \left\{4 \cot^2 \frac{2\pi t}{\lambda} + \left(\frac{Z_1}{Z_2} + \frac{Z_2}{Z_1}\right)^2\right\} \qquad (2.3)$$

where

t = thickness of the film

λ = wavelength of wave travelling through the film

$Z_1 = \rho_1 v_1$ = the specific acoustic impedance in the first medium

$Z_2 = \rho_2 v_2$ = the specific acoustic impedance in the thin film

For rock, say norite, $Z_1 = 17.5 \times 10^5$ g/sec-cm^2, and for air $Z_2 = 0.000413 \times 10^5$ g/sec-cm^2, the relationship between the ratio of reflected and incident energy as a function of t/λ was calculated from equation (2.3) and is shown graphically in Fig. 1.

It is seen from Fig. 1 that, for small value of t/λ, most energy is reflected while only a small fraction is transmitted into the second medium. As an example, for $t/\lambda = 0.75 \times 10^{-5}$, the ratio of reflected to incident energy is about 50%. If the

Fig. 1. Ratio of reflected to incident energy vs. t/λ for rock (norite) and air constrast.

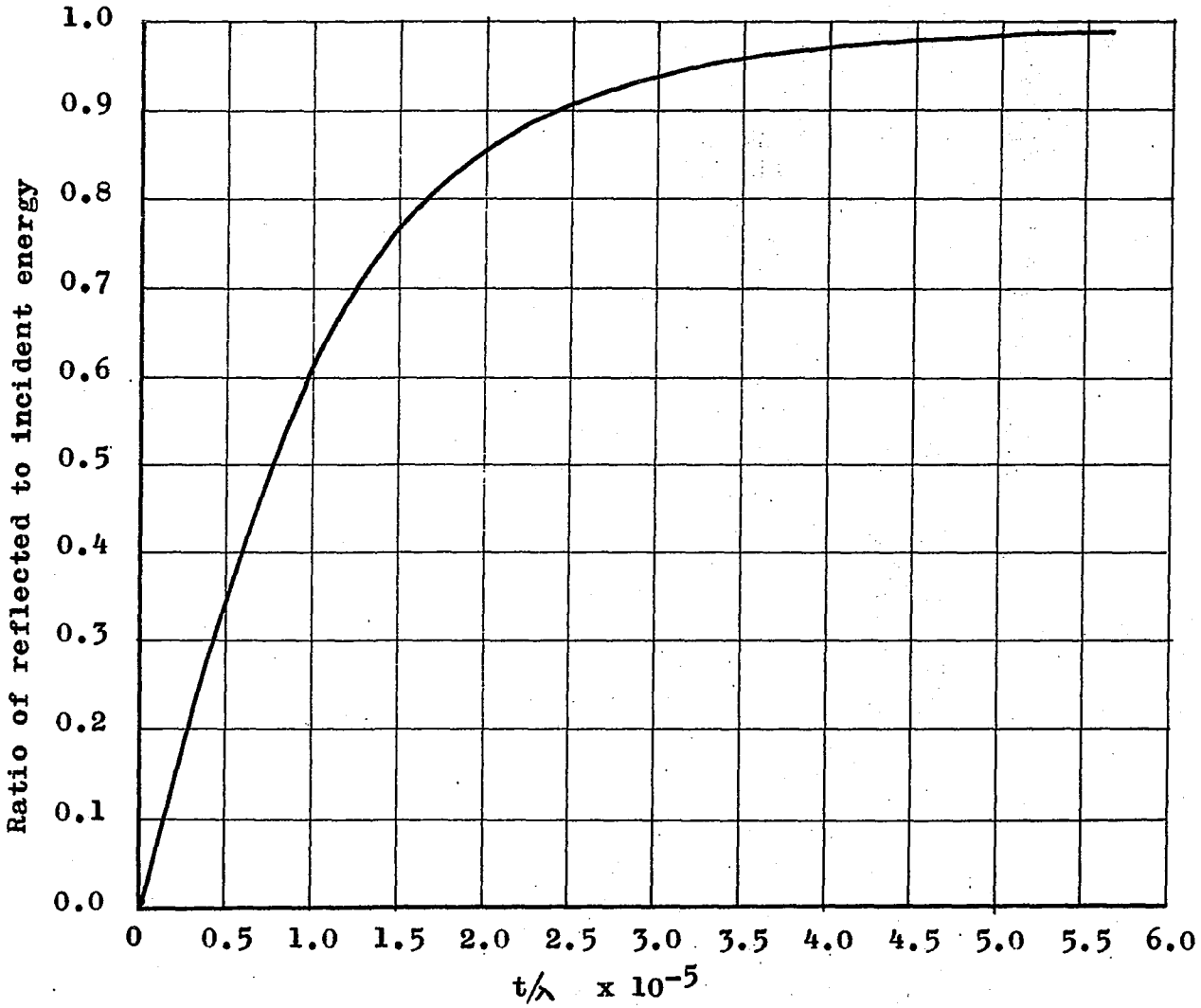

transmitted waves have the frequency of 500 kc/sec, then λ is of the order of 0.06 cm in air. Hence the thickness of the air gap which is capable of transmitting 50 % of energy is only 5×10^{-7} cm.

Nevertheless, Tarnóczy (7) in 1956, observed that, in practice, ultrasonic waves can penetrate through a thin air gap of thickness less than one wavelength in air of the transmitted wave, three orders of magnitude larger than that computed theoretically from Rayleigh's equation(2.3). Later in 1963, Tarnogzy's observation was confirmed by J. Szilárd (8) in further experiments.

It is interesting to note from equation (2.3), that when the thickness, t, of the film is equal to half the wavelength, $\lambda/2$, or multiples thereof, the energy transmitted through the film is a maximum. On the other hand, the transmitted energy is a minimum when the film thickness is an odd quarter wavelength, $\lambda/4$. These principles of energy transmission were used in designing the transition layer between the transducer and the testing specimen, and the back layer behind the transducer, as described in details in section (2.2.b).

An understanding of the beam geometry of ultrasonic waves, radiated in a medium, is very helpful in designing the transducer used in our equipment.

When an ultrasonic p-wave is radiated from a round transducer disc as a circular piston source, into a homogeneous medium, the radiated field in the medium can be divided into

two main regions (fig. 2), namely, the Fresnel region or the "near field" and the Fraunhofer region or the "far field".

In the near field, the distribution of pressure intensity, on the axis perpendicular to the center of the circular transducer disc, oscillates with increasing distance,X, up to the transition point,X_o, as shown in Fig. 3. In addition, there are separate pressure maxima along any one diameter in the near field of a circular piston. Hence, more than one reflected wave can be obtained from the same crack within the near field.

The length,X_o, of the near field is given by

$$X_o = \frac{r^2 - \lambda^2}{\lambda} = \frac{r^2}{\lambda} \quad \text{if} \quad r^2 \gg \lambda^2 \qquad (2.4)$$

where

r = the radius of the circular transducer

λ = the wavelength in the material concerned

Beyond the transition point,X_o, the field is called the far field. In the far field, the pressure intensity begins to diverge appreciably. The intensity,I_x, on the axis of the circular piston then falls off exponentially with increasing distance,X.

In the detection of fractures in materials, we are particularly interested in this far field. Fig. 4 shows the radiation pattern of a beam in the far field. The angle of divergence is given by

$$\theta = \sin^{-1} \; 1.22\lambda / D \qquad (2.5)$$

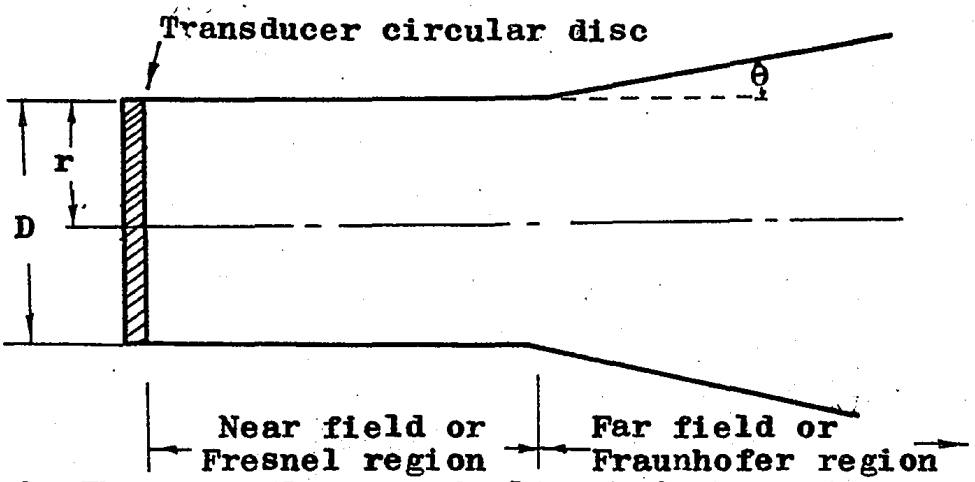

Fig. 2. The general form of ultrasonic beam from a circular piston source.

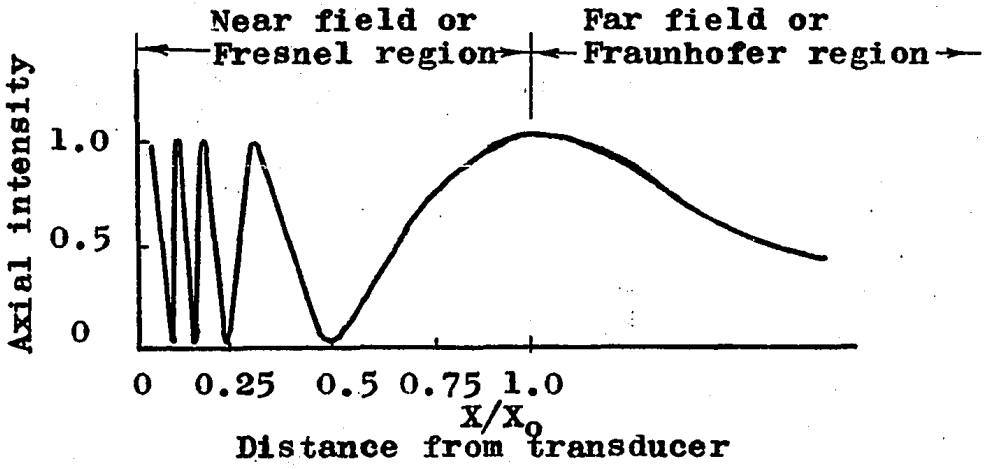

Fig. 3. Intensity variation on the axis of a circular piston source.

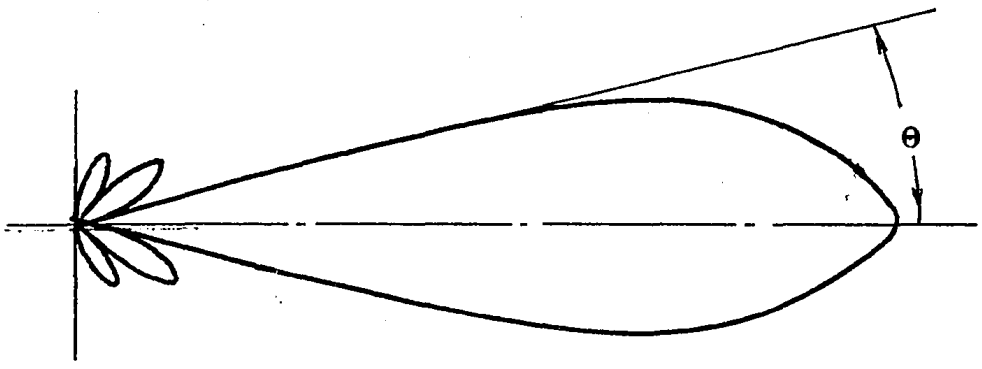

Fig. 4. Radiation pattern of ultrasonic p-wave beams in the far field.

where

θ = half the angle of the beam radiation

D = the diameter of the circular transducer

For example, when a circular transducer of diameter 1" radiates ultrasonic waves of frequency 450 kc into a medium of epoxy resin having a wavelength of 0.226" or 0.57cm, the length of the near field, by equation (2.4), is approximately 1.11". The angle of divergence in the far field is given by equation (2.5),

$$\theta = \sin^{-1} 0.276$$

$$= 17^{o}$$

From these calculations it is evident that in using a transducer of diameter 1" to measure cracks in epoxy resin, the cracks must lie at a depth greater than 1.11" from the face of the transducer, and they must lie within the conical angle of 34^{o}. If any crack is within the near field, then more than one indication of the reflected wave appears and makes the information unreliable.

The radiation pattern for most practical purposes can be regarded as that shown in Fig. 2, though in some cases, side lobes are produced and the beam pattern is more like that shown in Fig. 4. The number of side lobes depends on the ratio D/λ and the penetration of the beam depends on the ratio D/λ and the power of the source. Normally, the side lobes are small compared with the main lobe and do not give rise to spurious indications of reflected waves from cracks.

2.2 Ultrasonic Equipment

(a) General

The ultrasonic system consists of the following components:

1) Two 450 kc transducer probes and two 60 kc transducer probes
2) A modulated pulse generator
3) A trigger generator
4) A pulse amplifier
5) A preamplifier
6) A 1500 V DC power supply
7) Two 350 V DC power supplies
8) A dual beam cathode ray oscilloscope
9) An oscilloscope camera

A photograph of the entire assembly is shown in Fig. 5. A block diagram of the various components is also shown in Fig. 6.

Some accessories and materials used in the experiments are listed below.

1) A wooden tank having the dimension 4.0 ft. x 4.0 ft. x 1.0 ft.(height), containing water, for determination of the direction of crack planes by model studies.
2) An epoxy resin cylinder of diameter 6 in. and height 6.437 in. and a paraffin slab of dimension 10 in. x 8 in. x 1.5 in., for model study of fracture detection.
3) Two massive diorite slabs of dimension 2.5 ft. x 2.5 ft. x 3.5 ft. and 1.5 ft. x 2.0 ft. x 2.5 ft., for the detection of fractures in rock masses.

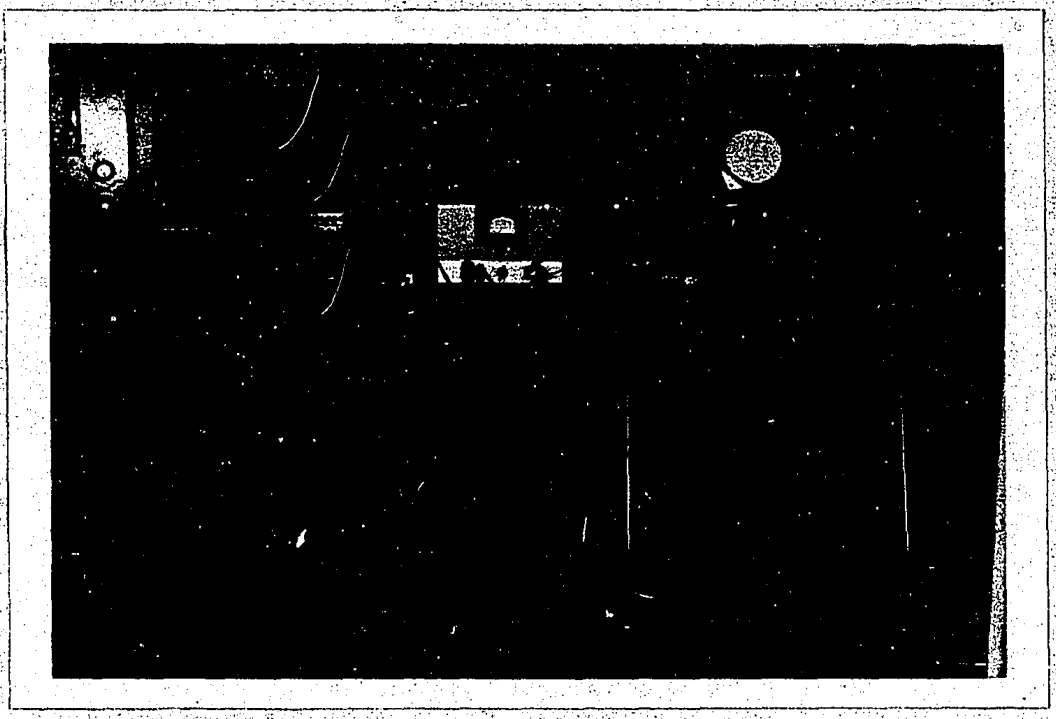

Fig. 5. An ultrasonic reflection system.

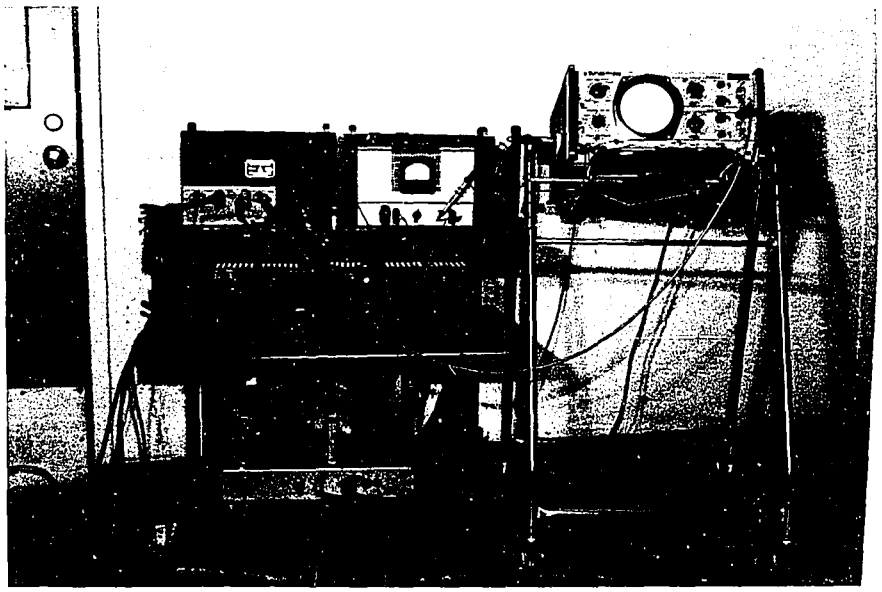

Fig. 5. An ultrasonic reflection system.

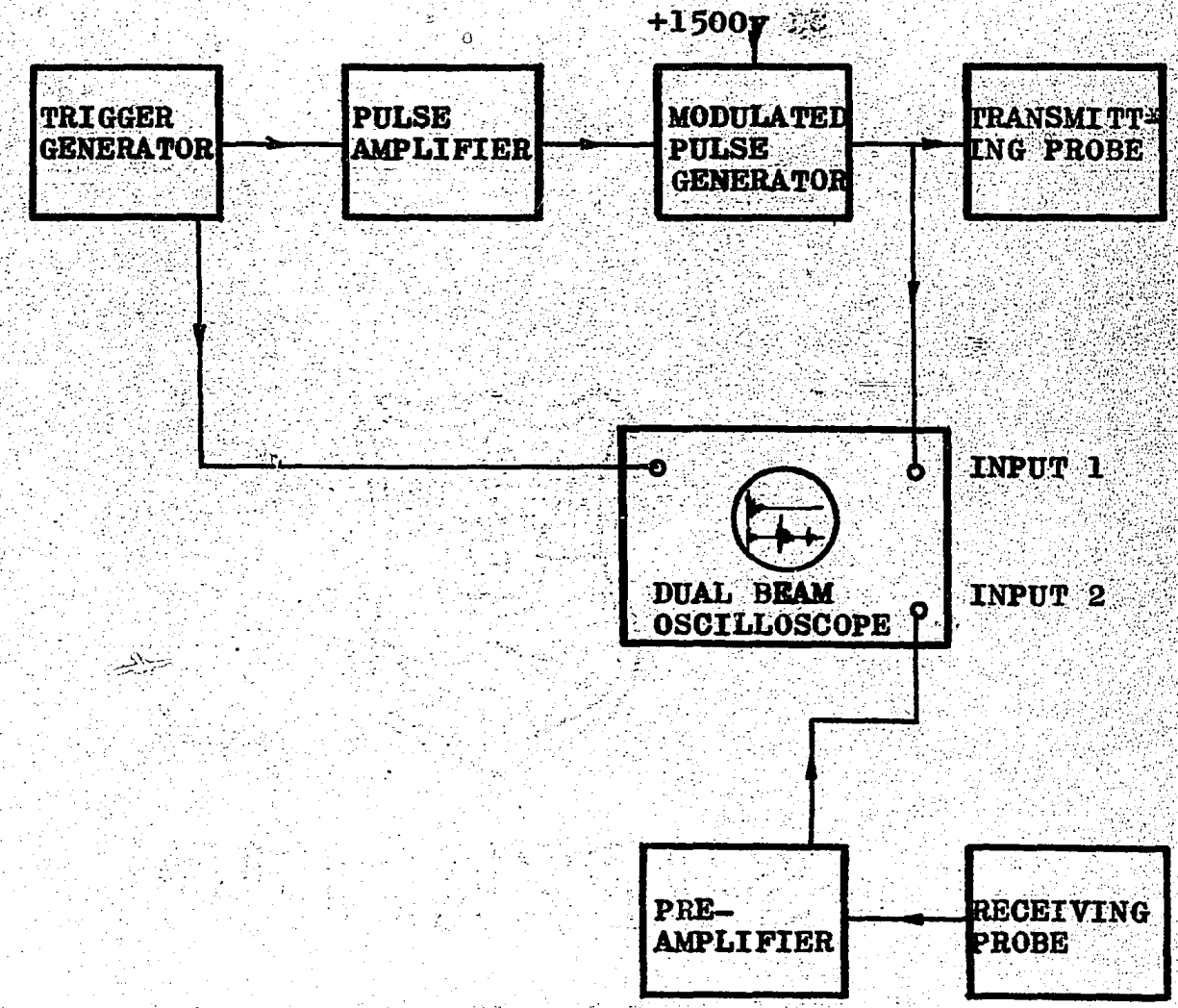

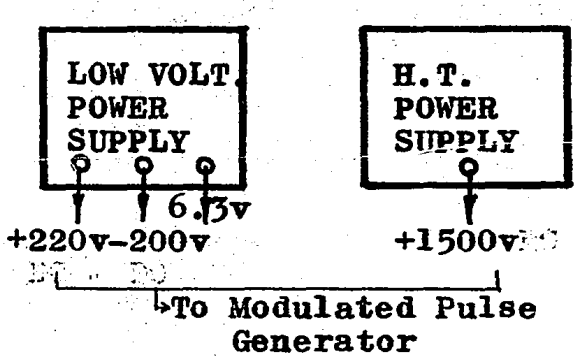

Fig. 6. Block diagram of ultrasonic reflection system.

4) Various specimens of variable lengths of epoxy resin, mortar, Trenton limestone, paraffin and some other materials for measurement of ultrasonic p-wave velocity, the former four specimens also being used for measuring the attenuation constant of ultrasonic waves.

All instruments and equipment listed above are described in detail in later sections.

(b) Transducer Probe

The function of the transducer probe is to convert electrical energy into mechanical energy or vice versa. When an oscillating voltage is applied to a transducer, there is alternate expansion and contraction of the transducer, giving rise to ultrasonic waves. Similarly, when the transducer is vibrated mechanically, the reverse process takes place, the transducer producing electrical signals.

There are several types of transducers used to produce ultrasonic waves. Some of them are the piezoelectric, the magnetostrictive and the ferroelectric (electrostrictive) transducers

Piezoelectric transducers, such as rochelle salt, lithium sulphate, quartz, etc., have been widely used for generating ultrasonic vibrations. Recently, the ferroelectric material of artificial polycrystalline compound, barium titanate, $BaTiO_3$, has largely replaced natural quartz crystals for signal generation and reception, since artificial barium titanate has two important advantages over natural quartz.

1) The artificial barium titanate transducer can be made to any shape and its cost is less than quartz.
2) Barium titanate has about 70 times larger loop gain (the total sensitivity of the transducer when used as transmitter and receiver) than that of quartz.

The table below shows the various constants of barium titanate and quartz(9,10).

Table 1

Constants of Barium titanate and Quartz.

Constants	Barium titanate	Quartz X-cut
Curie temperature ^{o}C	120	575
Longitudinal wave velocity, V, m/sec	4460	5750
Density, ρ, g/cm^3	5.4	2.65
Acoustic impedance, Z, $g/sec\text{-}cm^2$	24×10^5	15.2×10^5
Transmission sensitivity, d_{33}, $\frac{m/m}{v/m}$	140×10^{-12}	2.3×10^{-12}
Reception sensitivity, g_{33}, $\frac{v/m}{N/m^2}$	15×10^{-3}	58×10^{-3}
Modulus of elasticity, E, N/m^2	11×10^{10}	8.0×10^{10}
Dielectric constant, ε,	1050	4.5
Coupling coefficient, K, %	45	11
Dissipation factor, $\tan\delta$, %	1	0.02
Fraquency thickness constant, kc-mm	2840	2870

Because of its superior performance as a transducer elements, two barium titanate discs were used in our experiment for transmitting and receiving signals.

The attenuation of sound waves in rocks is a complicated phenomenon which is not yet thoroughly understood. Some features of the attenuation of sound waves in common materials are briefly described in section (3.2.a).

In the use of the ultrasonic technique for the detection of fractures in rocks, the relationship between frequency and attenuation is very important. Fig. 7 illustrates this for reef and quartzite rocks (1). It is seen that the attenuation of sound waves in quartzite and in reef is an exponential function of frequency. At lower frequencies, the increase in attenuation with frequency is small, but as the frequency increases beyond a critical value, the attenuation increases very sharply. The critical frequency for quartzite is observed at about 1000 kc/sec and for reef at about 600 kc/sec.

In designing a transducer unit, therefore, the frequency of the sound waves used should be below the critical frequency, so that high attenuation is not encountered. On the other hand, if the frequency of the sound wave is too low, the waves will not have sufficient energy to be reflected back from the small cracks which are to be detected.

Consequently, the frequency used should depend on two main factors, namely, the kind of rock tested, and the size of the fracture to be detected.

It can be seen from Fig. 7, that for both reef and quartzite, the relationship between attenuation and frequancy is a fairly flat curve below about 500 kc/sec. In this region,

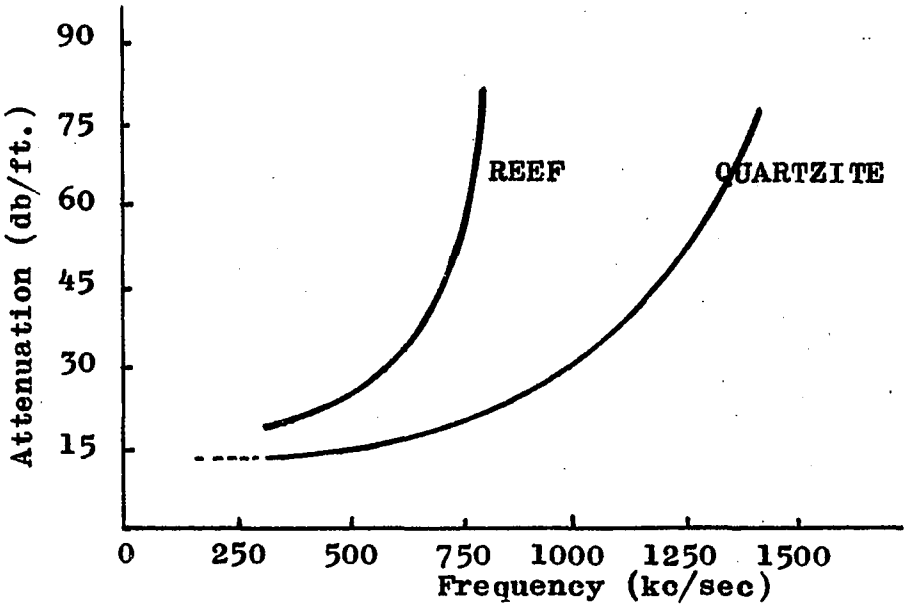

Fig. 7. Attenuation of ultrasonic waves in reef and quartzite vs. frequency.

therefore, the change in attenuation with frequency is small. The above phenomenon is believed to be true for other competent rocks similar to quartzite. Therefore, if the pair of probes chosen for our experiment have a natural frequency of approximately 500 kc/sec, the attenuation will be small and they should also be capable of detecting small cracks.

The detectability of rock fractures by the above pair of probes was compared with a second pair having a resonant frequency of 60 kc/sec made by Bruel & Kjaer (Model No, 4312).

The fundamental resonant frequency of the transducer, can be calculated from the relation:

$$F = \frac{V/2}{t} \text{ kc/sec} \qquad (2.6)$$

where

V = velocity of ultrasonic p-waves in transducer in m/sec

t = thickness of transducer disc in mm

From experimental observation it is found that in calculating the resonant frequency of barium titanate, equation (2.6) does not give an exact value; a better result is given by

$$F = \frac{2840}{t} \text{ kc/sec} \qquad (2.7)$$

As an example, the resonant frequency for a 0.25 in. thick barium titanate transducer, from equation (2.7), is equal to

$$F = \frac{2840}{0.25 \times 2.54} = 447 \text{ kc/sec}$$

The calculated value is very close to the actual resonant frequency of 450 kc/sec observed on the oscilloscope.

In order that the signals transmitted into the specimen,

or received from the specimen after reflection, have the maximum energy, it is necessary to have good impedance matching between the transducer face and the test specimen. A simple method of obtaining good impedance matching is by imposing a transition layer between the transducer face and the specimen.

From equation(2.3) it is seen that for $t = \lambda/4$ or even multiples of $\lambda/4$, the transmitted energy is a maximum. Hence the thickness of the transition layer can be fixed by the above relationship. Similarly, from the transmission line equations (2.8) or (2.9) (10) given below, the materials having the proper acoustic impedance for the transition layer can be chosen.

For even multiples of transition layers

$$Z_t = Z_s\left(\frac{Z_2.Z_4.....Z_{2n}}{Z_1.Z_3.....Z_{2n-1}}\right)^2 \qquad (2.8)$$

For odd multiples of transition layers

$$Z_t = Z_s\left(\frac{Z_1.Z_3.....Z_{2n+1}}{Z_2.Z_4.....Z_{2n}}\right)^2 \qquad (2.9)$$

where

Z_t = the apparent composite specific acoustic impedance of the transducer

Z_s = specific acoustic impedance of the specimen

$Z_1, Z_2, Z_3 ...$ = specific acoustic impedance of layers seen from specimen side

In selecting good impedance matching between the transducer and the specimen of paraffin, it was noted that Z_s for paraffin at room temperature is 1.3×10^5 g/sec-cm^2, and for barium titanate

24×10^5 g/sec-cm^2. Since the acoustic impedance of the two materials is very different, it is obvious that the energy transmitted into the paraffin will be very small.

For proper impedance matching between the transducer and the paraffin, two discs, one of aluminum and the other of bakelite were chosen. The thickness of the two discs were such that they were equal to one-quarter of the wavelength of sound waves in these materials at 450 kc/sec. For this the thickness of the aluminum disc is 0.14 in. and that of the bakelite 0.06 in.. Since the acoustic impedance of aluminum and bakelite are 17×10^5 g/sec-cm^2 and 3.63×10^5 g/sec-cm^2 respectively, from equation (2.8), the apparent composite acoustic impedance of aluminum, bakelite and paraffin is equal to

$$Z_t = 1.3 \left(\frac{17}{3.63}\right)^2 \times 10^5$$
$$= 28.5 \times 10^5 \text{ g/sec-cm}^2$$

The above value for acoustic impedance of the three materials (paraffin, aluminum and bakelite) is close to the acoustic impedance of barium titanate (24×10^5 g/sec-cm^2) and hence the impedance matching between the transducer and the specimen of paraffin has been achieved.

In addition to considering the transition layers for good impedance matching, it is also necessary to consider the effect of the back layer (the layer behind the transducer) for good resolution of the receiving signals. For this, the back layers should have the following properties:

1) high absorption, to achieve better damping for minimizing

ringing by waves reflected from the back of the absorber,
2) high rigidity, so that the amplitude of the first ultrasonic oscillation will be a maximum,
3) the layer should be one wavelength thick and should have good acoustic impedance matching with the transducer to minimize internal reflection of ultrasonic waves into the transducer.

For our 450 kc probes, a lead disc of thickness 0.22 in. (equal to one wavelength of sound wave in lead at frequency of 450 kc) had been used as the back layer in the transmitting and receiving probes. The acoustic impedance of lead is 26×10^5 g/sec-cm^2 which is close to the acoustic impedance of barium titanate (24×10^5 g/sec-cm^2) and lead also had high enough rigidity and large attenuation (11) as well.

The various parts of the 450 kc transducer assembly are shown diagramatically in Fig. 8. Fig. 9 shows the outside view of the 60 kc probes (small) and the 450 kc probes (large).

Besides the transition and the back layers, some electrical properties of the transducer should be taken into account in the design of a good probe. One of the main parameters to be considered is the dielectric constant of the piezoelectric disc. Because a transducer driven by a modulated pulse generator becomes the main load of the generator, the transducer can affect the characteristics of the transmitting pulses and the efficiency of power transmission of the modulated pulse generator.

The capacitance of a transducer disc can be defined as:

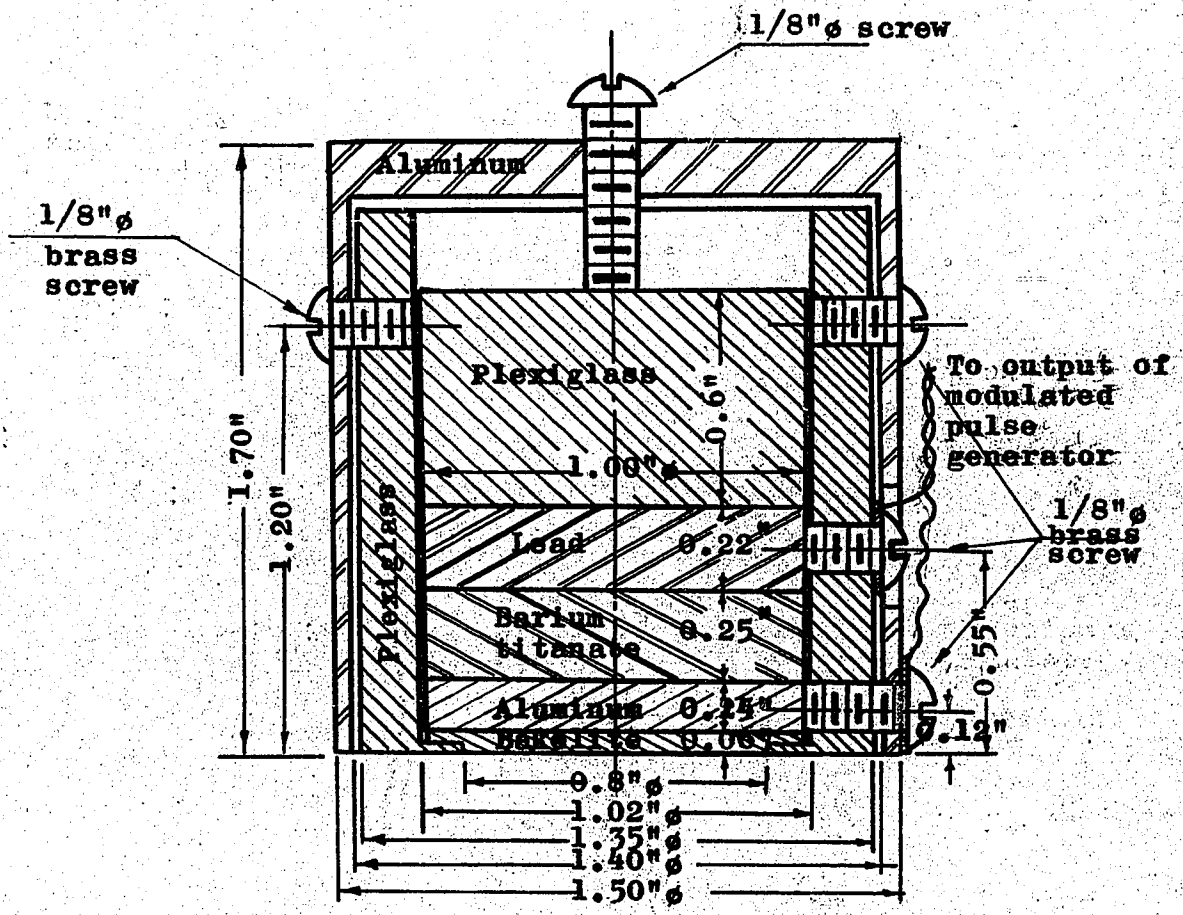

Fig. 8. Section of 450 kc transducer assembly(probe).

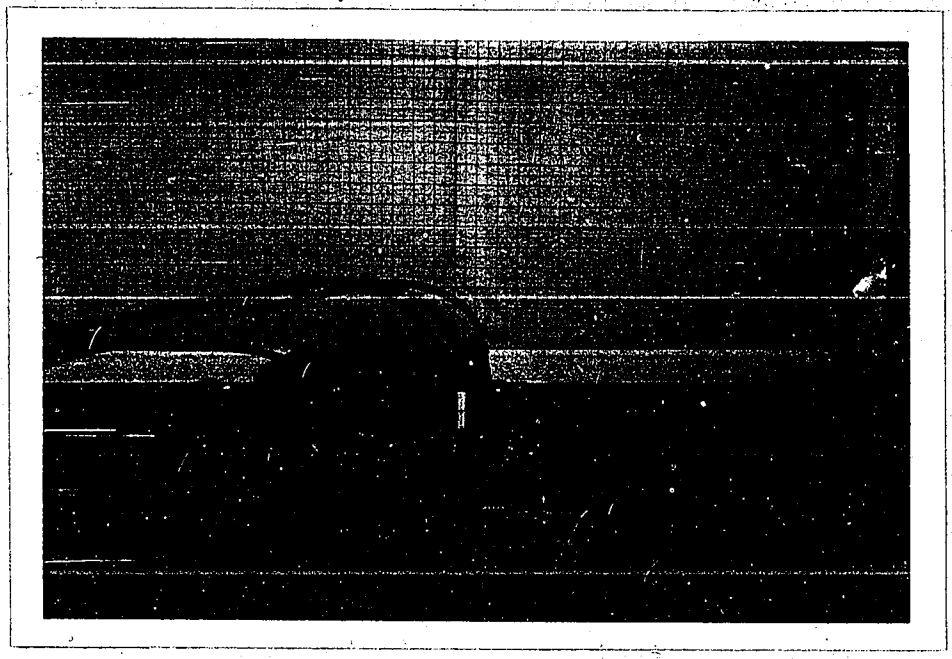

Fig. 9. Outside view of 60 kc(small) and 450 kc (large) probes.

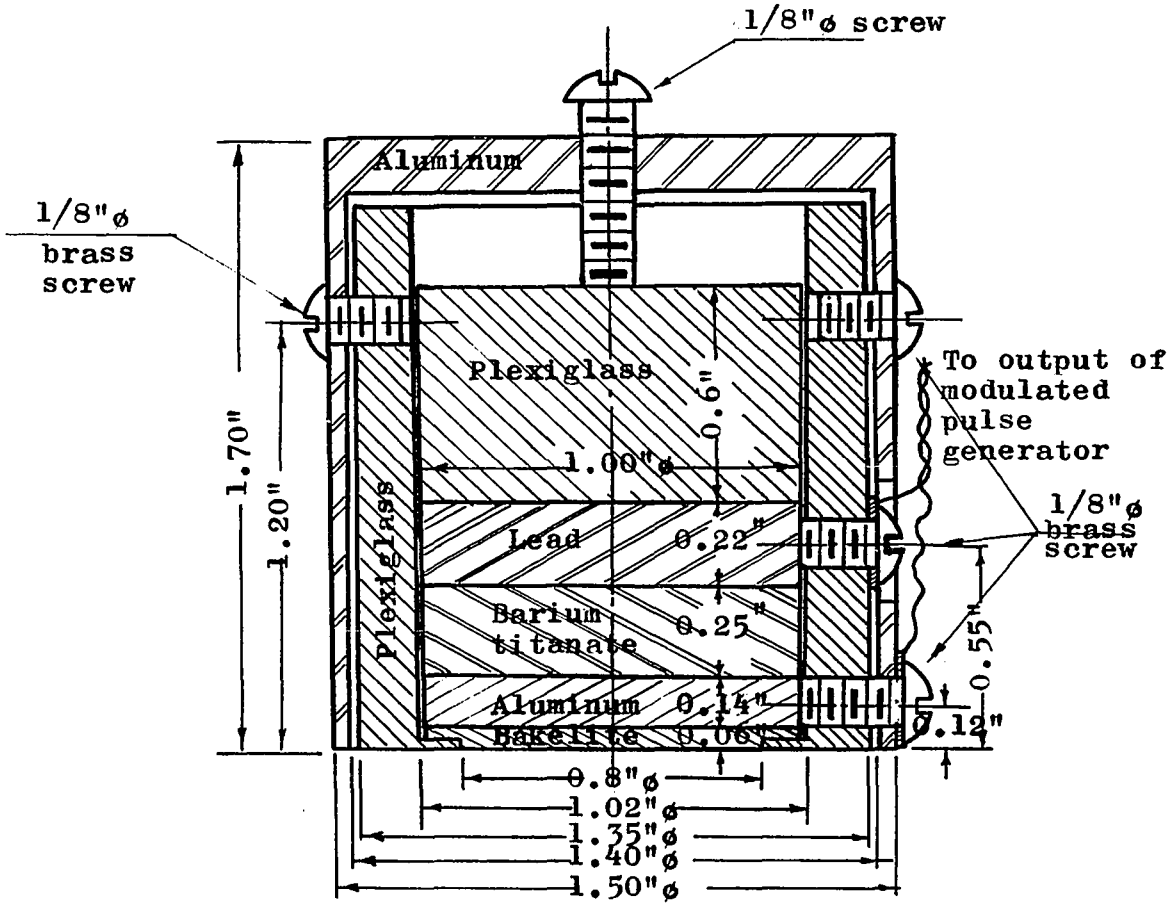

Fig. 8. Section of 450 kc transducer assembly(probe).

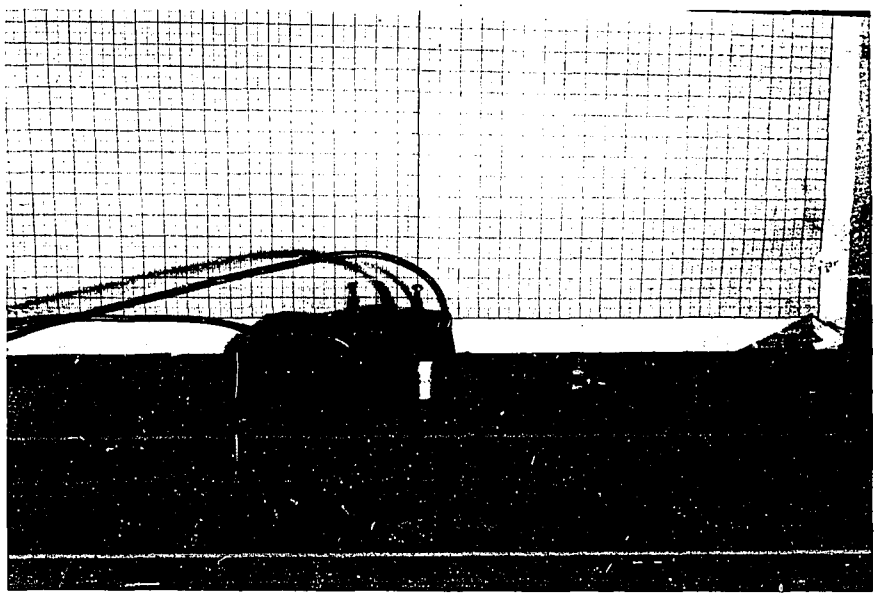

Fig. 9. Outside view of 60 kc(small) and 450 kc (large) probes.

$$C = \frac{A}{4\varepsilon t} \text{ pf} \qquad (2.10)$$

where

A = area of transducer disc in cm^2

t = thickness of transducer disc in cm

ε = dielectric constant (relative permitivity)

and the capacitive reactance, X_c, is given by:

$$X_c = 1/2\pi FC \ \Omega \qquad (2.11)$$

As an example, a barium titanate disc of diameter 1 in. has the following parameters.

area, A, = $5 cm^2$

thickness, t, = 0.63 cm (0.25 in.)

dielectric constant, ε, = 1050

Substituting the above values in equation (2.10), the capacitance of the transducer is C = 660 pf. At the frequency of 450 kc/sec, the capacitive reactance is, therefore, from equation (2.11), equal to $X_c = 500\Omega$.

In practice, the transducer capacitance, 660 pf, will combine in parallel with the stray capacitance in the co-axial cables and the distributed coil capacitance in the resonance cirsuit. This will make the effective capacitance of the circuit larger, and hence the capacitive reactance smaller.

The measured value of the combined capacitance of the 450 kc probe and the co-axial cables of length 4 ft. is about 0.0012 μf. For the 60 kc probe, it is about 0.0011 μf.

(c) Modulated Pulse Generator

The function of the modulated pulse generator is to generate a train of pulses for exciting the transmitting transducer. The modulated pulse generator (Fig. 10) was built to produce a train of damped pulses, having two bands of frequencies at 60 kc/sec and 450 kc/sec. The pulses have a maximum amplitude of 1500 Volts peak to peak. The frequencies of the modulated pulses — 60 kc/sec (fig. 11) and 450 kc/sec (Fig. 12), are slightly adjustable in order to match the 60 kc and 450 kc transducers to their own resonant frequencies. The pulse amplitude can be varied continuously in the range of 100 Volts to 1500 Volts peak to peak, by changing the plate voltage of the modulated pulse generator.

Fig. 13 shows the schematic circuit diagram of the modulated pulse generator. As the frequency selection switch is turned to 450 kc, a negative triggering signal of 200 Volts, taken from the pulse amplifier, is imposed on the grid of the twin triode V_1 (12AU7). During cutoff a transient oscillation of 450 kc/sec occurs in the cathode inductance(12). These oscillating pulses, however, do not contain sufficient voltage and power to energize the transmitting transducer for practical use. A further stage is, therefore, required to amplify them. In this stage, a twin beam power tube V3 (3E29) is used.

A L–C tuned circuit is employed for generating a train of damped pulses at their natural resonant frequency of 450 kc/sec. The inductance has a low stray capacitance and is connected in

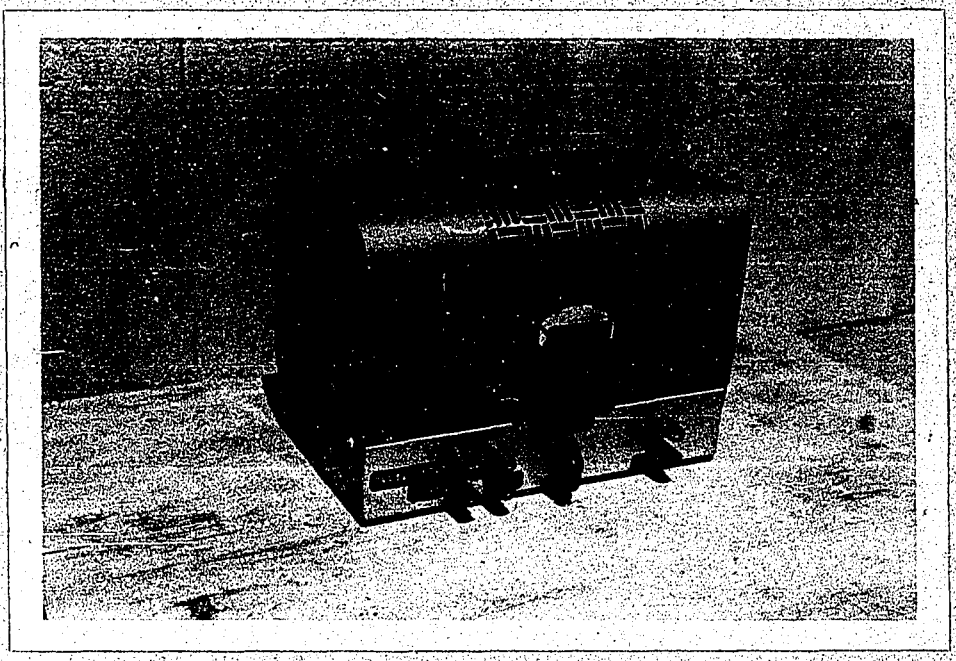

Fig. 10. A modulated pulse generator.

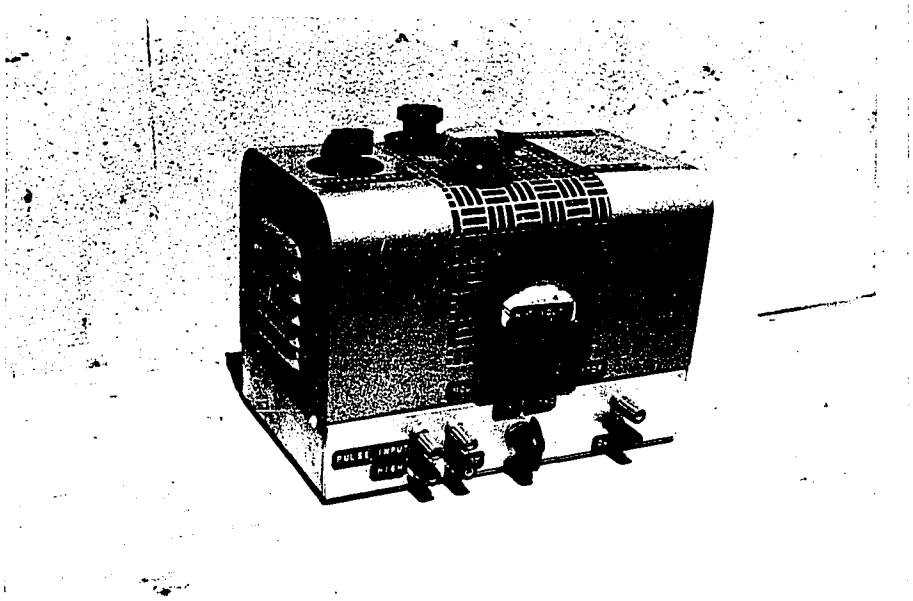

Fig. 10. A modulated pulse generator.

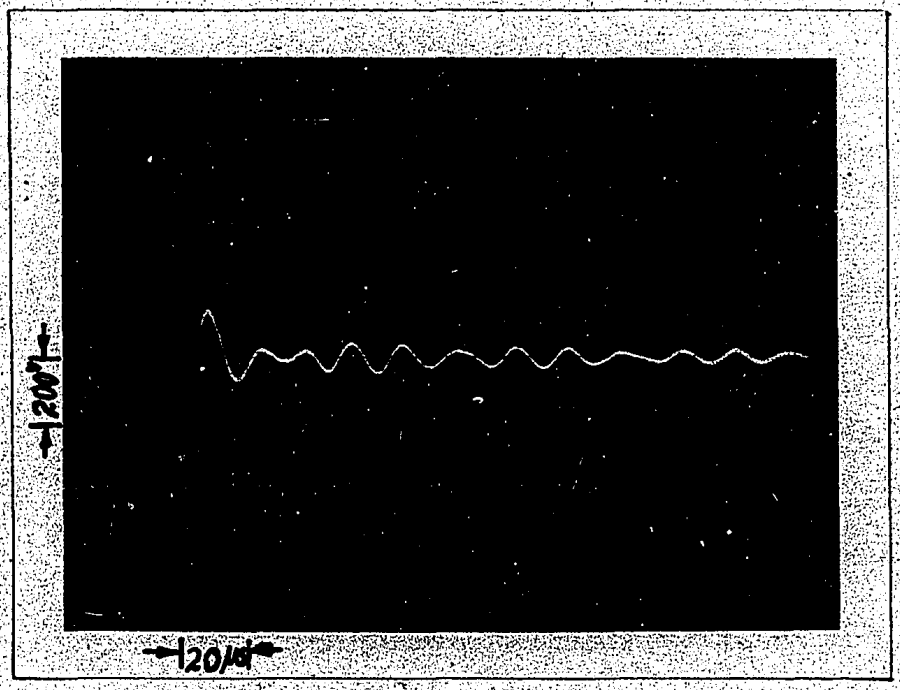

Fig. 11. 60 kc transmitted pulses from the modulated pulse generator.

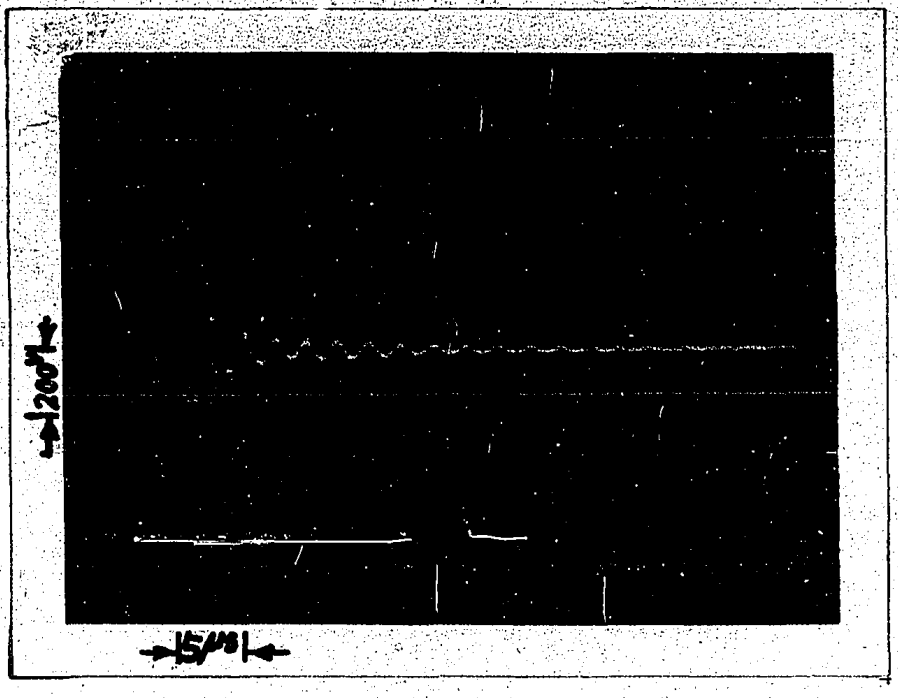

Fig. 12. 450 kc transmitted pulses from the modulated pulse generator.

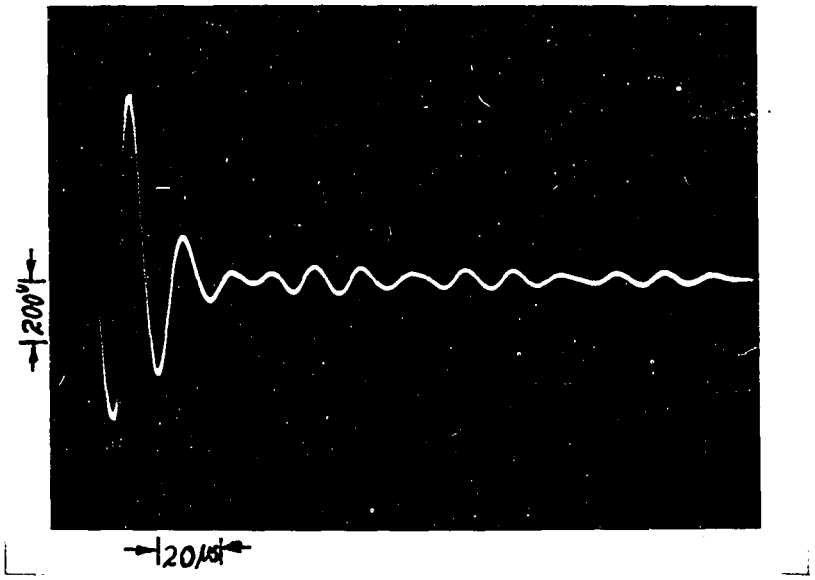

Fig. 11. 60 kc transmitted pulses from the modulated pulse generator.

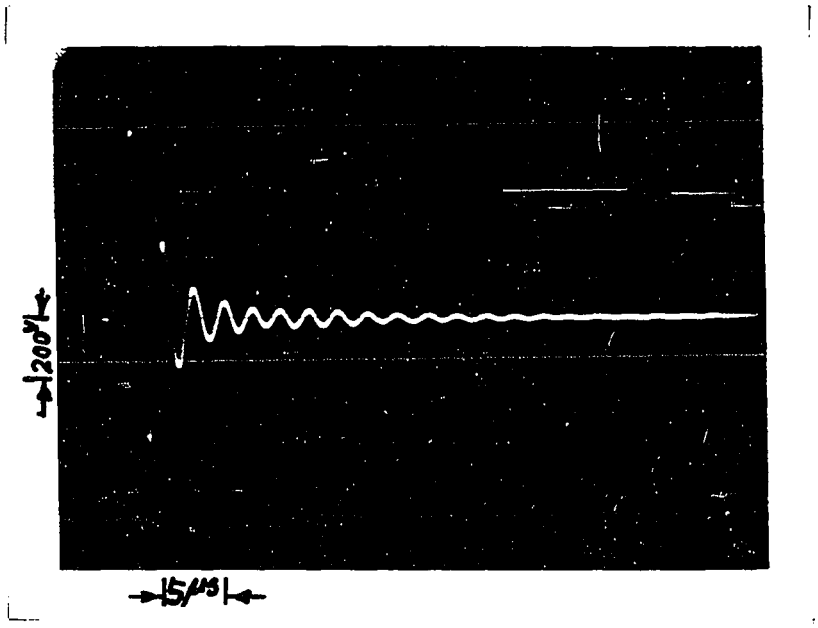

Fig. 12. 450 kc transmitted pulses from the modulated pulse generator.

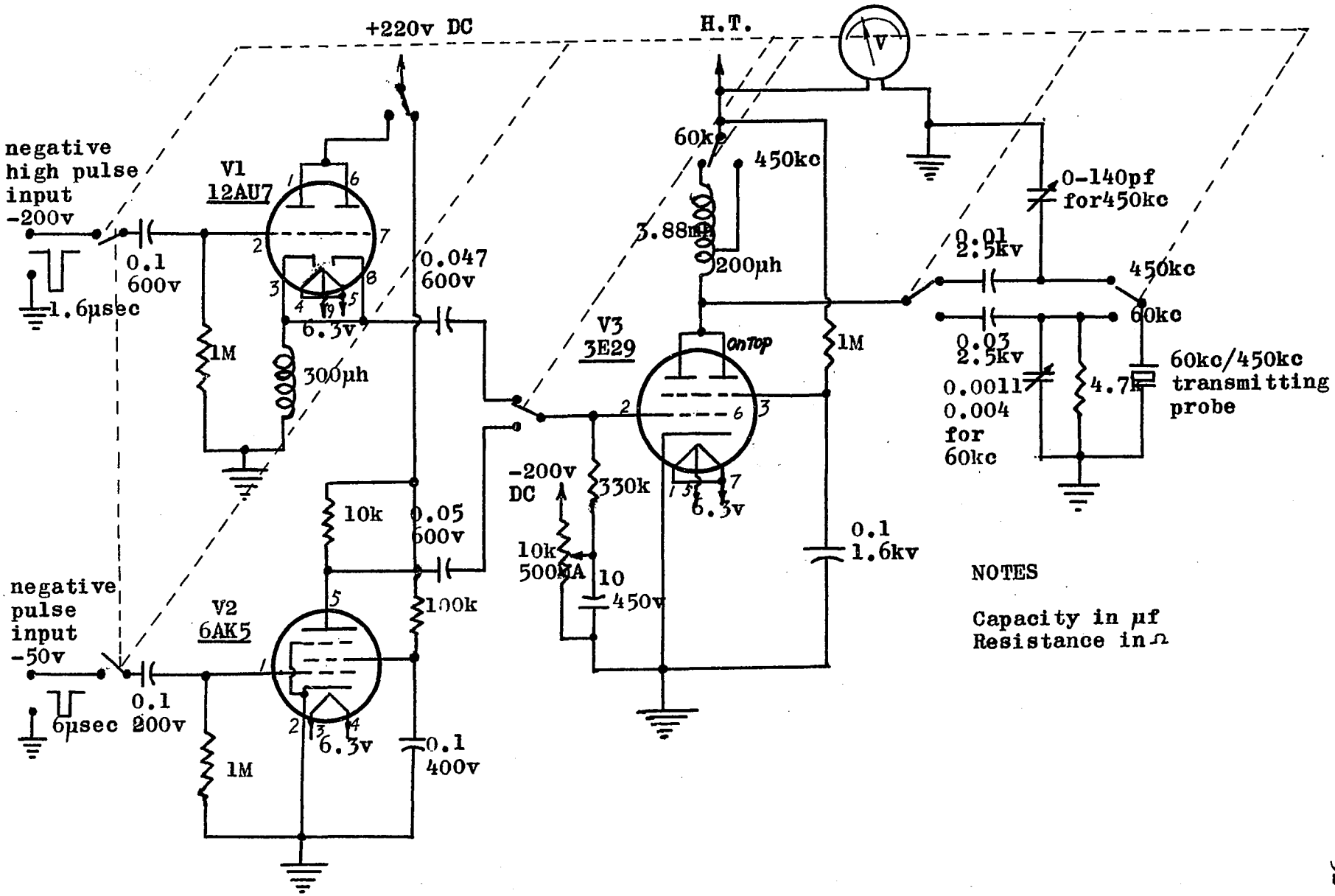

Fig.13. Schematic diagram of modulated pulse generator.

parallel with the variable capacitance. It is noted that the resonant frequency of the tuned L-C combination is also affected by the fairly large capacitance of the transducer and the connecting co-axial cables since they are connected in parallel with the L-C circuit.

The frequency of the modulated pulse, therefore, can be adjusted for frequency matching with the natural frequency of the transducer by tuning the variable capacitance. The degree of damping of the modulated pulses can be increased, if necessary, by adding a suitable resistance in parallel with the L-C circuit.

Turning the frequency selection switch to 60 kc, a negative triggering signal of 60 Volts, taken from the trigger generator, is imposed on the grid of the pentode V_2 (6AK5). V_2 simply serves as a voltage amplifier and produces a phase shift of 180^{o}. The amplified positive pulse from the plate of V_2 is large enough to drive tube V_3 which is usually cut off by the high negavive grid bias. A steady current will flow through the tube and the inductance as the tube V_3 starts conducting as a result of the high positive pulse on its grid. The induced current, therefore, flows into the capacitor and oscillations start at the resonant frequency of the L-C-R tuned circuit.

The L-C-R circuit, as described above, consists of the inductance, the variable capacitance, the capacitance in the transducer and the co-axial cables, and the damping resistance. The elements of the L-C-R circuit are so arranged that they have the resonant frequency of 60 kc/sec.

A 4.7 kΩ resistor is connected across the variable capacitor to obtain proper damping in the oscillation of the modulated pulses. The variable capaciotr makes the frequency of the modulated pulses slightly adjustable.

(d) Trigger Generator

A General Radio (Type 1217-A) Unit Pulser is used as a synchronizer to trigger the time base of the oscilloscope at any one of the 12 selected repitition rates, from 30 cps to 100 kcps. The trigger generator produces a negative pulse of 60 Volts maximum to drive the modulated pulse generator for energizing the 60 kc modulated pulse, and also a positive 20 Volts pulse for pulse amplifier to trigger the 450 kc modulated pulse. The duration of the pulses can be continuously varied within the range 0.2 μsec to 60,000 μsec.

The trigger generator essentially consists of, a blocking oscillator, a monostable multivibrator, a limiter-type amplitude control circuit, and an output cathode follower.

An elementary schematic circuit diagram of the trigger generator is shown in Fig. 14. Further details about the trigger generator are contained in the operating manual of General Radio Company Type 1217-A Unit Pulser.

(e) Pulse Amplifier

The Unit Amplifier (General Radio Type 1219-A) is driven by a positive pulse from the trigger generator. The output

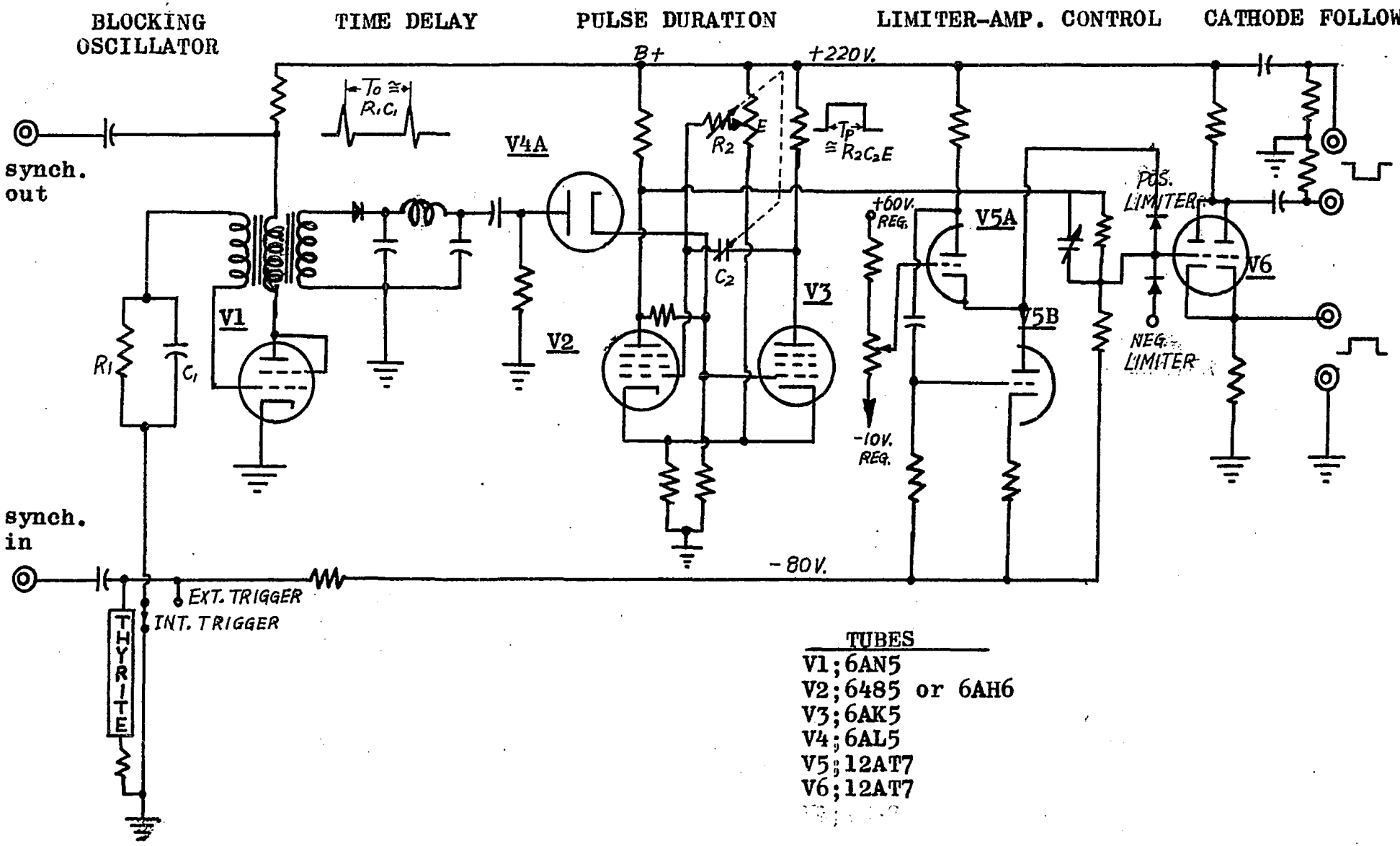

TUBES
V1; 6AN5
V2; 6485 or 6AH6
V3; 6AK5
V4; 6AL5
V5; 12AT7
V6; 12AT7

Fig. 14. Elementary schematic circuit diagram of trigger generator.

negative pulse, which is applied to the input of the modulated pulse generator, is large enough (-200 volts) to maintain the twin triode V_1 (Fig. 13) cutoff during the transient oscillation in the cathode circuit.

An elementary schematic circuit diagram of the pulse amplifier is shown in Fig. 15. The main parts of the amplifier consists of a two stage driver and a power amplifier.

(f) Receiver preamplifier

A preamplifier (Fig. 16) is used on the receiver to amplify very small signals, of the order of a few micro volts, from the receiving transducer for display on the cathode ray oscillescope.

The four stage, R-C coupled amplifier was constructed to have a gain of 4000 (70 db). In order to obtain high fidelty of the signals from the probe, the circuit was designed with the aim of achieving frequency response within 5 % from 10 cps to 1 mc/sec.

The maximum output voltage without serious distortion is approximately 3 volts peak to peak.

The schematic diagram of the preamplifier is shown in Fig. 17. Four pentodes (6AK5) are used and the circuit has two feedback pairs connected in cascade to reduce noise and increase stability. The gain is controllable by adjusting the input of the third stage. Extra gain, when necessary, may be obtained by taking out the feedback. However, the noise and

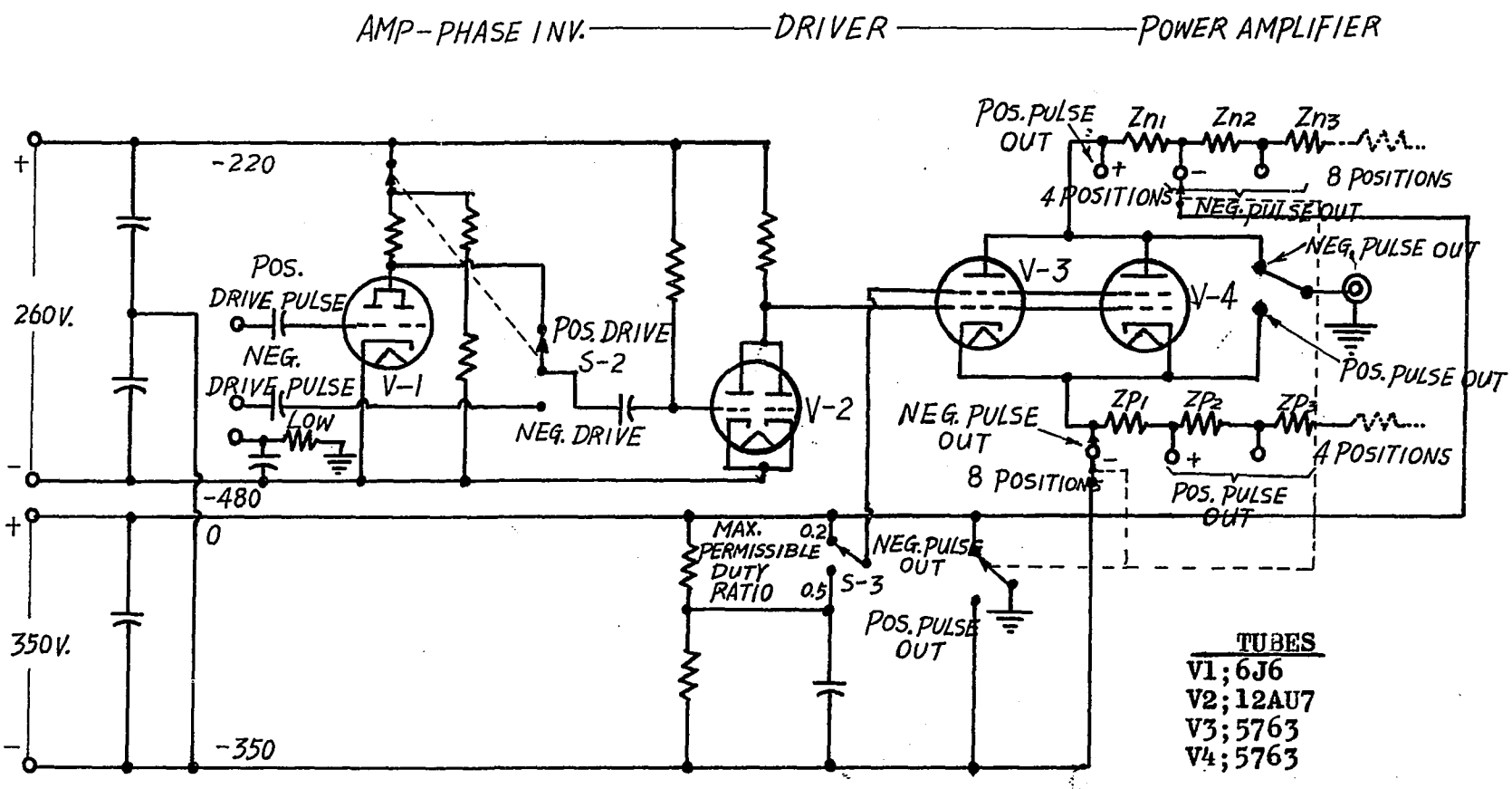

Fig. 15. Elementary schematic circuit diagram of pulse amplifier.

Fig. 16. A four stage preamplifier.

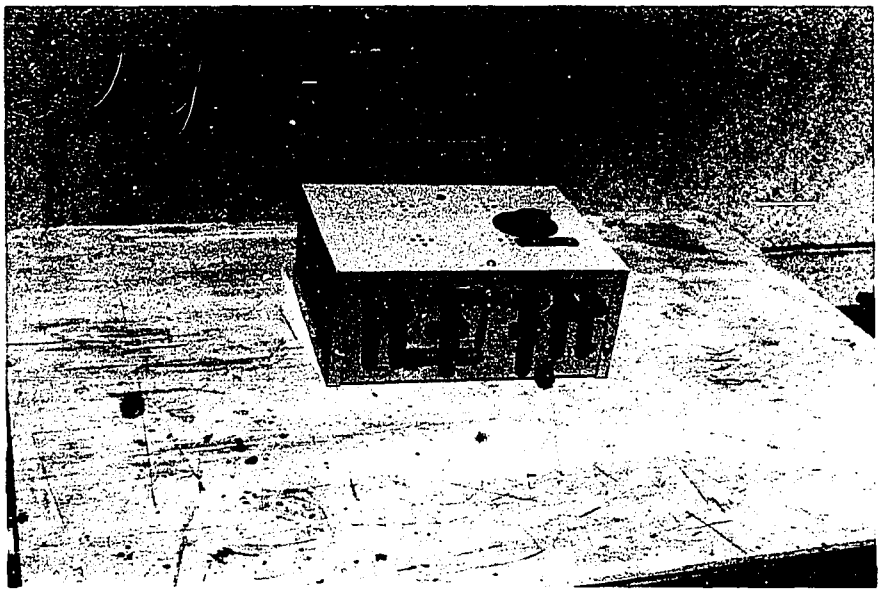

Fig. 16. A four stage preamplifier.

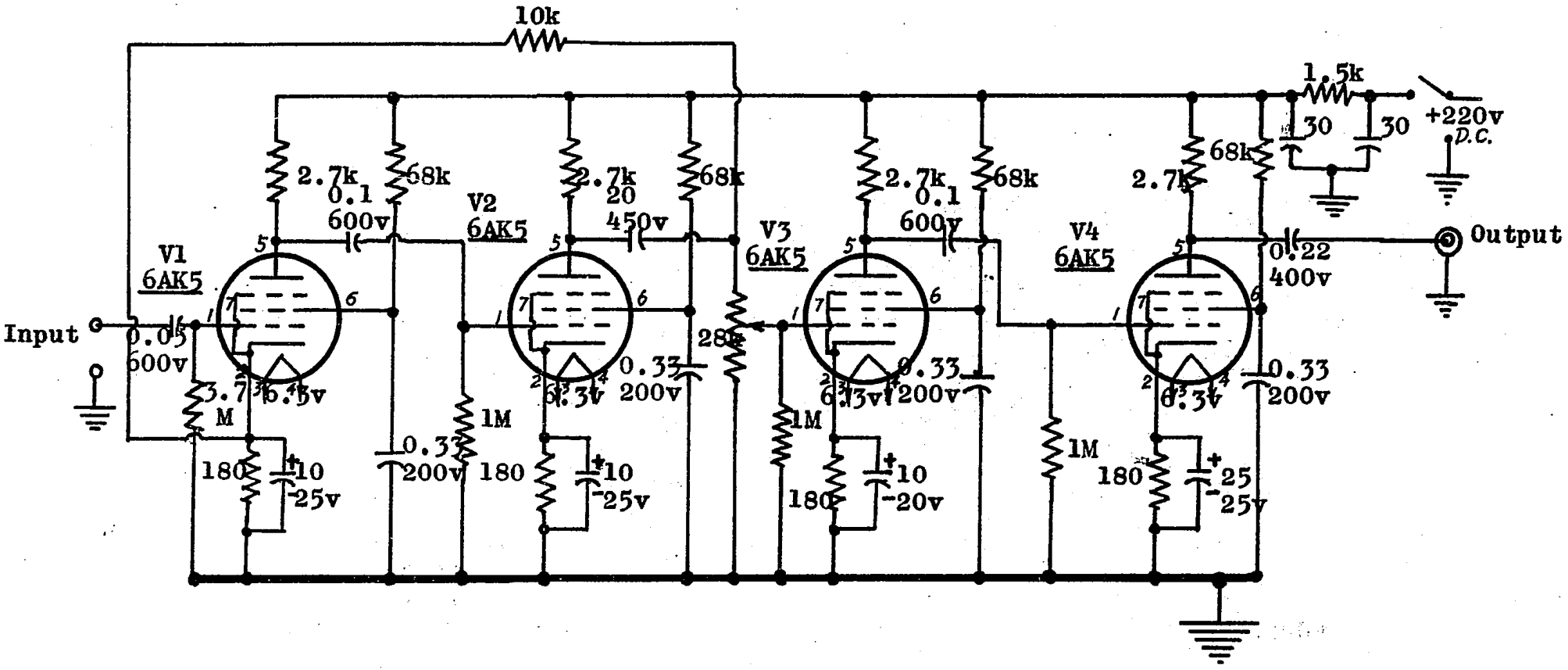

Notes

Capacity in μf
Resistance in Ω

Fig. 17. Schematic diagram of preamplifier.

instability are found to increase without the feedback. The overall performance of the preamplifier was found to be very satisfactory.

(g) 1500 V DC Power Supply

A power supply, having output of 1500 volts DC, 100 ma and 6.3 volts AC, 2 amp, supplies the plate, screen and heater voltages of the output stage driving the transducer. The half-wave rectification is achieved by the rectifier tube 8013, as shown in Fig. 18. A variac is used to adjust the input voltage of the 1500 V DC power supply, which permits variation of the pulse voltage on the transducer.

(h) 350 V DC Power Supply, Cathode Ray Oscilloscope and Oscilloscope Camera

Two Lambda Model 25 regulated power supplies provide the B +, the negative grid bias and the heater voltages.

A Hewlett Packard 132 A dual beam oscilloscope is used to amplify and display the received signals.

A Hewlett Packard 196 A oscilloscope camera accompanies the dual beam oscilloscope to take photographs from the screen of the oscilloscope.

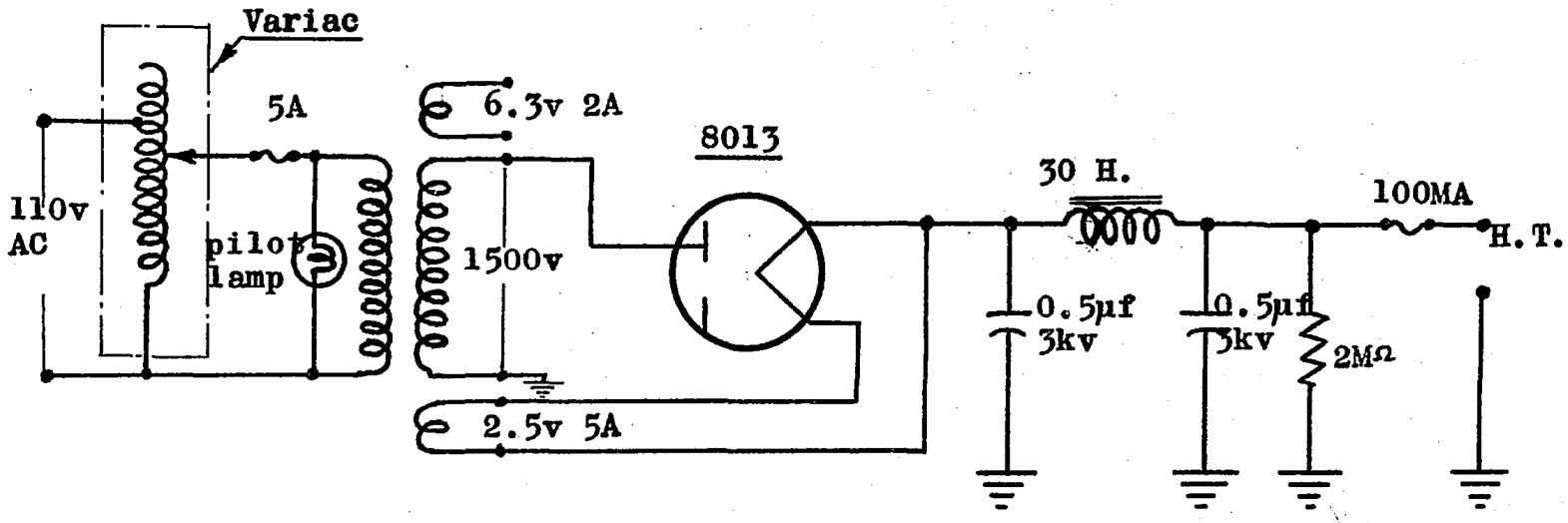

Fig. 18. Schematic diagram of 1500 v DC power supply.

C H A P T E R III

MEASUREMENTS IN LABORATORY

3.1. Velocity of Ultrasonic Longitudinal Waves in Solids

(a) General

In the application of ultrasonic p-waves for detection of fractures in rocks, one measures the travel times of the waves reflected from the fractures. In order to obtain the locations of fractures, a knowledge of the wave velocity in the testing materials is, evidently, a primary requirement.

The velocities of ultrasonic p-waves in the specimens of paraffin, epoxy resin, mortar, some rocks and some other materials were measured by using the ultrasonic system. The measured values of the sound wave velocity in the above specimens were then used to calculate the acoustic impedances of the specimens. As mentioned in a previous chapter, a knowledge of the acoustic impedances of the specimens is necessary for designing the equipment used in the model study.

The measured values of the velocities and the acoustic impedances are compared with those given by other authors in Table 2. As seen in the table, the agreement between the different sets is very good in most cases.

(b) Experimental Procedures

At least two specimens of different lengths for each material were prepared for most measurements. Two faces were cut parallel and polished on each specimen. The surfaces of

the specimens were coated with a thin layer of vaseline for easy transmissions of energy between the probes and the specimen. The specimen was then mounted between the 450 kc transmitting and receiving probes as shown in Fig. 19. The distance between the two points where the two probes were placed should be known very accurately. A moderate pressure should be applied on the probes by tightening the bolts on the frames so that there is no air gap between the probe and the specimen. The impedance matching between the probe and the specimen need not be considered because of the energy available from the probe and the short length of the specimens tested.

The circuit diagram for all the instruments of the ultrasonic system is shown in Fig. 20. It was observed that when the 450 kc probes were used the duration of the triggering pulses to the modulated pulse generetor should be about 1.6 μsec and for the 60 kc probes around 6 μsec. The trigger pulse length can be varied by adjusting the pulse duration dial on the trigger generator. At a particular high tension voltage, the maximum output voltage of the transmitted pulses can be obtained by adjusting the grid bias of the tube V_3 in the modulated pulse generator to a proper value.

The high tension voltage on the modulated pulse generator should be switched on after all other electronic instruments have been turned on so that over voltage may not damage the voltmeter and the tube V_3 (3E29). It was found very necessary to ground all instruments properly. A 60 cps repetition rate

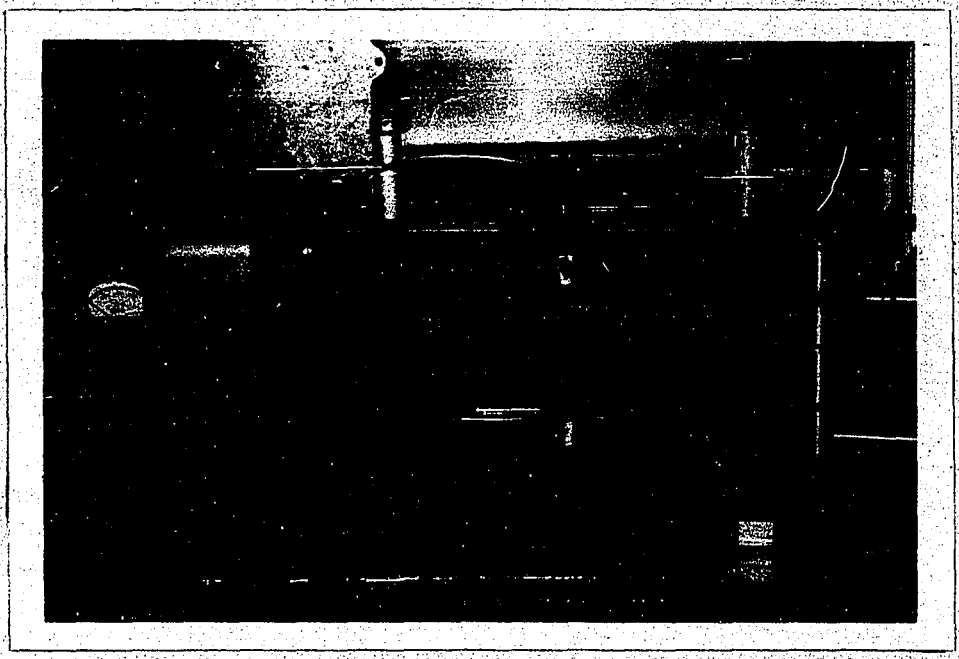

Fig. 19. Set-up used for velocity and attenuation measurements.

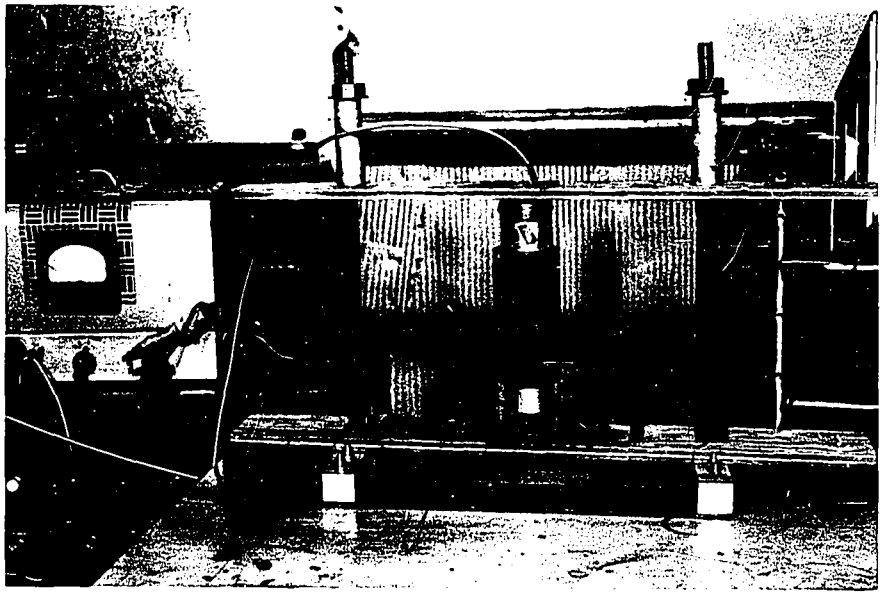

Fig. 19. Set-up used for velocity and attenuation measurements.

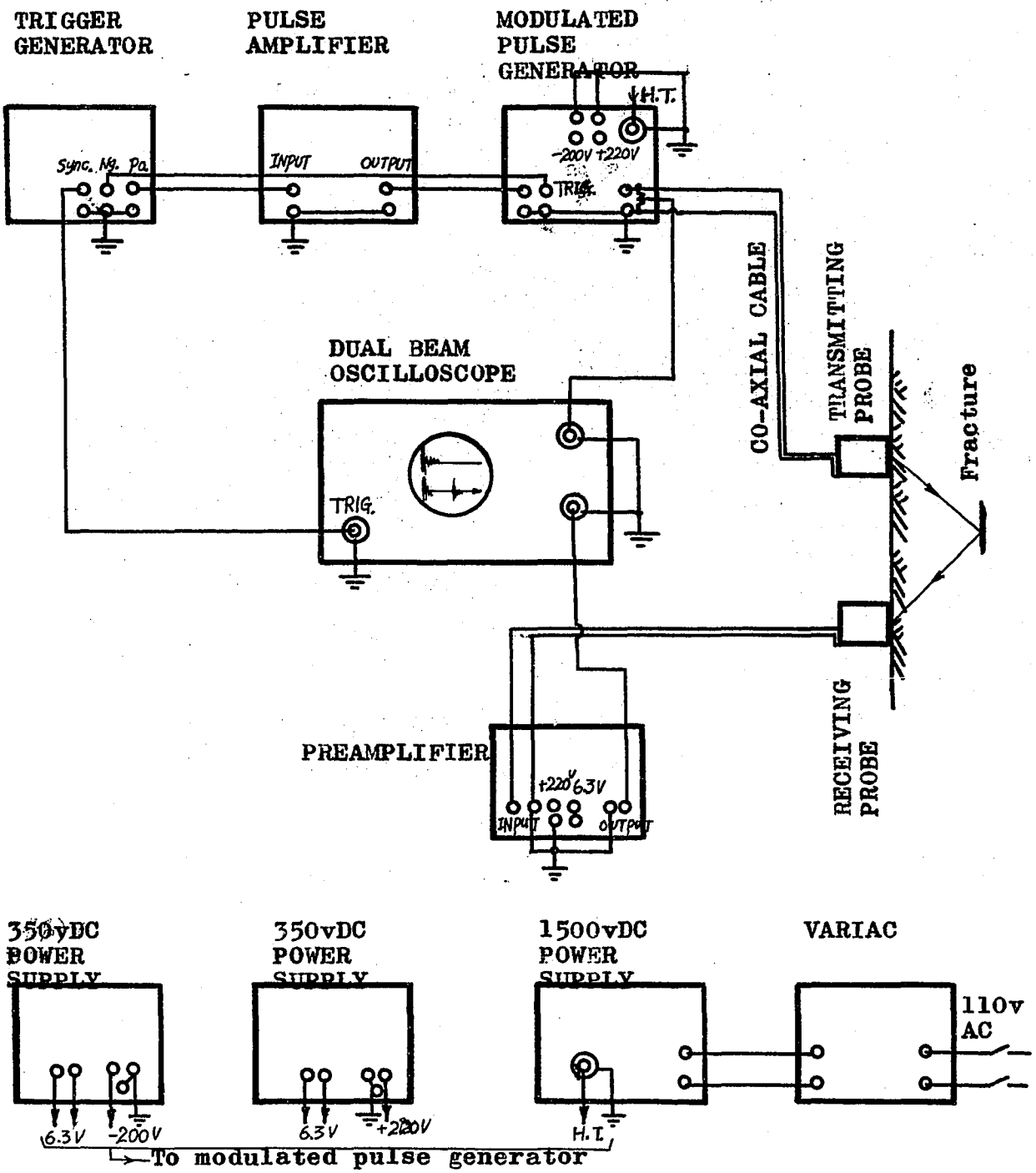

Fig. 20. Connecting diagram of ultrasonic apparatus.

of the synchronizing pulses was found to be most suitable for carrying out all the experiments.

The apparent travel time of the wave in the specimen was read from the screen of the calibrated oscilloscope. The sweep time between the starting trace of the oscillogram and the break in the first arrival waves shows the apparent travel time. A curve is then plotted between the lengths of the specimens tested and the travel time in these specimens. If abscissa values are the lengths and ordinates the travel times, the reciprocal of the slope of the straight line obtained, will give the average velocity of ultrasonic p-waves in the specimens.

(c) Experimental Results

The velocities of ultrasonic p-waves in various solids, under normal conditions, were measured with ultrasonic waves of frequency 450 kc.

Fig. 21 shows the pattern of the first arrival waves in a specimen of paraffin. The break in the first arrival is clearly visible. Hence the travel time could be read very accurately.

The travel times vs. the lengths of the specimens of epoxy resin and Trenton limestone were plotted in Fig. 22 and Fig. 23. The average velocities of epoxy resin and Trenton limestone obtained from the graphs respectively are 2,560 m/sec and 6,642 m/sec.

The intercepts of the fitted lines on the time-ordinate

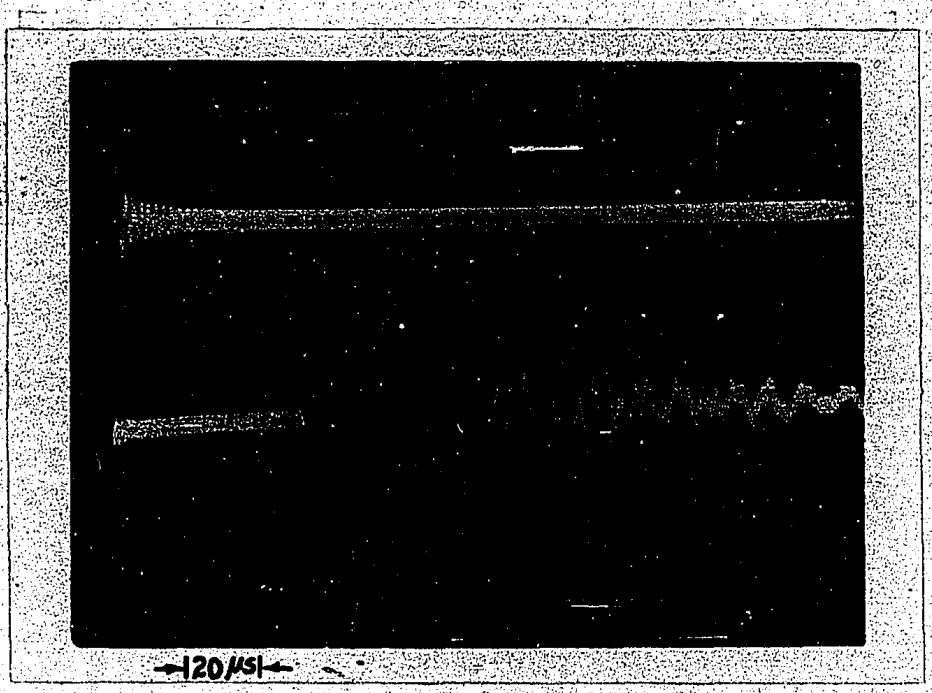

Fig. 21. The first arrival signal in a paraffin specimen.

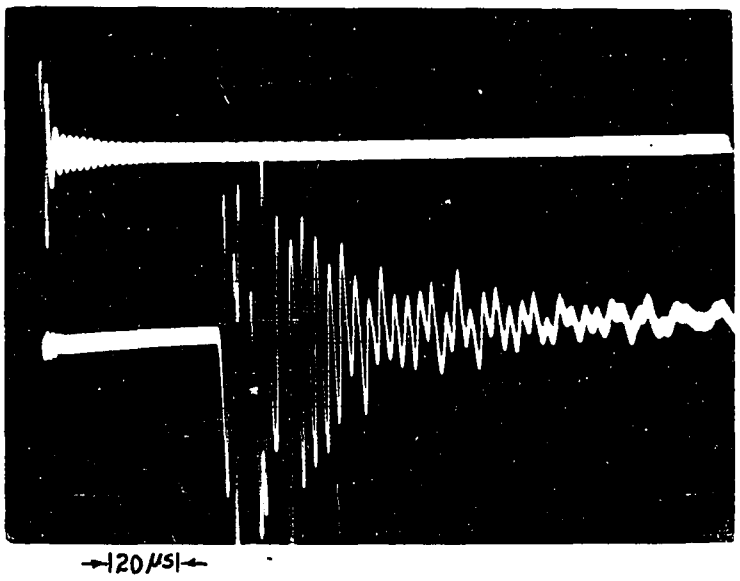

Fig. 21. The first arrival signal in a paraffin specimen.

Fig. 22. Travel times of ultrasonic p-waves vs. lengths of epoxy resin specimens.

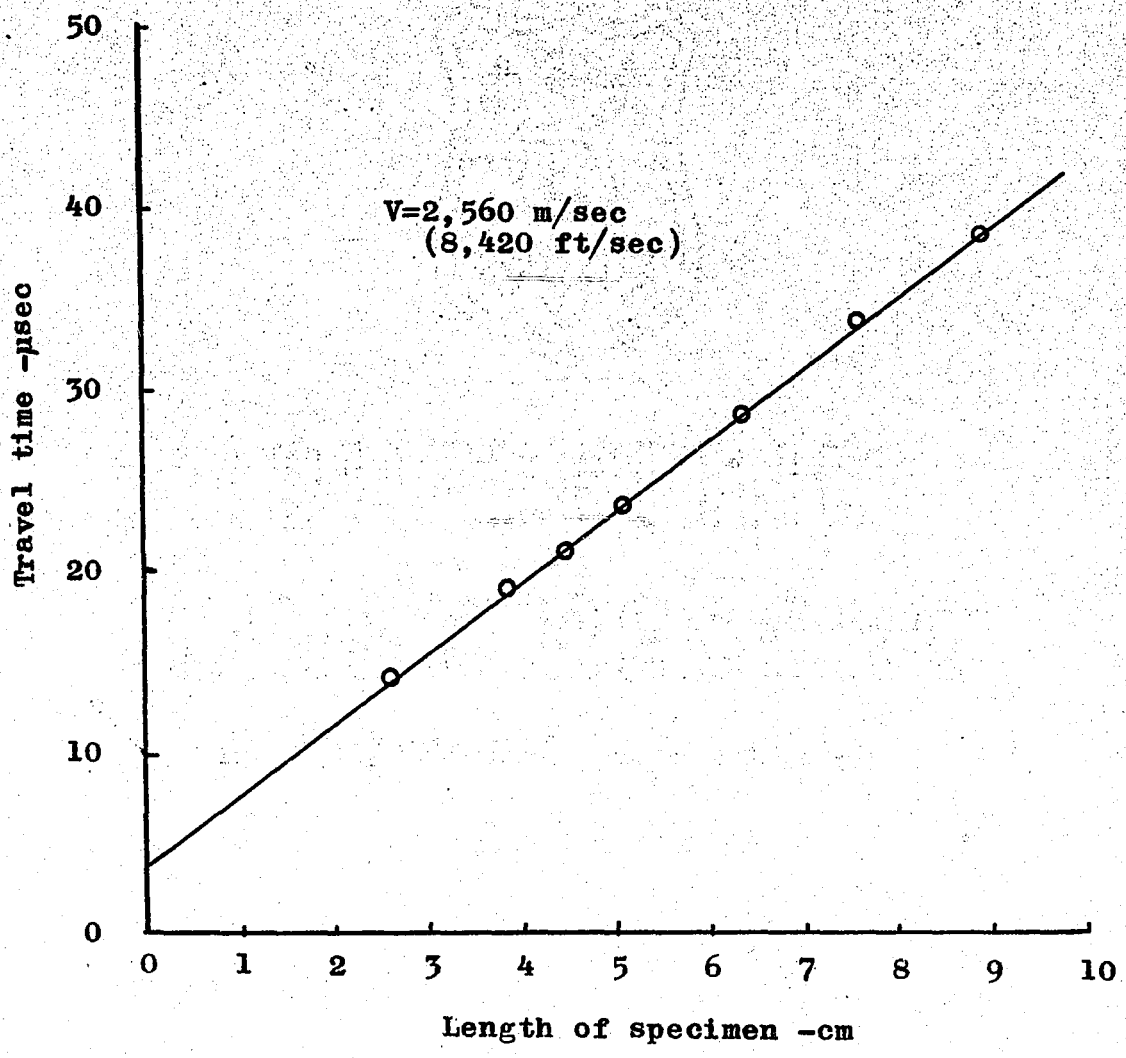

Fig. 23. Travel times of ultrasonic p-waves vs. lengths of Trenton limestone specimens.

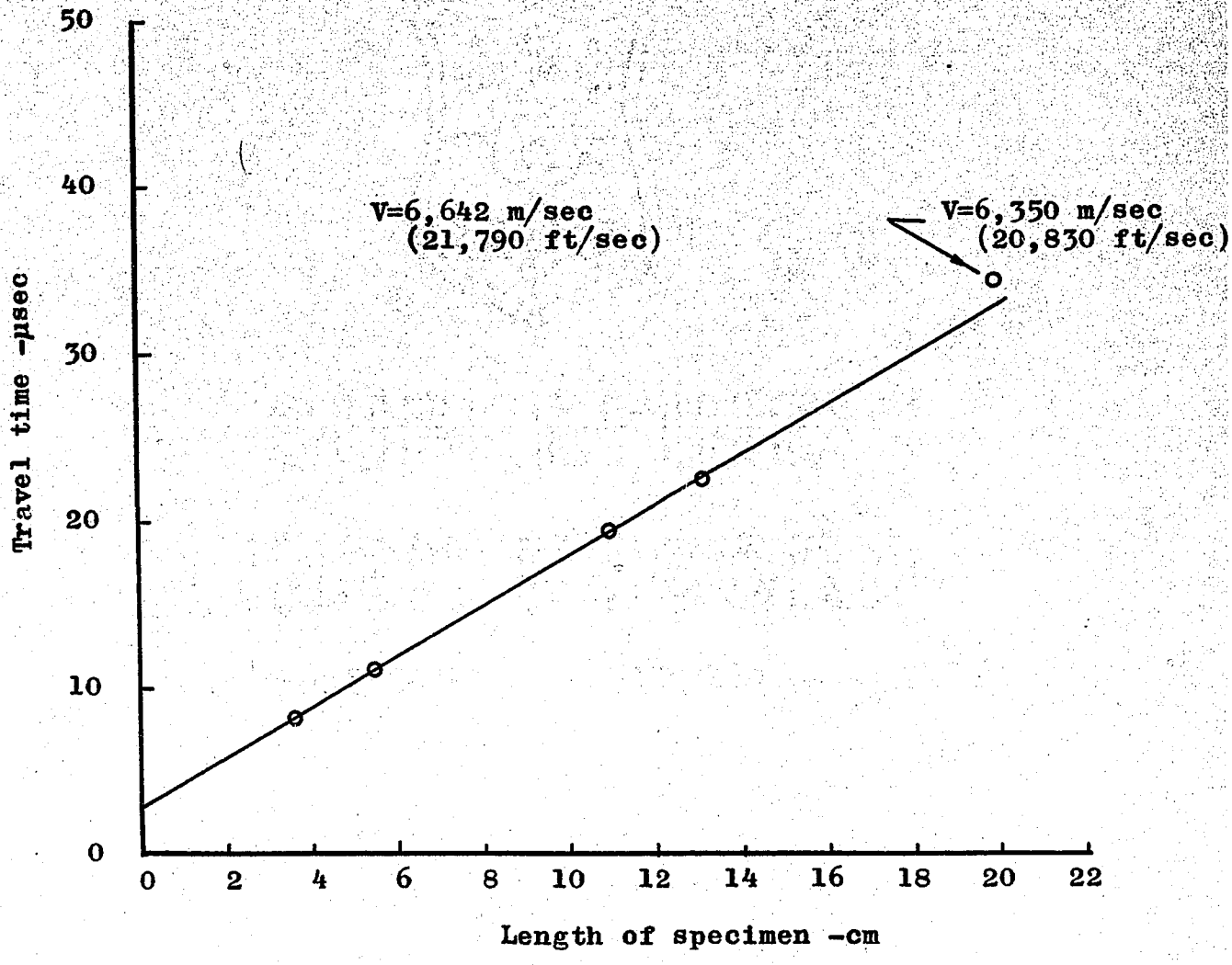

show the travel time for zero length. The zero length observed from our observation is about 3 μsec, and it indicates the time taken in passing through the transition layers in probes and also some extra delay caused in the electronic instruments. If only one measurement is to be made on a specimen this value must be substracted from the apparent travel time to obtain the true travel time through the specimen in calculating the velocity. Generally, however, it is preferable to measure several lengths and obtain the velocity from the slope. The results of the measurements are summarized in Table 2.

3.2. Attenuation of Ultrasonic Waves in Solids

(a) General

The intensity of a sound wave decreases as its distance from the source is increased. This phenomenon is generally called the attenuation of sound waves. The main reasons for the attenuation of sound waves in a solid medium are the following.

1) spreading of the sound beam,

2) absorption of the sound wave energy in the medium.

It is shown in an earlier section (see Fig. 4) that the sound beam spreads outwards with an angle of 2θ ($\theta=\sin^{-1}1.22\lambda/D$) in the far field or the Fraunhofer region. This effect of spreading of the sound waves is called Fraunhofer diffraction.

As the wave travels through a perfectly elastic medium, the wave energy changes back and forth from kinetic to potential form while theoretically, the total energy remains constant.

TABLE 2

Velocities of Ultrasonic P-wavesin Solids under Normal Conditions.

Material		Density gr./cm^3	Ultrasonic P-Wave Velocity m/sec	Ultrasonic P-Wave Velocity ft./sec	Acoustic Impedance x10^{5}gr/sec-cm^2	No. of Tests
Aluminum	(measured)	2.60	6,494	21,300	16.9	2
"	"	2.70	6,557	21,510	17.7	2
"	(13)	-	6,416	21,050	-	-
"	(14)	-	6,507	21,350	-	-
"	(15)	2.65	6,220	20,410	17.0	-
"	(9)	2.81	6,360	20,870	17.9	-
Brass	(measured)	8.39	4,417	14,490	37.1	3
"	"	8.52	4,234	13,890	36.1	2
"	(16)	-	4,300	14,110	-	-
"	(15)	8.5	4,238	13,900	-	-
Epoxy resin	(measured)	1.39	2,560	8,420	3.5	5
Resin	(16)	-	2,443	7,970	-	-
Lead	(measured)	10.6	2,454	8,052	26.0	3
"	(15)	11.4	2,130	6,988	27.3	-
Mortar	(measured)	2.2	3,880	12,720	8.5	5
Norite	(measured)	2.8	6,388	20,960	17.9	2
"	(11)	-	6,220	20,410	-	-
Paraffin	(measured)	0.92	2,140	7,030	1.97	9
"	(17)	0.9	1,460	4,780	1.3	-
Steel	(measured)	7.84	5,873	19,270	46.0	1
"	"	7.88	5,892	19,330	46.4	1
"	(18)	7.82	5,880	19,290	-	-
Trenton limestone	(measured)	2.73	6,642	21,790	18.1	4
Dense limestone	(16)	-	5,900 -7,000	19,350 -22,960	-	-

Practically, however, during the alternation between kinetic and potential energy, some energy is lost in the form of heat. Coupled with this heat loss, a sound wave may also lose energy due to 1) internal friction (viscous-damping losses), 2) diffusion, 3) irreversible thermal effects, 4) scattering by grains and minute irregularities. An ultrasonic wave, in passing through a medium, encounters losses mainly due to scattering effect and due to minute irregularities present in the medium.

For plane wave propagation, it has been found experimentally that the absorption is given by (19)

$$A / A_0 = \exp (-\alpha x) \qquad (3.1)$$

where

A / A_0 = the ratio of the wave amplitude between two points, distance x apart, on the axis of a source radiating a sound wave.

α = the attenuation constant of the medium

The attenuation constant can be expressed explicitly as:

$$\alpha = \frac{- \text{Ln } A / A_0}{x} \text{ népers/cm} \qquad (3.2)$$

The attenuation constant, α, is a function of the frequency of the sound waves.

Based on certain assumptions, the attenuation constant can be measured experimentally. First, we assume that the operation of the equipment was unchanged during the entire experiment, so that the transmitting probe generates ultrasonic

waves of constant energy. Secondly, if the surfaces of the specimens are treated identically, the coupling between the probe and the specimen will be approximately the same for any one material and hence each sample of that material will have equal transmissivity for sound waves. Once the conditions mentioned above are fulfilled, the attenuation constant can be found by measuring the amplitudes of the head wave travelling through specimens.

(b) Experimental Procedures

The specimens (Fig. 24), prepared for the measurement of velocity, were also used for the measurement of attenuation constant. Since the surfaces of the specimens were treated in the same manner, it is believed that they had the same smoothness and the same coupling for wave transmission between the probe and the specimen. The same set-up used for the measurement of velocity was also used for the measurement of attenuation constant.

For measuring the attenuation constant the instrument was kept fixed for measurements on several specimens of the same material but different lengths. It is observed that for maximum energy of the received signals, the position of the probes should be adjusted properly.

The amplitudes of the head waves were read from the screen of the oscilloscope. By plotting the amplitudes in the natural logarithm scale vs. the lengths of the specimens in the linear scale, the attenuation constant can be found from the slope of the fitted line.

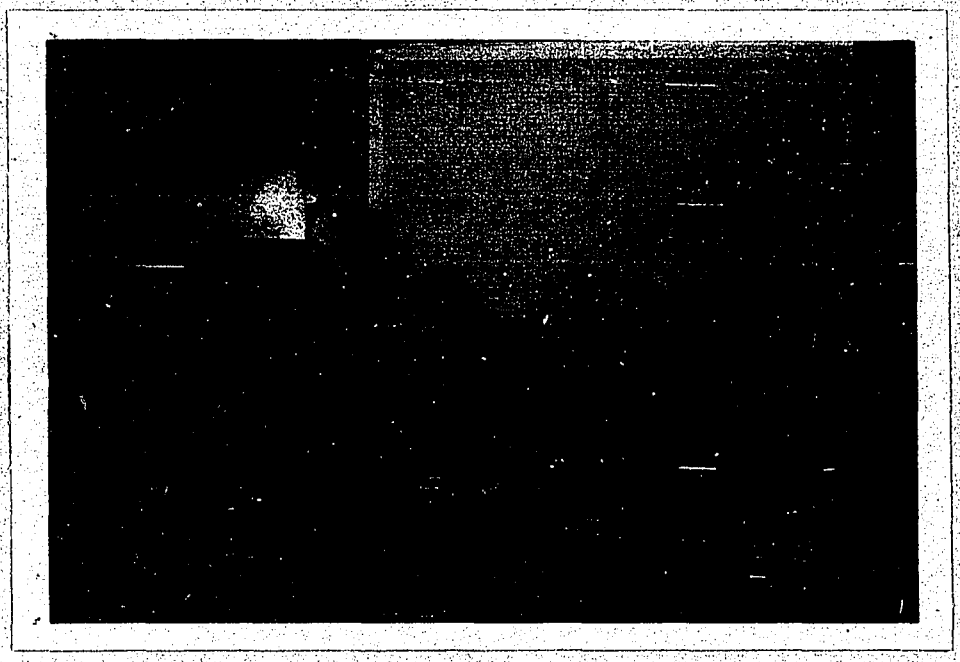

Fig. 24. Some specimens of paraffin, epoxy resin, mortar and Trenton limestone.

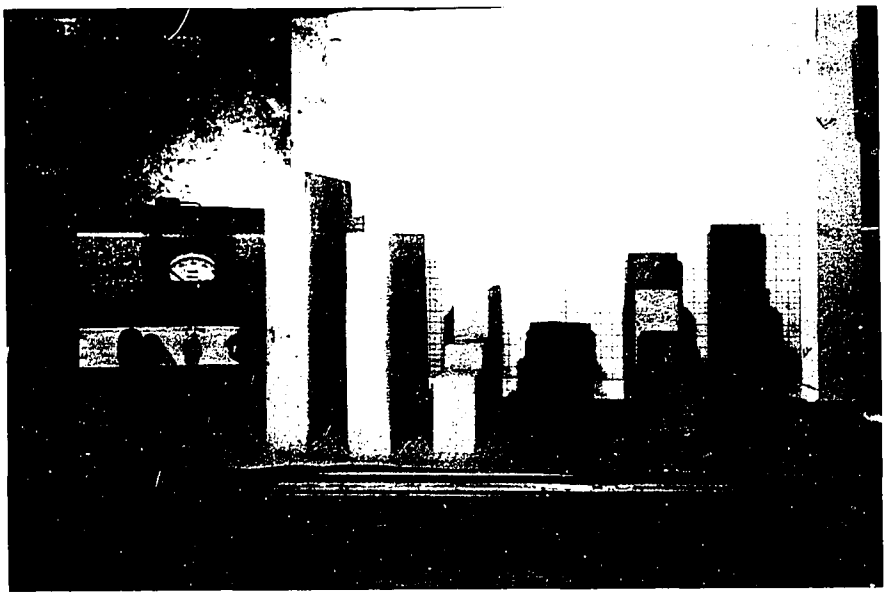

Fig. 24. Some specimens of paraffin, epoxy resin, mortar and Trenton limestone.

(c) Experimental Results

Using ultrasonic waves of frequency 450 kc/sec, measurements were made on specimens of epoxy resin, mortar, Trenton limestone and paraffin. As mentioned in section (2.2.b) the attenuation also varies with frequency.

The complete data for all the experiments are given in Appendix A-1 to A-4. Plotted results appear in Fig. 25 to Fig, 28. The results could not be compared with any other author since there is no report of any work with the same experimental conditions as ours.

3.3 Measurement of Degree and Depth of Fractures in Solids

(a) General

As described in section (2.1), ultrasonic waves travelling in solid media are reflected back from the planes of fractures or other discontinuities. The number of reflected waves observed on the oscilloscope indicates the degree of fracture while the travel times of the reflected waves determine the position of each fracture.

A round hole of diameter, 1/8 in., was drilled perpendicular to the curved surface of the epoxy resin cylinder, and also a plane fracture, thickness, 1/8 in., was made parallel to the plane surface of the cylinder by means of a saw. Reflected pulses from the hole, the plane fracture and the bottom of the cylinder were then observed on the oscilloscope.

The reflection from a round hole of diameter, 1/8 in., in the specimen of paraffin, and also from the bottom of the

Fig. 25. Amplitudes vs. lengths of epoxy resin test specimens.

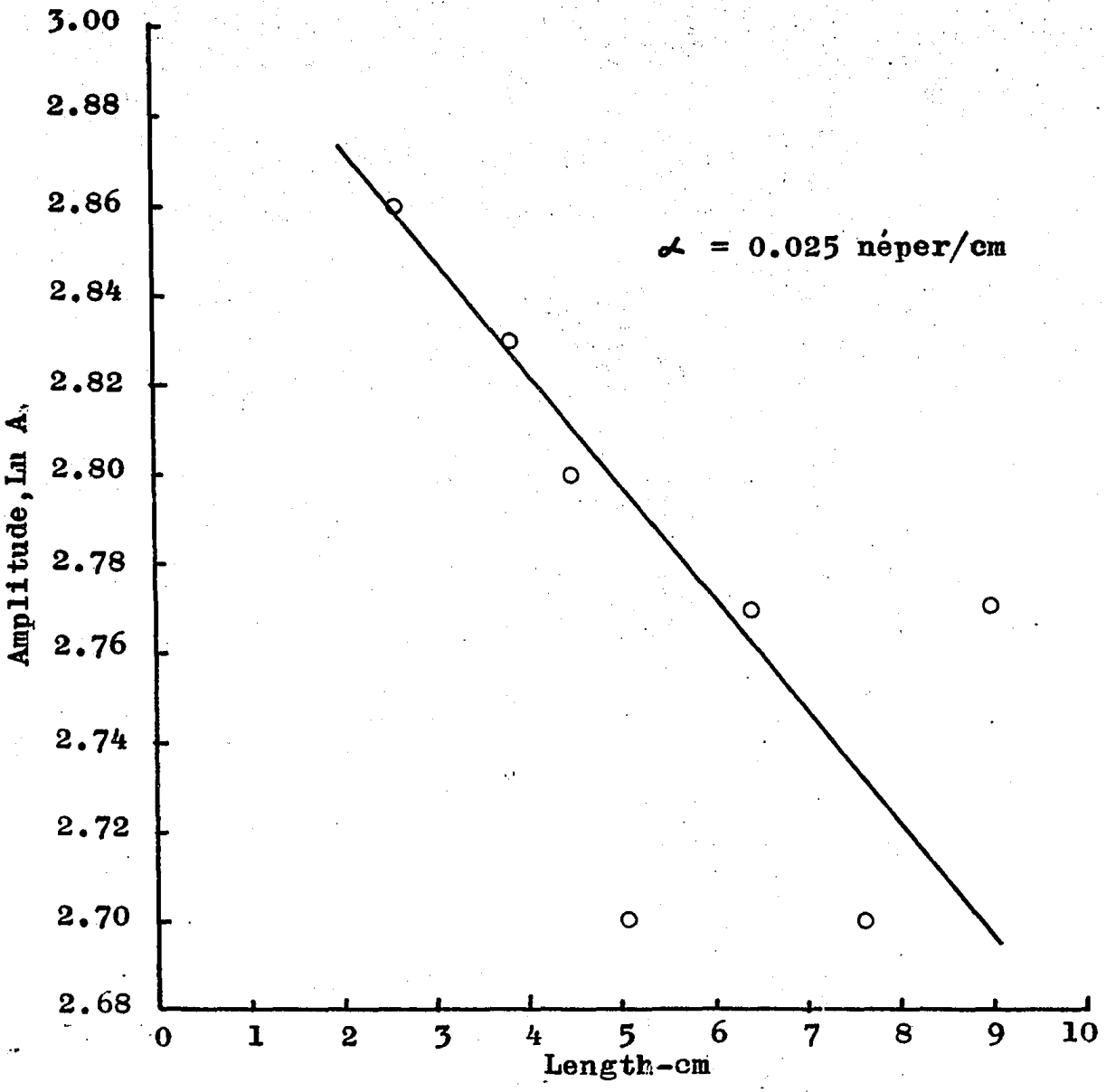

Fig. 26. Amplitudes vs. lengths of mortar test specimens.

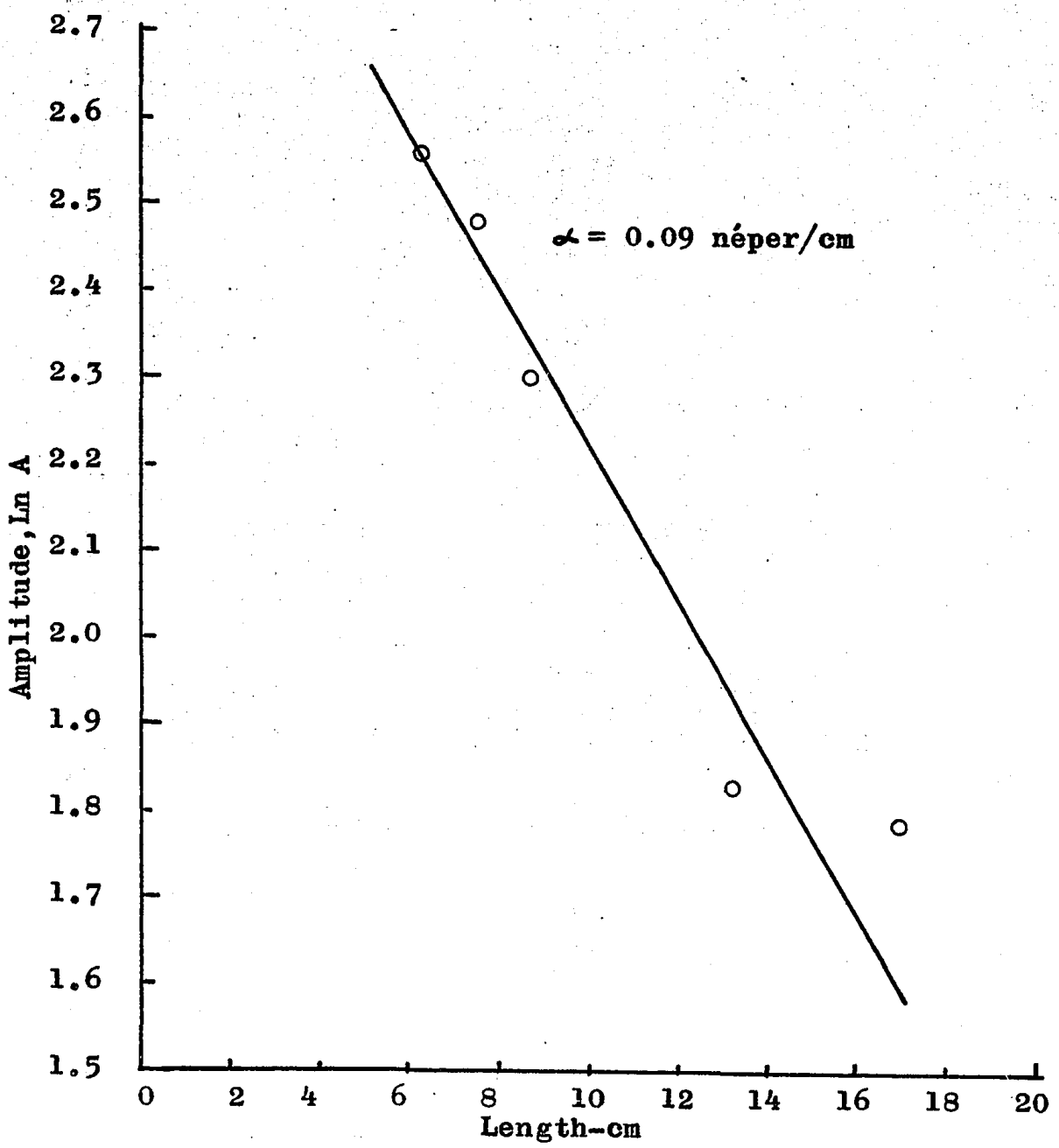

Fig. 27. Amplitudes vs. lengths of Trenton limestone test specimens.

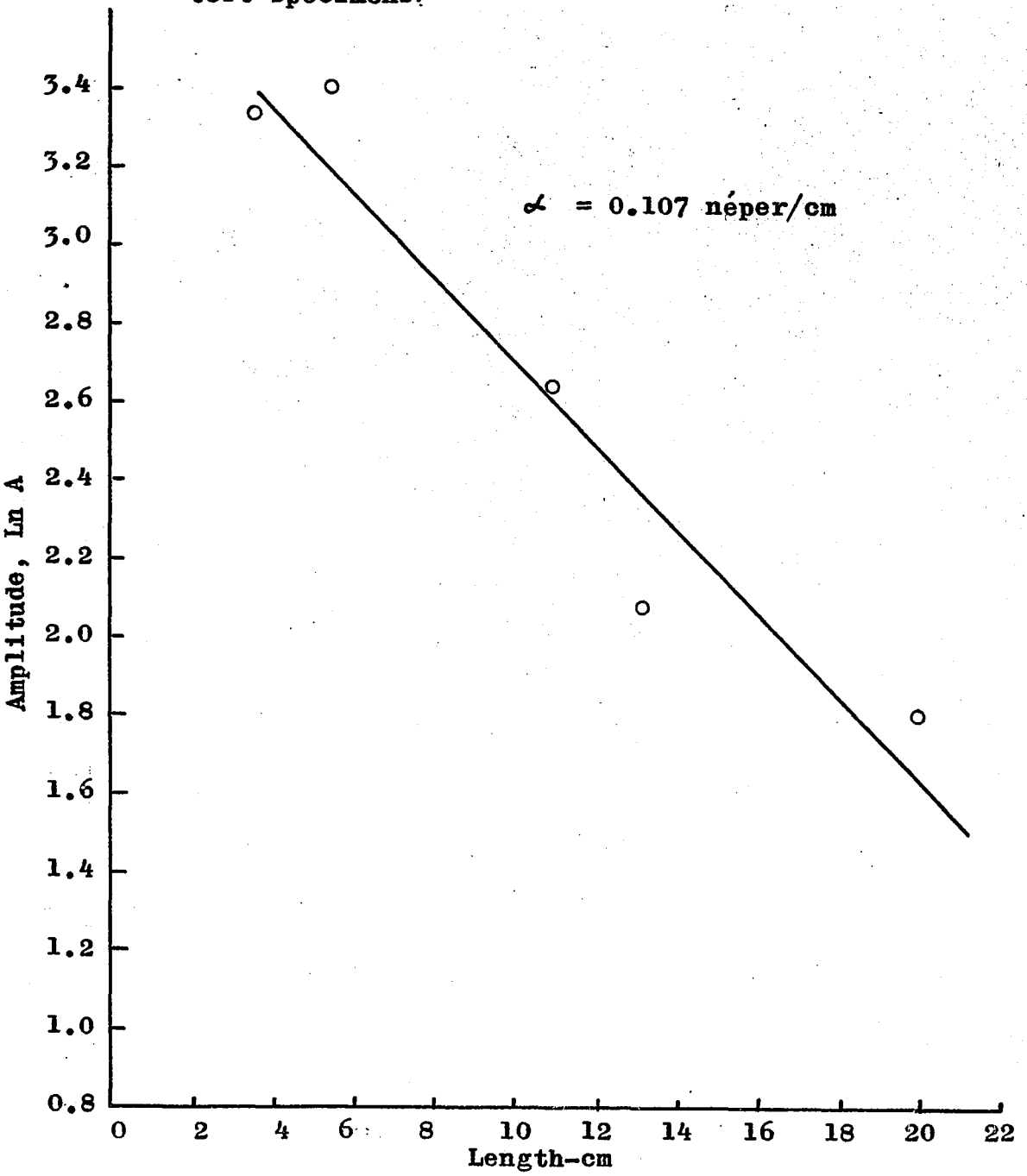

Fig. 28. Amplitudes vs. lengths of paraffin test specimens.

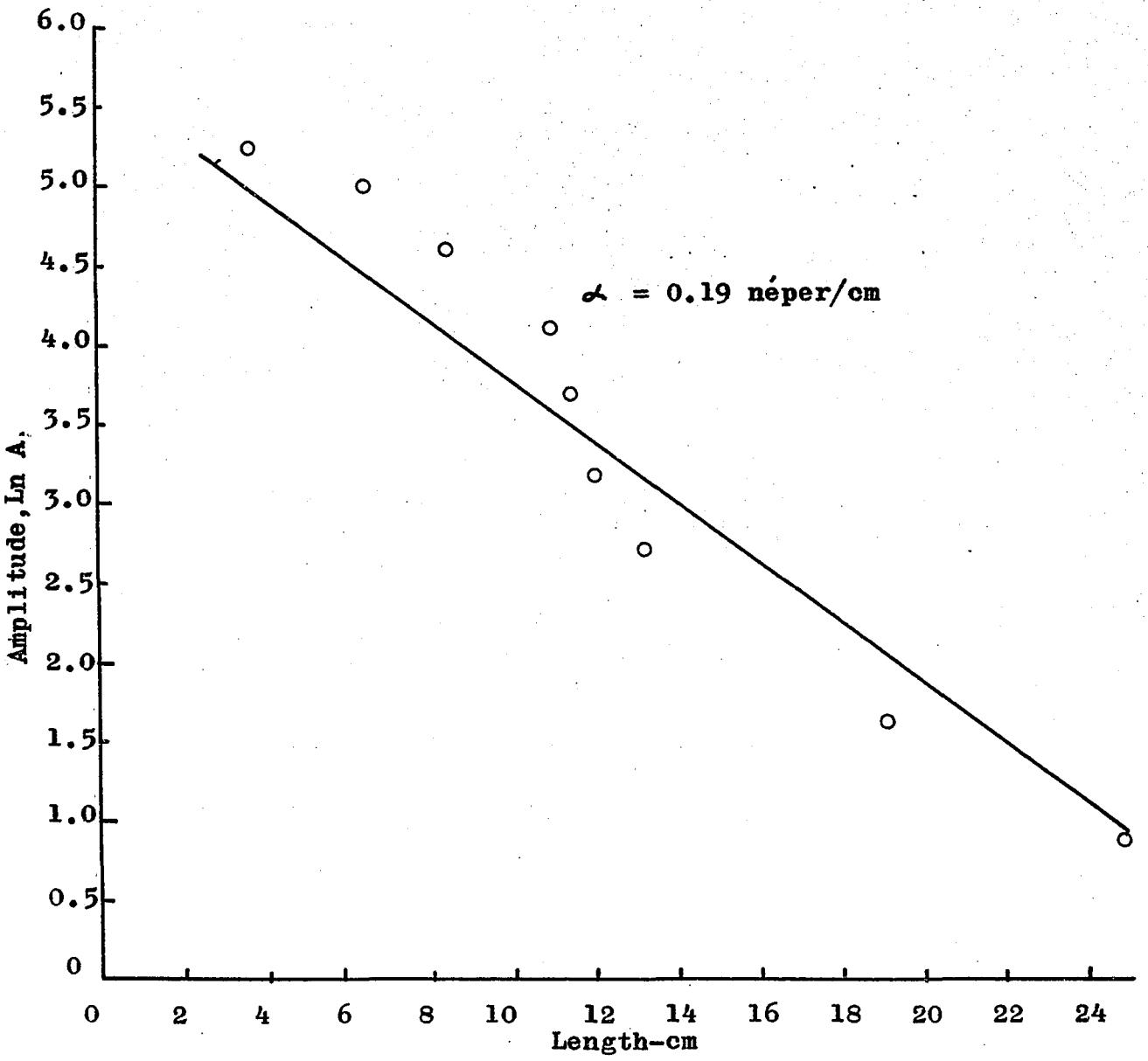

paraffin were observed.

(b) Experimental Procedures

The surfaces of the specimens were polished, and then a thin layer of vaseline or heavy oil was applied to the surfaces. For reflection measurements both the transmitting and the receiving probes were placed on the same surface of the specimen, applying a moderate pressure for good contact between the probes and the specimen. A preamplifier was used to amplify very small receiving signals. A semi-conductor diode was connected to display the positive or the negative halves of the waves; this clarified the reflected wave traces somewhat. The circuit arrangement is shown in Fig. 29.

(c) Experimental Results

The detection of fractures in the epoxy resin cylinder (Fig. 30) was found to be very satisfactory. In the oscillogram of Fig. 31, the bright line in the extreme left shows the starting point of the transmitted waves. The first large pulses with the travel time of 59.4 μsec were observed to be the reflected waves from the surface of the hole. Substracting the delay time of 3 μsec from this value gave a true travel time of 56.4 μsec. From the true travel time of the reflected waves, the approximate depth to the hole from the surface of the cylinder is estimated by taking half the true travel time and then multiplying it by the velocity of ultrasonic p-waves in the cylinder. The depth to the hole from the top surface of

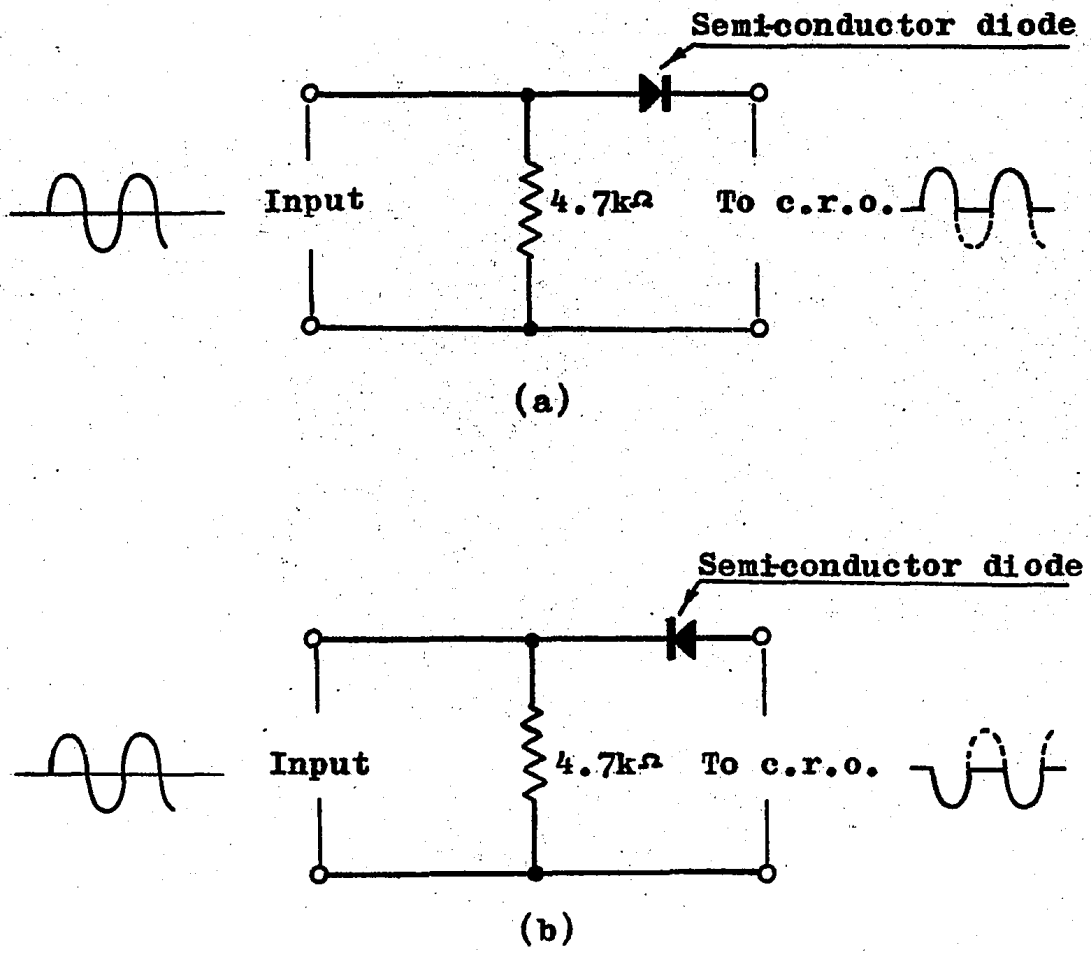

Fig. 29. Clipping circuit diagram for upper half-wave display(a) and for bottom half-wave display(b).

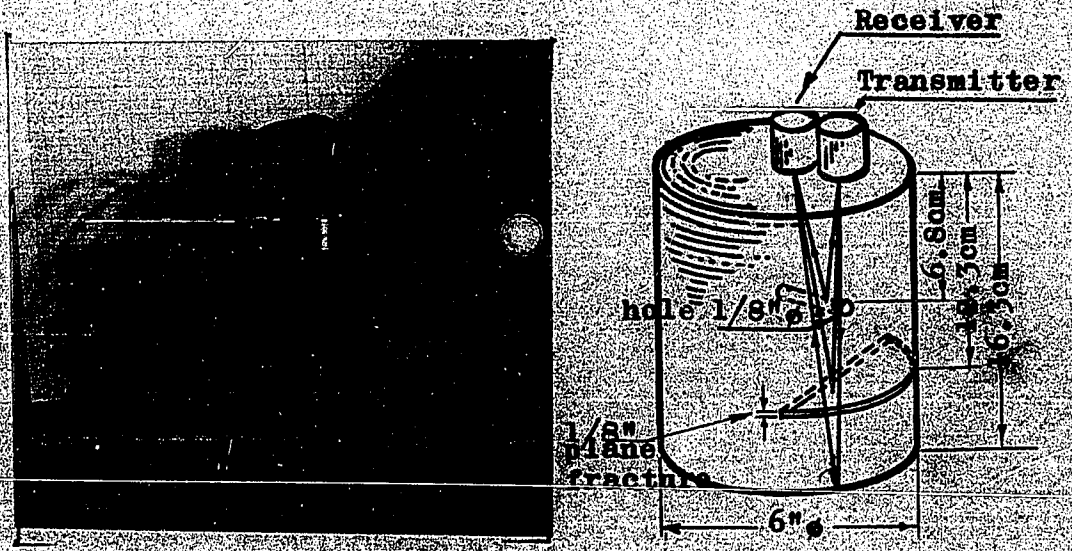

Fig. 30 (a) (b). Measurement in epoxy resin cylinder.

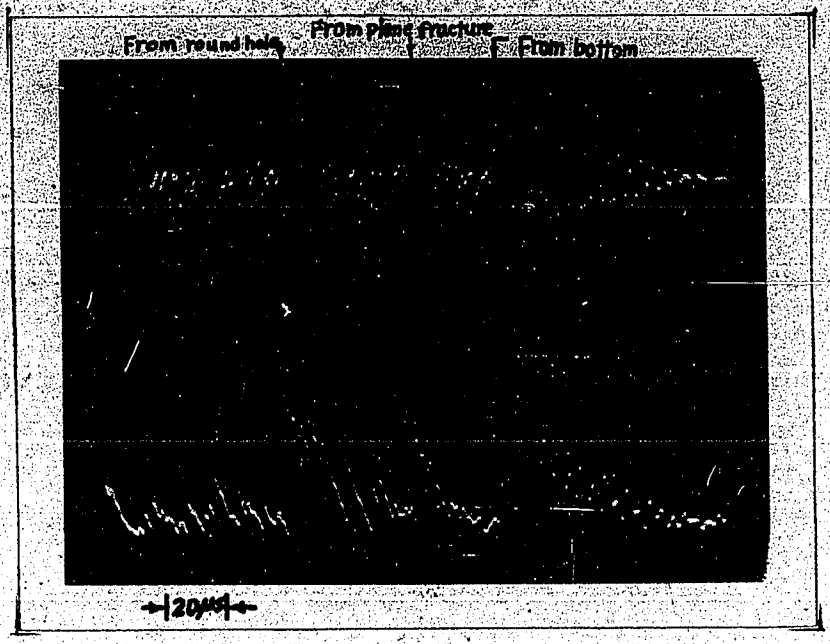

Fig. 31. Reflected pulses in the epoxy resin cylinder.

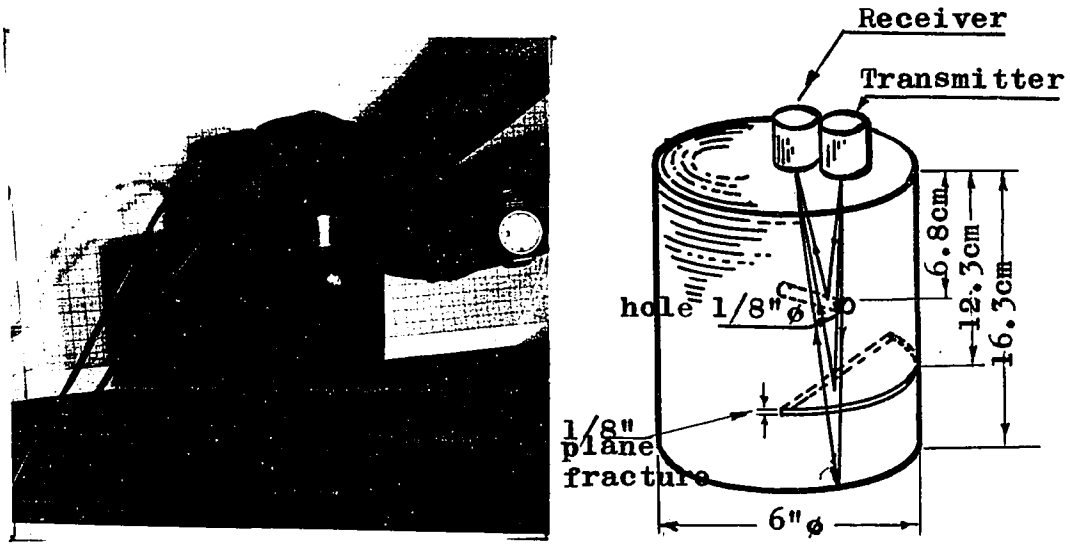

Fig. 30 (a) (b). Measurement in epoxy resin cylinder.

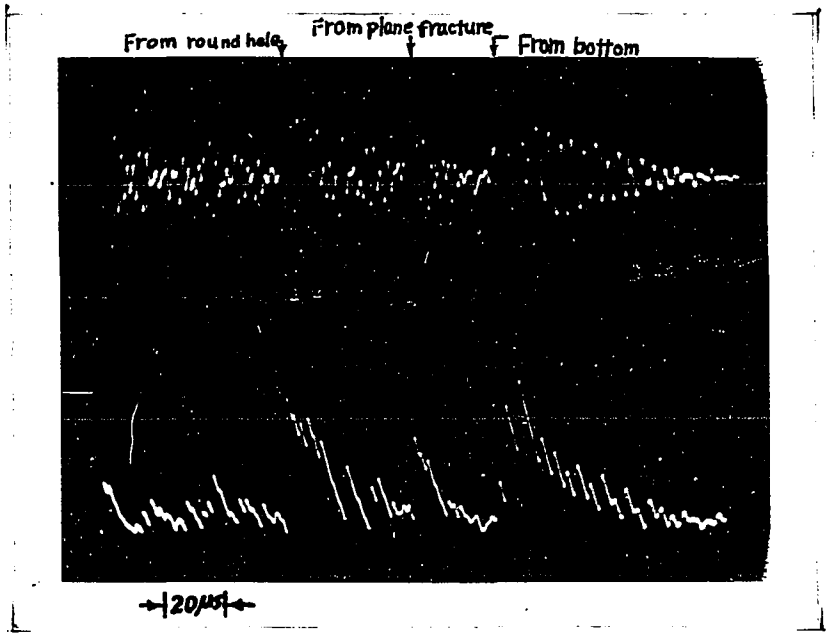

Fig. 31. Reflected pulses in the epoxy resin cylinder.

the cylinder was found to be 7.2 cm, and the actual measured depth is 6.8 cm. The second large pulse at 100.8 μsec, indicating a depth of 12.5 cm, is the reflected wave from the plane fracture. The third pulse at 130.4 μsec, corresponding to a depth of 16.3 cm, is found to be the reflection from the bottom of the cylinder. Actual measured depth from the surface of the cylinder to the fracture plane and the bottom of the cylinder are 12.3 cm and 16.3 cm respectively.

As can be seen in Fig. 31, all the reflected waves are clearly visible. The half wave display, shown in the bottom half of Fig. 31, gives a clearer picture of the reflected waves.

Fig. 32 (a& b) show the specimen of paraffin to be tested. It is seen from Fig. 33 that the first large pulse with the travel time of 148.5 μsec is the reflected wave from the round hole and the second large pulse at 239 μsec is from the bottom of the paraffin. The estimated depths to the hole and the bottom of paraffin from the top surface (taking the measured velocity of ultrasonic p-wave in the paraffin to be 2,140 m/sec) are found to be 15.5 cm and 25.1 cm, whereas the actual measured values are 14.7 cm and 24.7 cm respectively.

3.4 Determination of Geometry of Fracture Planes in Rocks by Model Studies

(a) General

All large fractures in rocks usually possess fracture

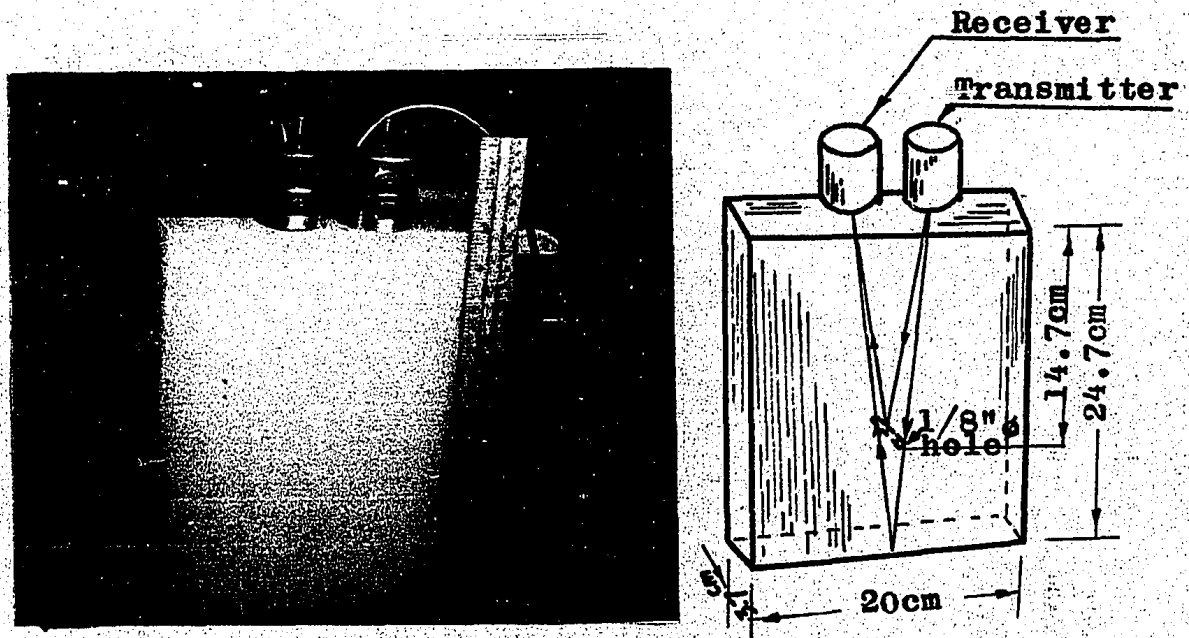

(a) (b)

Fig. 32 (a) (b). Fracture measurement in the paraffin specimen.

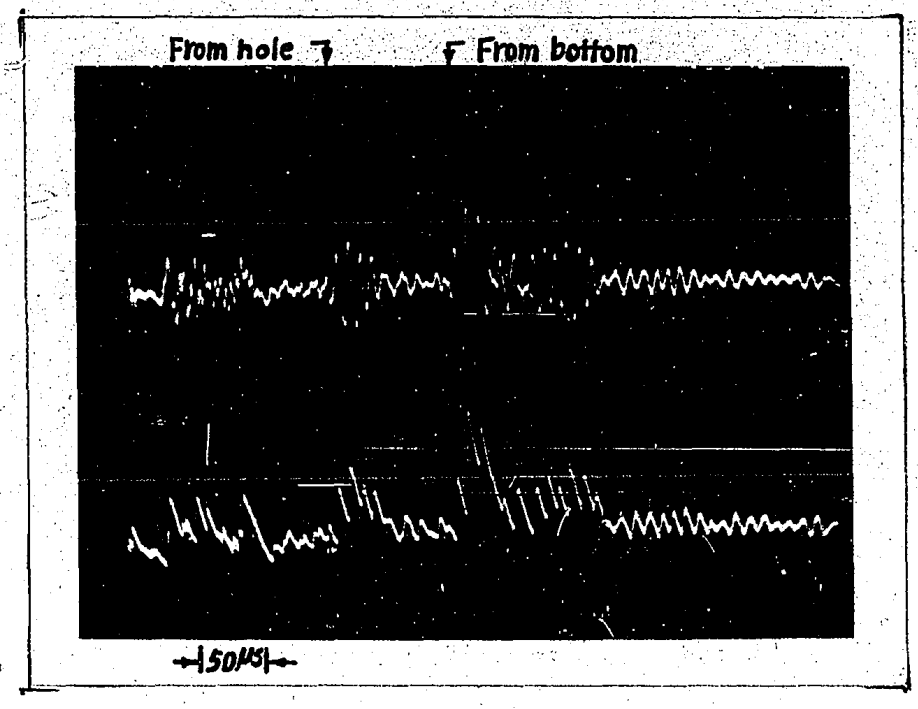

Fig. 33. Reflected pulses in the paraffin specimen.

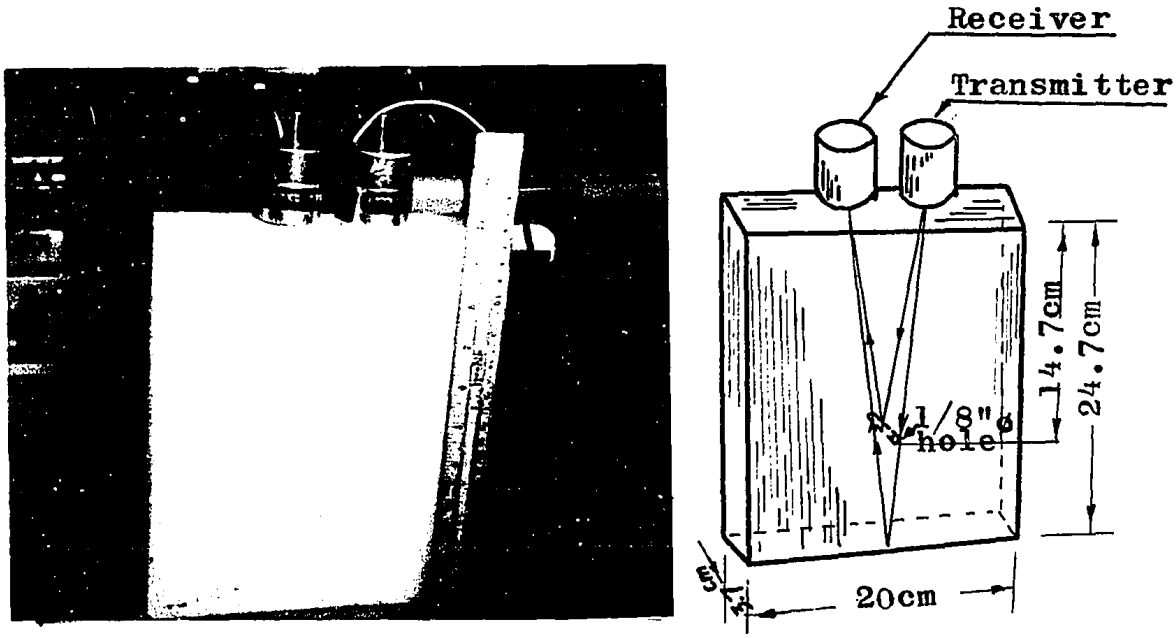

Fig. 32 (a) (b). Fracture measurement in the paraffin specimen.

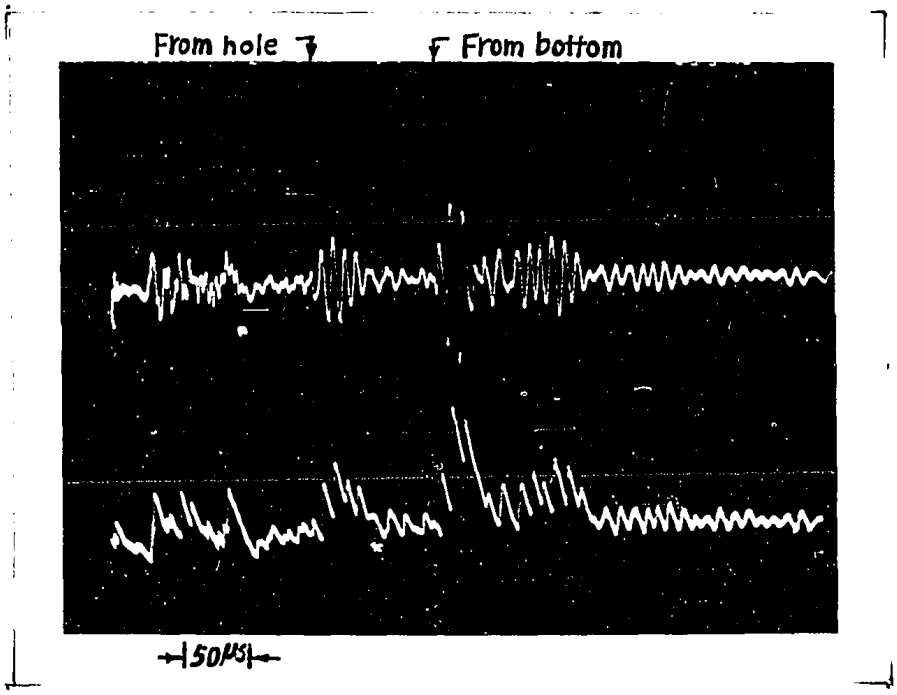

Fig. 33. Reflected pulses in the paraffin specimen.

planes. The geometry of the fracture planes can be determined by the ultrasonic equipment using seismic reflection techniques.

By means of models, the velocity of p-wave in the medium and the various parameters of the geometry of fracture planes were determined. The parameters measured were the direction of strike of fractures, the apparent dip angle of fractures, the true dip angle of fractures and the depths of the fractures.

The direction of strike is analogous to the geologic term "strike" and is defined as the acute angle between any measuring line, say the X axis, on the rock face, and the line of intersection between the fracture plane and the rock face.

The dip angle of fracture is defined as the acute angle between the rock face and the fracture plane. When the dip angle is measured along the direction of the line normal to the X axis on the rock face, it is called the apparent dip angle, and when the dip angle is measured at right angles to the strike, it is called the true dip angle.

The depth to the fractures is the vertical depth of the fracture plane under the transmitting probe.

In order to make measurements on complete fracture planes, a three dimensional model of some volume is necessary. The first attempt was made on a wooden tank, constructed in the laboratory at one time for seismic model studies. The tank had been filled with concrete in the bottom and paraffin in the upper part, with an interface between the two layers. Experiments with the above set-up, however, had to be abandoned because of

the following reasons: 1) Due to presence of vaporized holes in the paraffin, there were very few reflected waves, 2) Attenuation of ultrasonic waves in paraffin is very high (0.19 néper/cm) as indicated by the measurement of attenuation constant in paraffin, described in the last section.

An attempt was then made to replace the paraffin by a type of epoxy resin, called the Laminac polyester resin 4151 made by Cyanamid Ltd.. From previous tests it was observed that the epoxy resin has a much smaller attenuation constant (0.025 néper/cm) than paraffin and also it is fairly easy to obtain homogeneous blocks of resin on which experiments could be performed. The use of this material was not successful either, mainly because of the difficulty in constucting a homogeneous volume of epoxy resin layers. Inorder to prevent cracking of of the epoxy during molding, the volume must be built up by pouring successive thin layers(1/8 in.), one on top of the other. Due to the large shrinkage of the epoxy resin during gelling, the resin surface was pulled up around the edges and from the face of the bottom concrete layer.

Finally it was decided to use a tank filled with water and containing a thin aluminum plate immersed at an angle. The plate was used to simulate a fracture plane in rocks.

In the seismic reflection technique, there are several methods for determining the direction of strike, the dip angle and the depth of the fracture plane, and the p-wave velocity in the medium. The following method, however, was found to be most suitable for our model study purposes.

First of all, the ultrasonic p-wave velocity in water was determined by the $T^2 - X^2$ method (20). The travel times of the reflected wave were taken using the process described in the following experimental procedure. The squares of the travel times, T^2, are plotted against the squares of the displacement, X^2, The slope of the straight line gives $1/V^2$. With the slope, and thus the value of the velocity of ultrasonic p-wave in water, V, can be determined. The vertical depth, Z, from the transmitting probe to the plane of reflection can be calculated from the observed intercept, which is $4(Z/V)^2$.

Subsequently, the travel times of waves reflected from the aluminum plate were measured using the methods described in the following experimental procedure. Using the travel times, the following measurements were made; the direction of strike of the aluminum plate, the apparent dip angle of the aluminum plate, the true dip angle of the plate and the depth to the plate.

Equations used for the calculation of the above quantities are listed below.

<u>For the direction of strike</u>:

$$\phi = \tan^{-1} \left| \frac{t_{x2} - t'_{x2}}{t_{y2} - t'_{y2}} \right| \qquad (3.5)$$

where

ϕ = the direction of strike with respect to an arbitary X axis

t_{x2}, t'_{x2} = the travel times of reflected wave with

the transmitting probe at T, and the receiving probe at X_2 and X_2' on the X axis (see Fig. 35)

t_{y2}, $t_{y'2}$ = the travel times of reflected wave with the transmitting probe at T, and the receiving probe at Y_2 and Y_2' on the Y axis (see Fig. 35)

For the apparent dip, θ_p,

$$\theta_p = \sin^{-1} \frac{V}{2L} \left[(t_{x2} - t_{x'2})^2 + (t_{y2} - t_{y'2})^2 \right]^{1/2} \qquad (3.6)$$

where

V = the velocity of ultrasonic p-wave in water

L = the distance from the transmitting probe at T to the extreme receiving probe at X_2, X_2', Y_2, and Y_2' (see Fig. 35)

For the true dip, θ_t,

$$\theta_t = \tan^{-1} \frac{\tan \theta_p}{\sin(90^b - \phi)} \qquad (3.7)$$

For the vertical depth, D, of the plate below the transmitting probe(21)

$$D = 1/2 \left\{ V^2 \left[\frac{\Delta L (t_{y1}^2 - t_{y2}^2)}{L - \Delta L} + t_{y1}^2 \right] + L x \Delta L \right\}^{1/2} \qquad (3.8)$$

where

L = the distance from the transmitting probe at T to the receiving probe near the transmitting probe at X_1, X_1', Y_1, Y_1' (see Fig. 35)

(b) Experimental Procedures

The wooden tank, used in the experiment and shown in Fig.34, had dimension of 4 ft. x 4 ft. x 1 ft. (deep). The tank was filled with water and fitted with an inch scale on the top for conveniently locating the probes.

For conducting velocity measurement by the $T^2 - X^2$ method, the bottom surface of the water tank was made horizontal, The transmitting probe was then fixed at the center of the water surface and the travel times of reflected wave from the bottom of the tank were taken when the receiving probe was moved from point to point along a row with a fixed increament in distance. By plotting the squares of the travel times against the squares of the displacement, the velocity of ultrasonic p-wave in water can be found from the slope of the straight line.

A thin aluminum plate of dimension 2.5 ft. x 1.5 ft. was then placed at the bottom of the tank so that it had a strike direction of 18° with respect to one wall of the water tank, say X axis, and a dip angle of 12°. The transmitting probe was then placed at the water surface near the center of the plate at T (Fig.35). The receiving probe was placed at the same water level as the transmitting probe along two lines at right angles to each other. The point of intersection of the two orthogonal lines is the point, T, as shown in Fig. 35. The distance between the transmitting probe and the positions of the receiving probe at X_1, X_1', Y_1, and Y_1' is ΔL and the distance between the transmitting and the receiving probe at X_2, X_2', Y_2

Fig. 34. A wooden tank containing water and a thin aluminum plate for model studies.

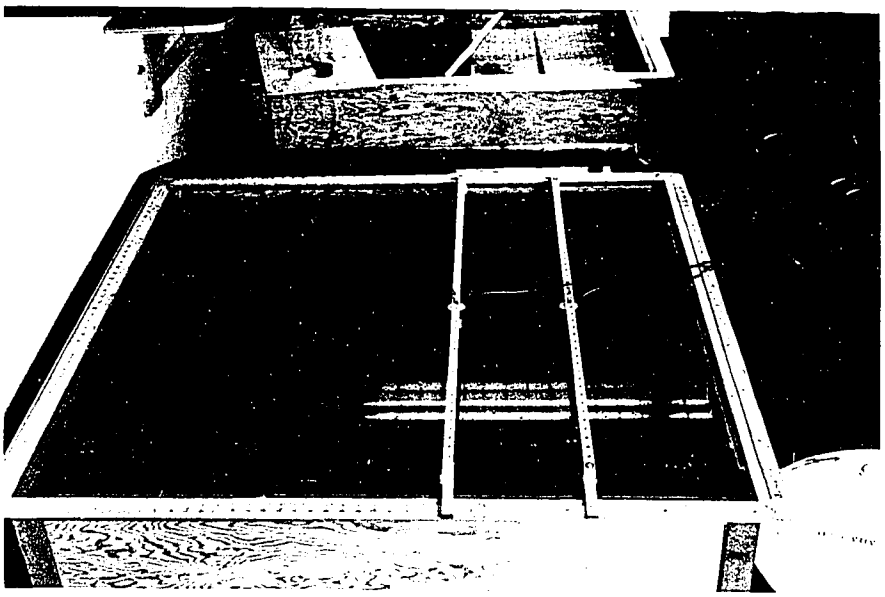

Fig. 34. A wooden tank containing water and a thin aluminum plate for model studies.

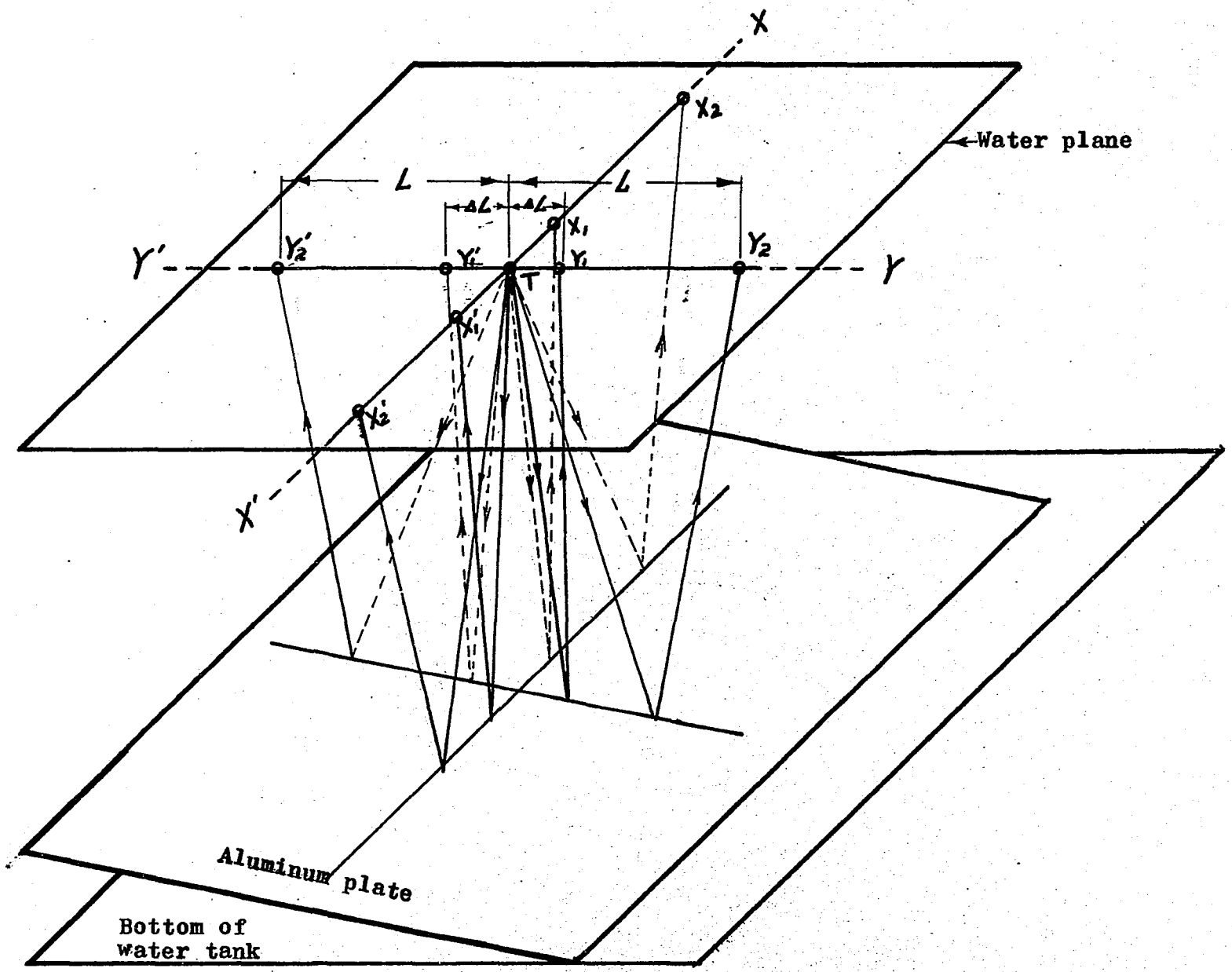

Fig. 35. Cross spread layout for determining the strike and the dip angle.

and Y_2' is L. The ratio of ΔL to L is 1/4.

By placing the transmitting probe at T and the receiving probe at Y_1, Y_2, Y_1', Y_2', X_1, X_2, X_1' and X_2' respectively, a series of readings for the travel times of the first reflected wave was obtained. Substituting the travel times for each point into the equations given above, the various quantities were calculated.

(c) Experimental Results

The velocity of ultrasonic waves in water determined by the $T^2 - X^2$ method gives an average value of 1594 m/sec compared to the accepted value of 1490 m/sec. The vertical depth, Z, to the bottom of the tank from the transmitting probe is calculated to be 23.8 cm whereas the actual measured value is 23.5 cm.

The squares of the travel times vs. the squares of the displacement were plotted in Fig. 36, and the detailed data are shown in Table 3.

The true travel times of reflected wave from the aluminum plate when the transmitting probe is at T and the receiving probe is at points Y_1, Y_2, Y_1', Y_2', X_1, X_2, X_1' and X_2' (see Fig. 35) were measured as follow;

t_{y1} = 250.5 μsec t_{y2} = 294.0 μsec

$t_{y'1}$ = 237.0 μsec $t_{y'2}$ = 231.0 μsec

t_{x1} = 241.5 μsec t_{x2} = 260.0 μsec

$t_{x'1}$ = 245.5 μsec $t_{x'2}$ = 275.5 μsec

L = 20.32 cm ΔL = 5.08 cm

Fig. 36. Determination of average velocity by $X^2 - T^2$ method.

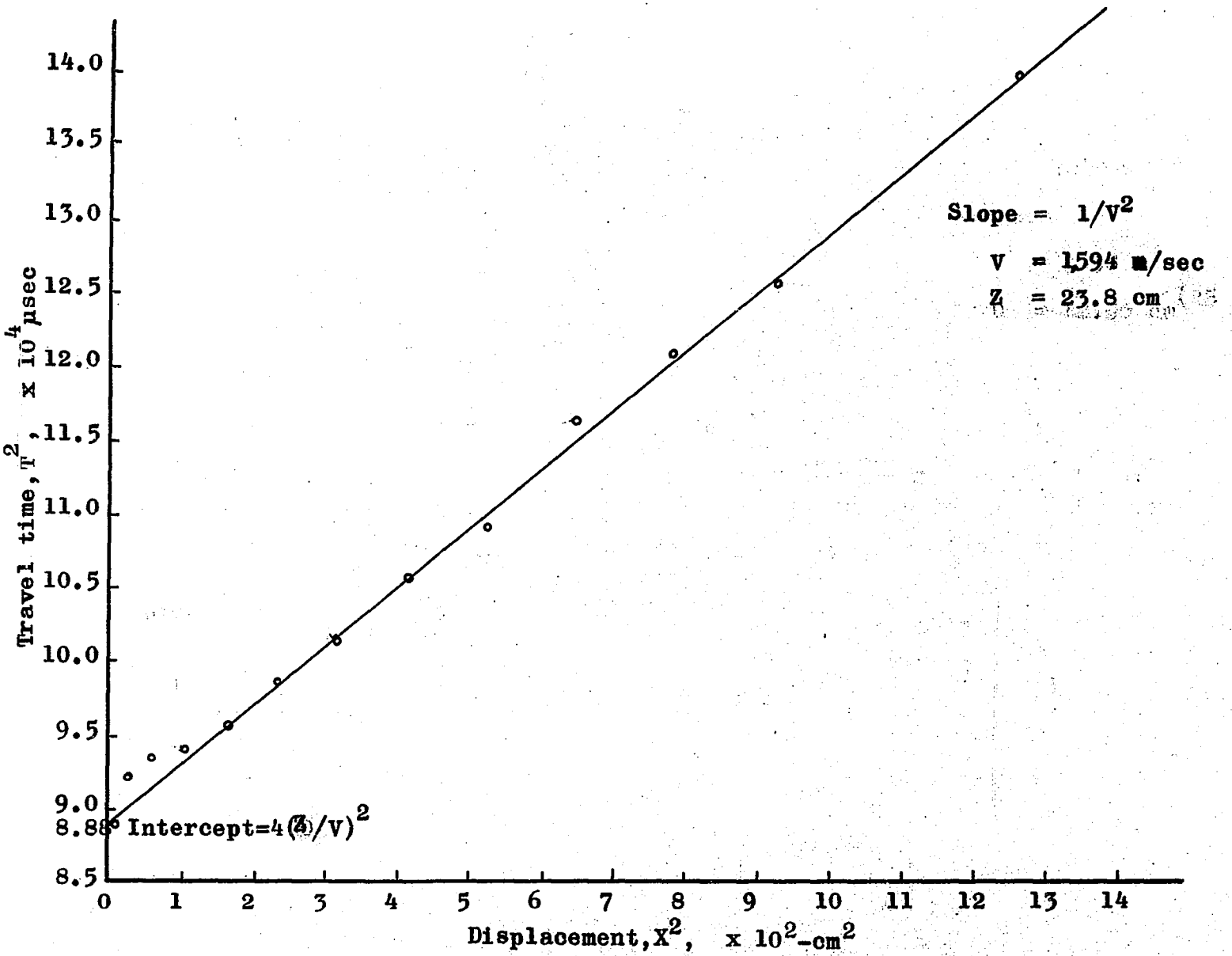

TABLE 3

Transmitter-receiver Displacements vs. Travel Times.

Location of receiver	1	2	3	4	5	6	7	8	9	10	11	12	13
Displacement, X_r (cm)	5.08	7.62	10.16	12.70	15.24	17.78	20.32	22.86	25.40	27.94	30.48	--	35.56
X^2 (cm^2)	25.8	58.1	103.2	161.3	232.3	316.1	412.9	522.6	645.2	780.0	929.0	---	1264.5
Travel time, T, x50μsec	6.13	6.17	6.19	6.24	6.34	6.43	6.57	6.67	6.88	7.00	7.14	--	7.52
$T_{corre.}$ x50μsec	6.07	6.11	6.13	6.18	6.28	6.37	6.51	6.61	6.82	6.94	7.08	--	7.46
$T^2_{corre.}$ x10^4 μsec^2	9.21	9.33	9.39	9.55	9.86	10.14	10.59	10.92	11.63	12.04	12.53	--	13.91

Using the above data the various parameters of the inclined aluminum plate calculated fron the equation(3.5 - 3.8) are as follows.

from equation (3.5), the direction of strike with respect to X axis is $16^{o}20'$ (18^{o}actual)

from equation (3.6), taking the measured value of velocity V = 1594 m/sec the apparent dip angle, θ_p, is $13^{o}20$ ($11^{o}30'$ actual)

from equation (3.7), the true dip angle, θ_t, is 14^{o} ($12^{o}10'$ actual)

from equation (3.8), the vertical depth, D, of the aluminum plate from the transmitting point, T, is 19.9 cm (18.3 cm actual).

3.5 Measurement of Fractures in Rocks

(a) General

To find a suitable frequency range of the ultrasonic waves for detecting fractures in rocks, two series of waves with frequencies 60 kc/sec and 450 kc/sec were transmitted into the diorite block. The block had dimensions 2.5 ft x 2.5 ft. x 3.5 ft. and had a plane fracture about 0.001 in. thick (measured at the rock face) parallel to one of its flat faces. By transmitting ultrasonic waves of frequency 450 kc/sec, A reflected wave was received, but no evidence of reflection for waves of frequency 60 kc/sec was obtained.

A measurement was also made to find the detectability of ultrasonic waves of frequency 450 kc/sec for detecting

fractures in rocks. It was observed that with ultrasonic waves of 450 kc/sec it was possible to detect very small fractures, the thickness of which could not be measured by the thickness gauge.

A grinder, made by fixing a grinding disc on the portable drill as shown in Fig. 37, was used to polish rock faces for measurement. The grinding sand disc of diameter $2^3/4$ in. and thickness 5/8 in. was cemented on a round steel plate with cement. A steel bar was soldered on the back of the steel plate for attachment to the drill head. This grinder was suitable for polishing rock faces smooth enough for our measurements.

(b) Experimental Procedures

Fig. 38 shows the entire set-up of the ultrasonic equipment used for measuring fracture planes on a diorite block outside the laboratory.

The rock faces were polished by using the portable grinder. A thin layer of vaseline was coated on the rock faces before the transmitting and the receiving probes were placed for measurements.

(c) Experimental Results

A fracture in a diorite block (Fig.39) was detected by the ultrasonic equipment which transmitted ultrasonic waves of frequency 450 kc/sec. The receiver and transmitter were spaced side by side on the top surface. The large pulses reflected from the fracture (Fig. 40) were observed to have

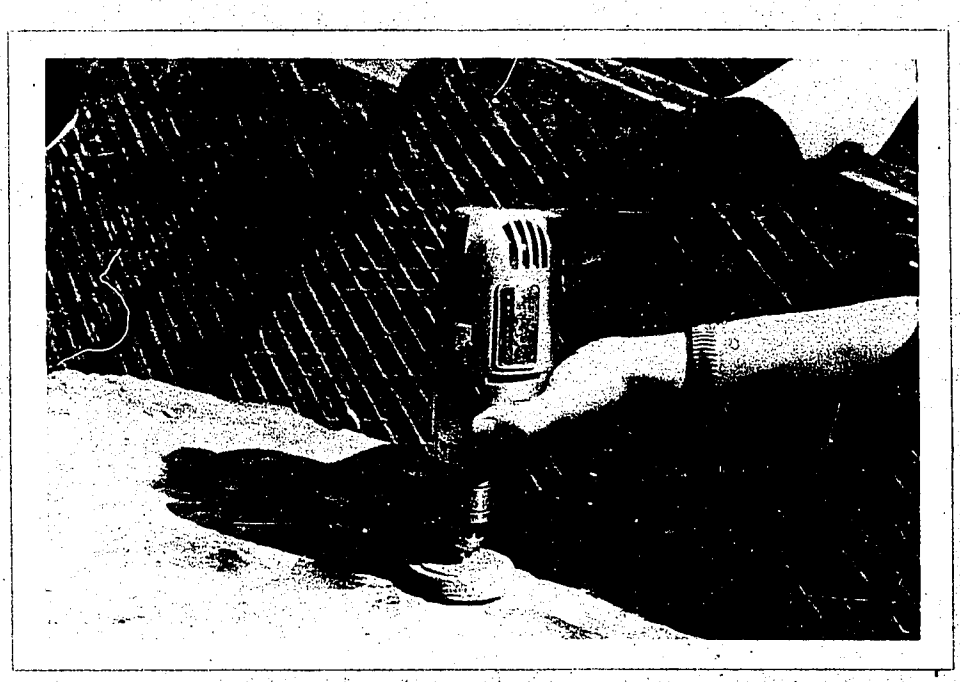

Fig. 37. Portable grinder used for polishing rock faces.

Fig. 38. Ultrasonic equipment and the diorite block.

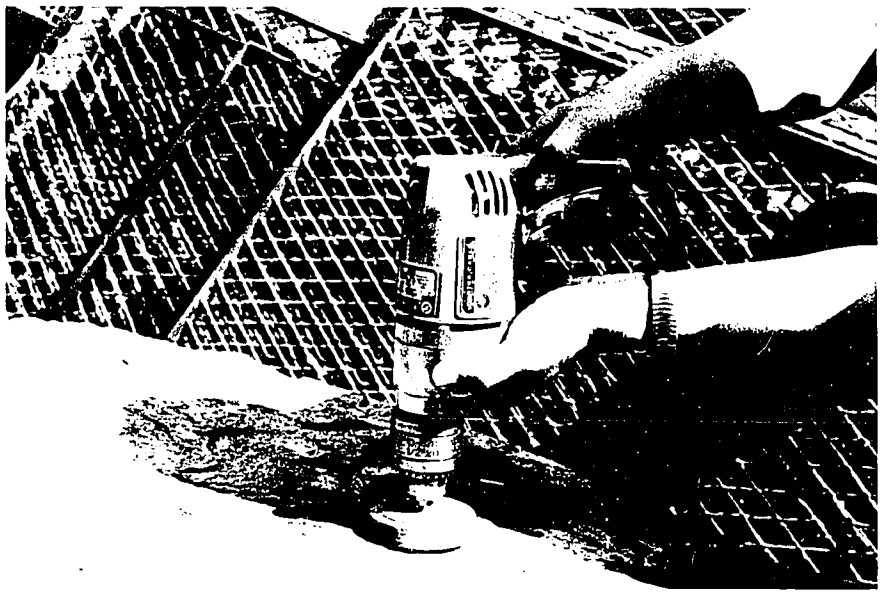

Fig. 37. Portable grinder used for polishing rock faces.

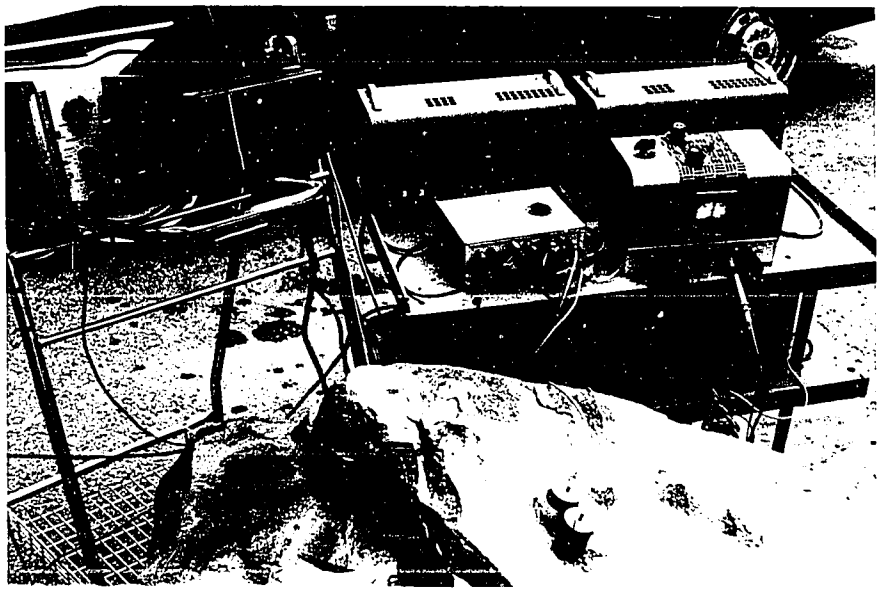

Fig. 38. Ultrasonic equipment and the diorite block.

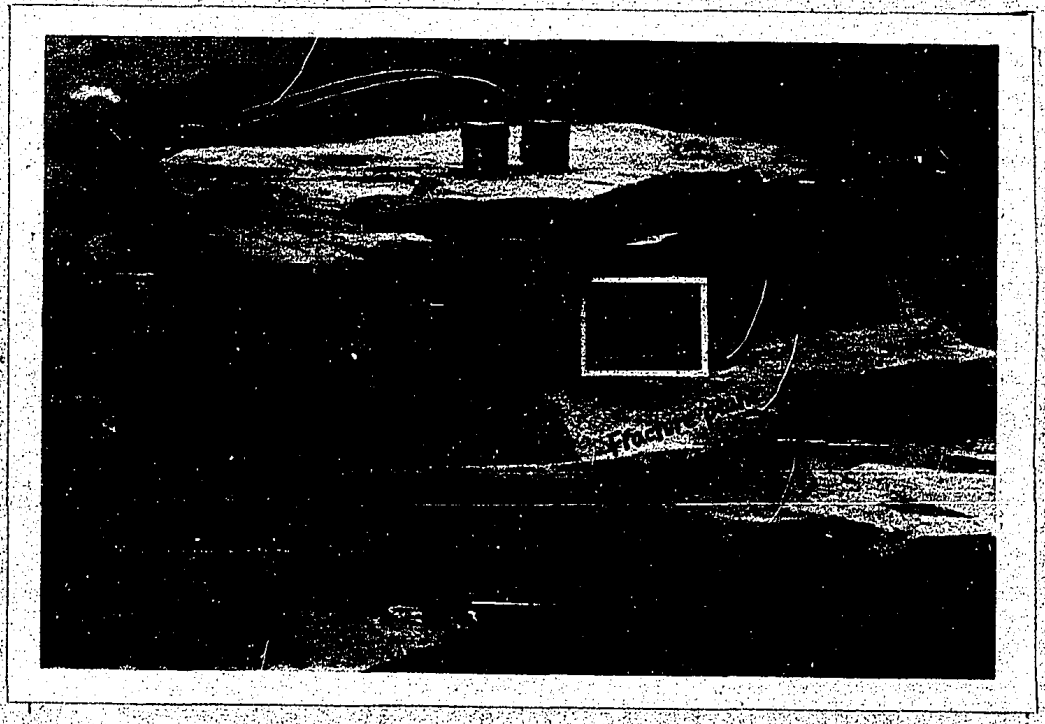

Fig. 39. Fracture plane in the diorite block.

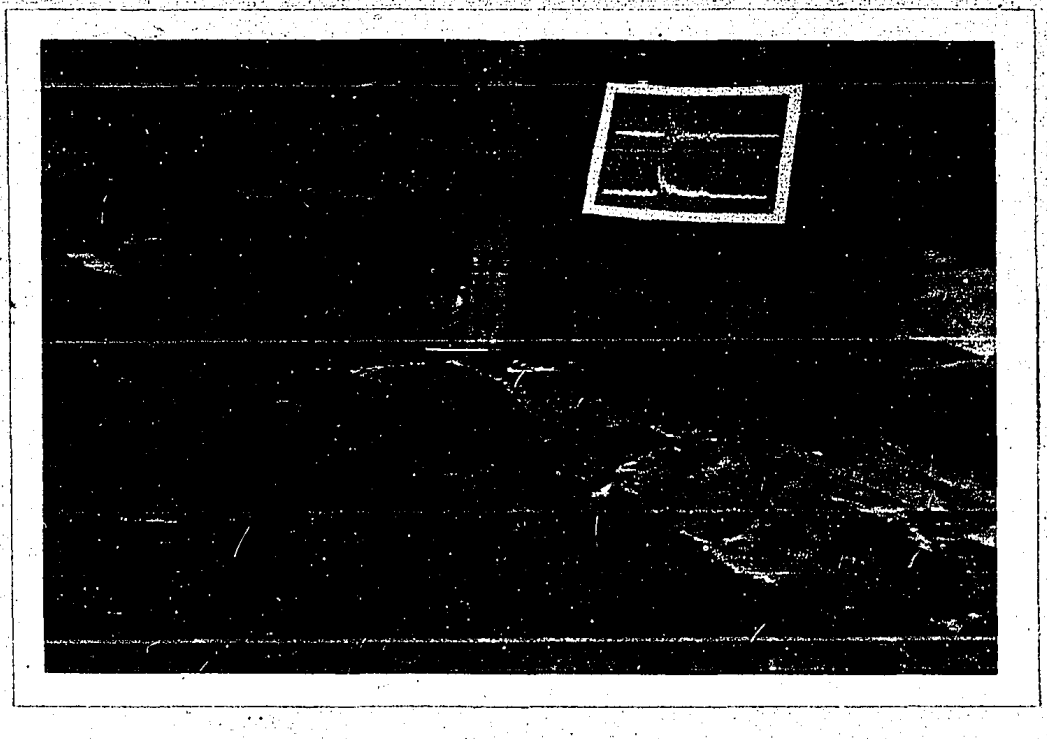

Fig. 40. Side view of the fracture plane.

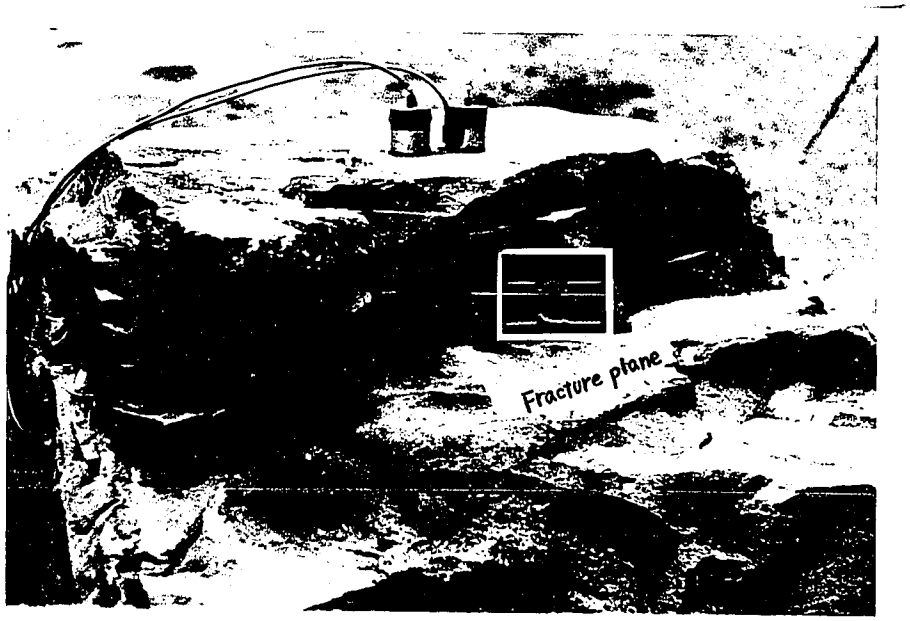

Fig. 39. Fracture plane in the diorite block.

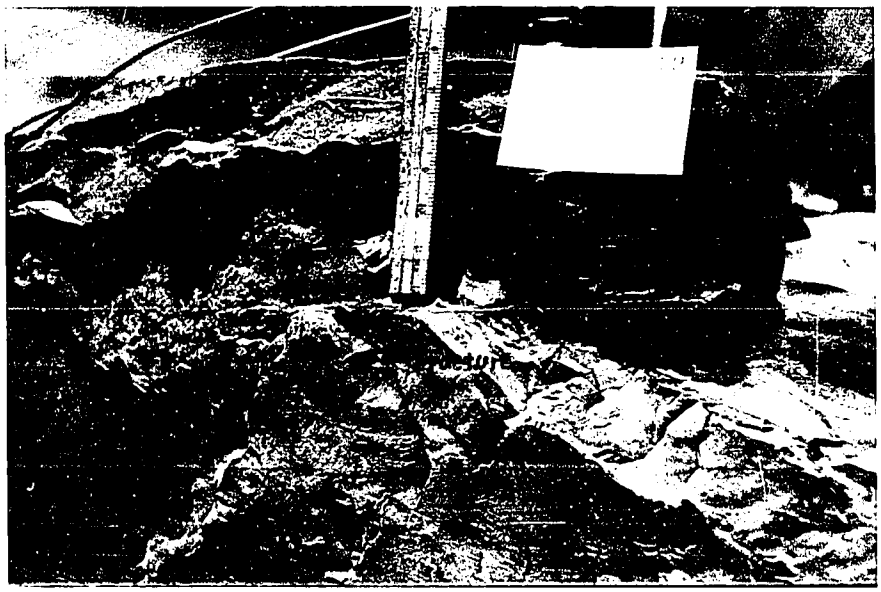

Fig. 40. Side view of the fracture plane.

a travel time of 60.2 μsec, as shown in Fig. 41. From the travel time of the reflected pulses, the depth to the fracture from the face was estimated to be 17.2 cm. (taking the measured velocity of ultrasonic p-wave in the rock 6020 m/sec). The actual measured value of the depth to the fracture is approx. 17 cm. When ultrasonic waves of the frequency of 60 kc/sec were transmitted into the same rock, no reflected pulses from the fracture were observed, but there were reflected pulses from the bottom of the rock with a travel time of 315 μsec, as shown in Fig. 42. From the travel time of the reflected waves the depth to the bottom of the rock is estimated to be 95 cm. The actual value of the depth to the bottom could not be measured accurately since the bottom of the rock is not very flat, but a rough measurement gave a depth of 85 cm.

Fig. 43 shows the measurement when the 450 kc transmitting and receiving probes were placed 4.5 in. apart on the top face of the diorite block. The surface and reflected waves from the fracture were clearly observed, as shown in Fig, 44. As the probes were moved closer together on opposite sides of a vertical crack having an air gap about 0.003 in. thick (measured from the rock surface) and extending to the fracture plane, as shown in Fig. 45, the amplitude of the surface and reflected waves were found to decrease significantly (Fig. 46).

The above measurement was also made using the 60 kc probes. The same phenomenon of decrease in the amplitude of the surface wave was also observed.

Fig. 47 shows the measurement on another diorite block

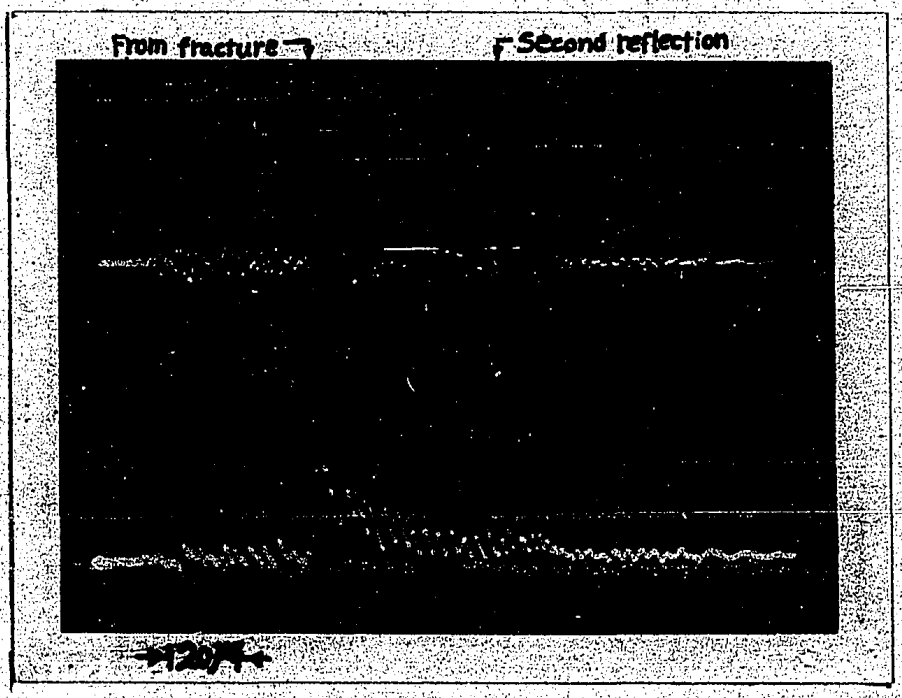

Fig. 41. Reflected waves from the fracture plane in the diorite block.

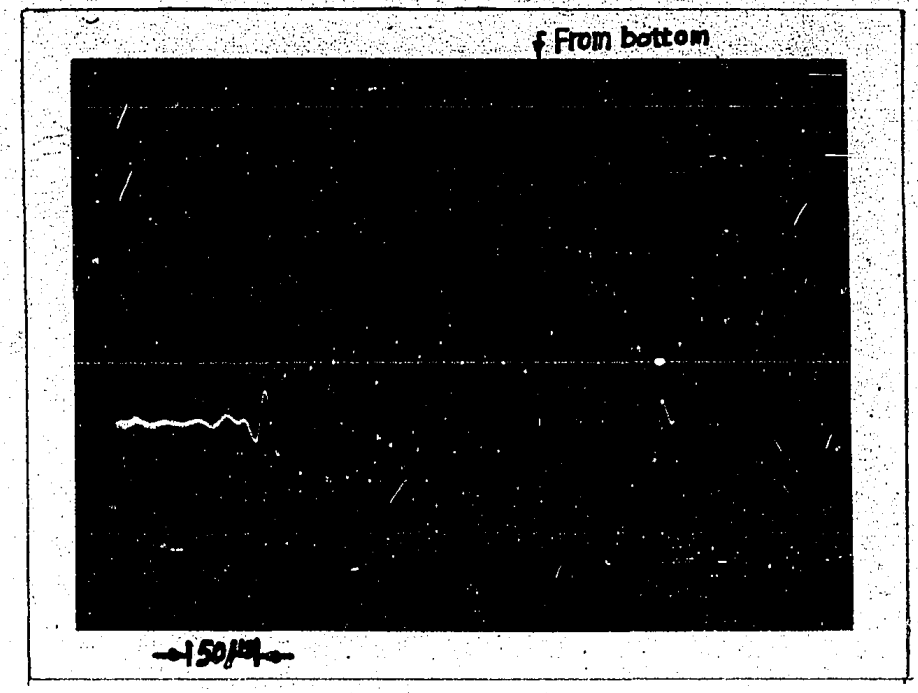

Fig. 42. Reflected waves from the bottom of the diorite block.

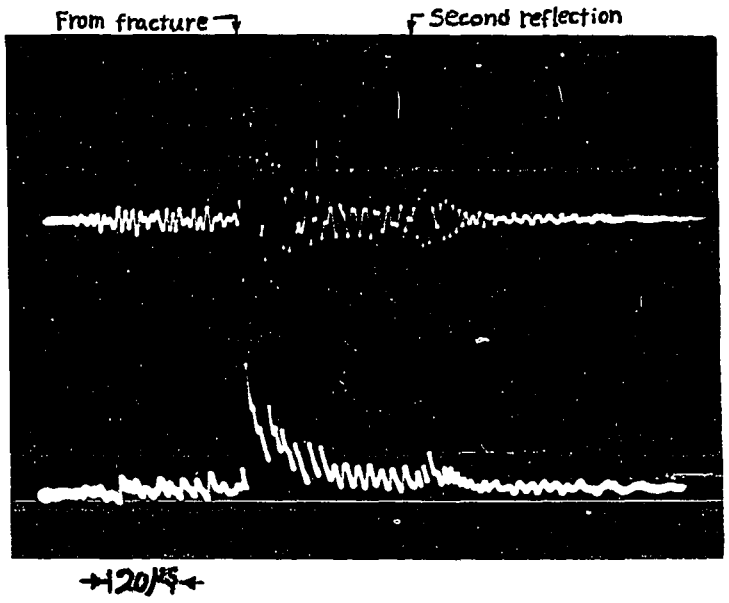

Fig. 41. Reflected waves from the fracture plane in the diorite block.

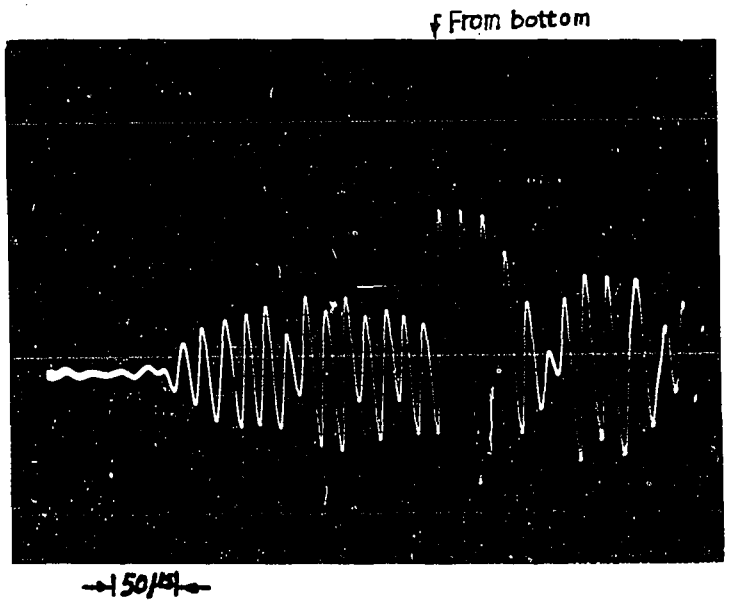

Fig. 42. Reflected waves from the bottom of the diorite block.

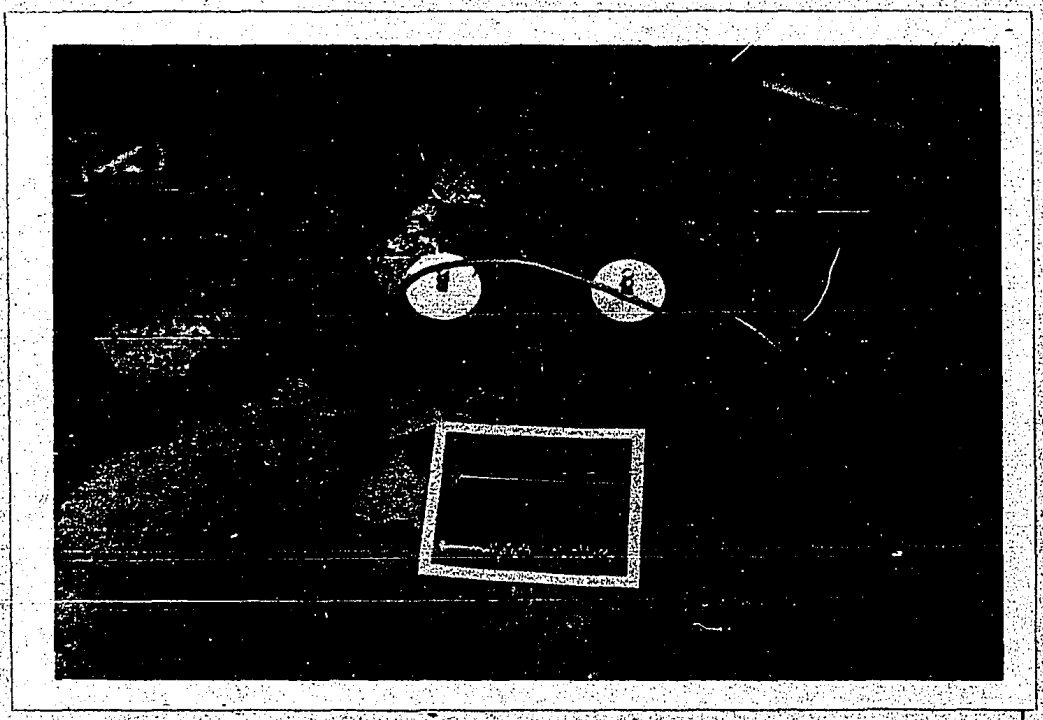

Fig. 43. 450 kc probes on the rock face.

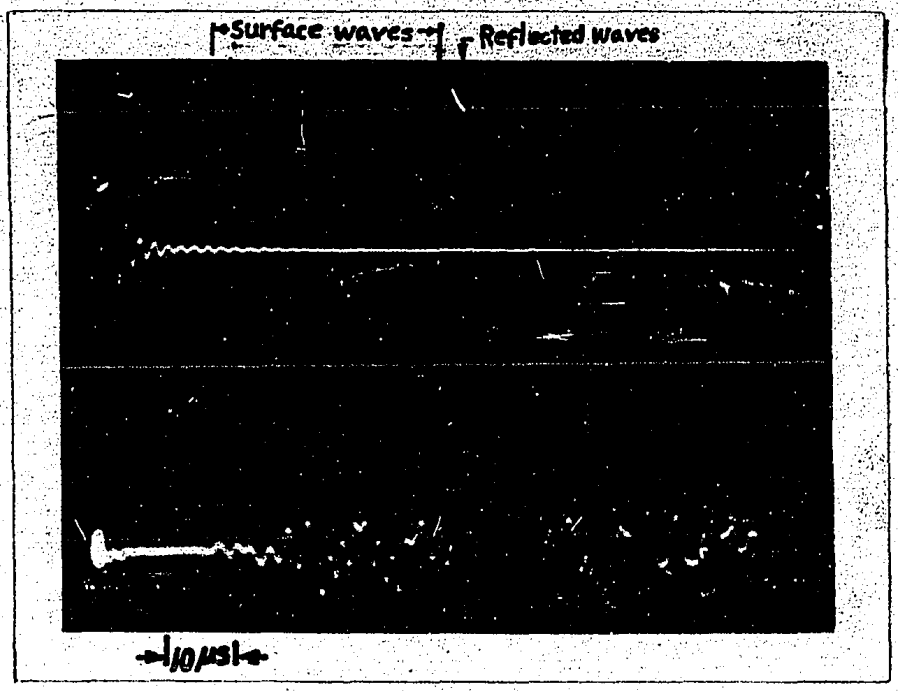

Fig. 44. Surface and reflected waves from the rock face and the fracture plane using 450 kc probes.

Fig. 43. 450 kc probes on the rock face.

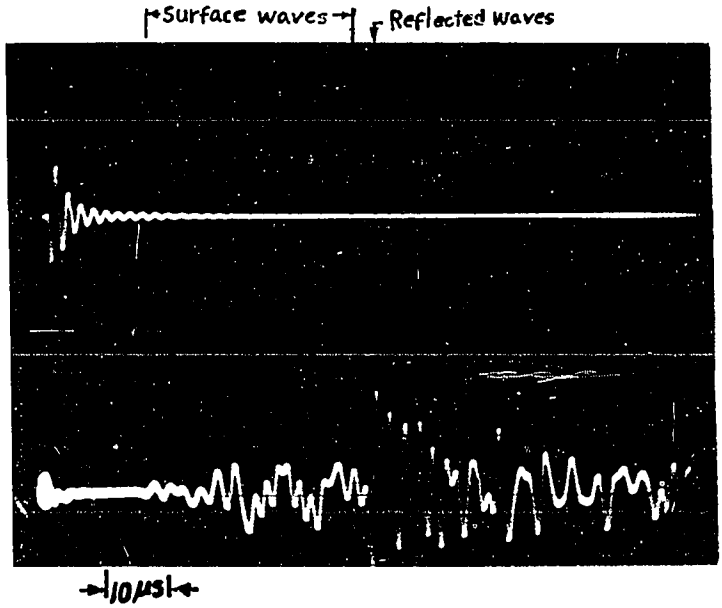

Fig. 44. Surface and reflected waves from the rock face and the fracture plane using 450 kc probes.

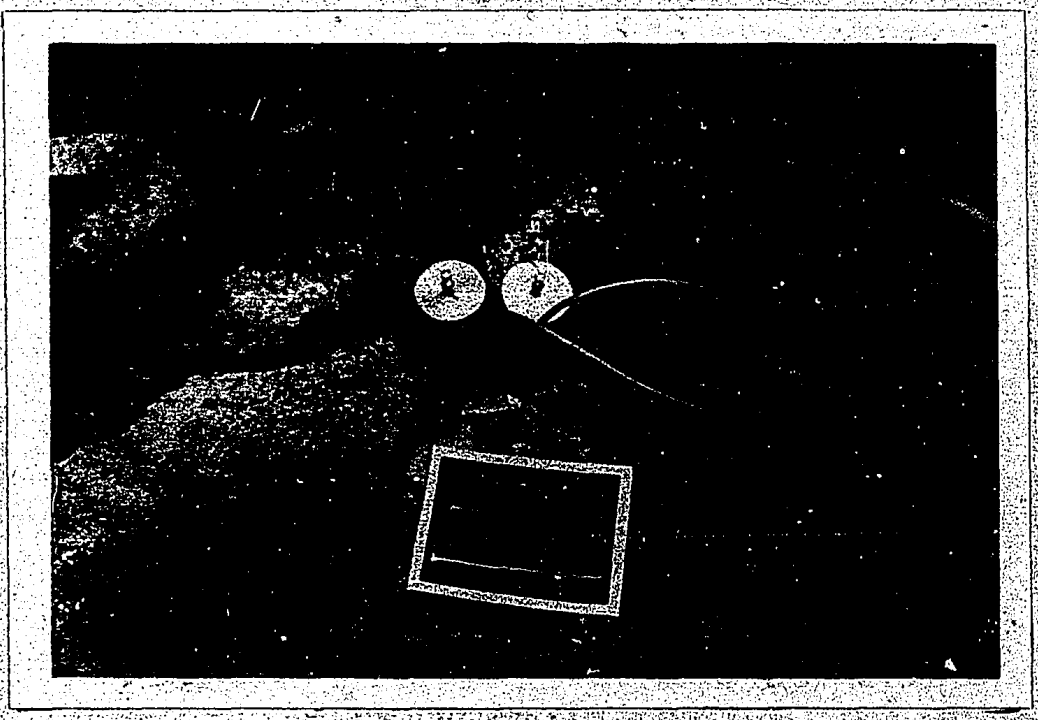

Fig. 45. A vertical crack between the two probes.

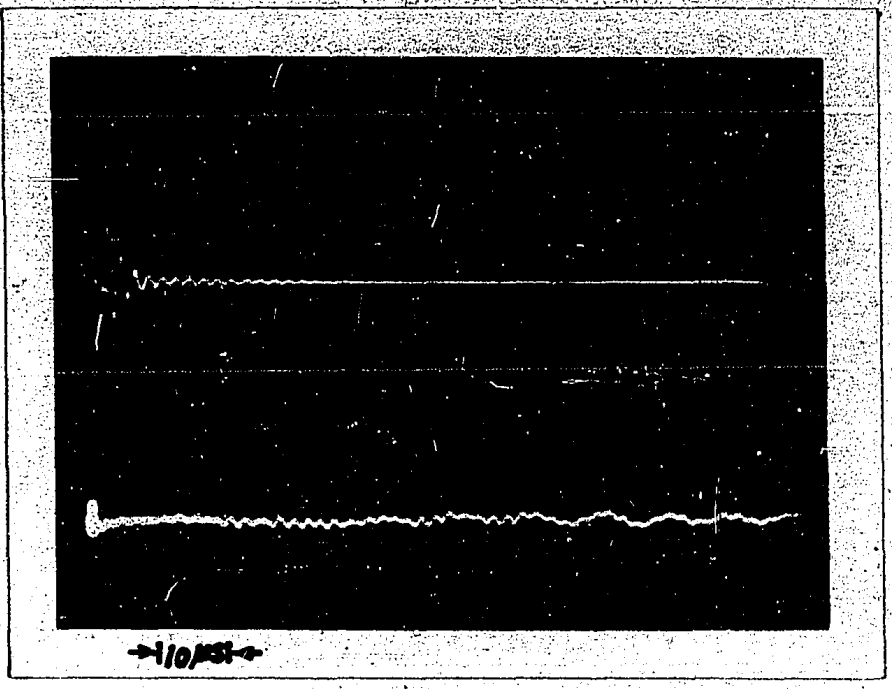

Fig. 46. Decrease in amplitude of waves with probes placed on the opposite sides of the crack.

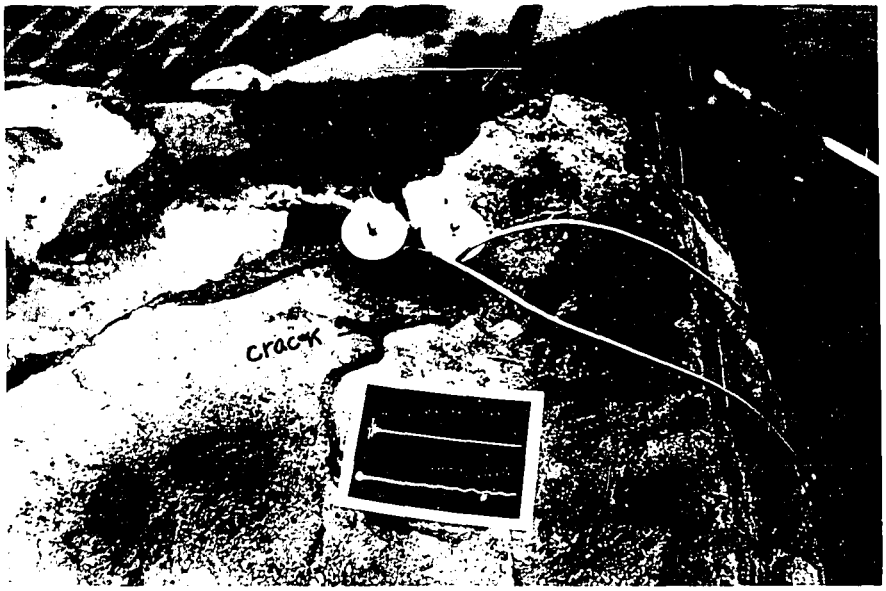

Fig. 45. A vertical crack between the two probes.

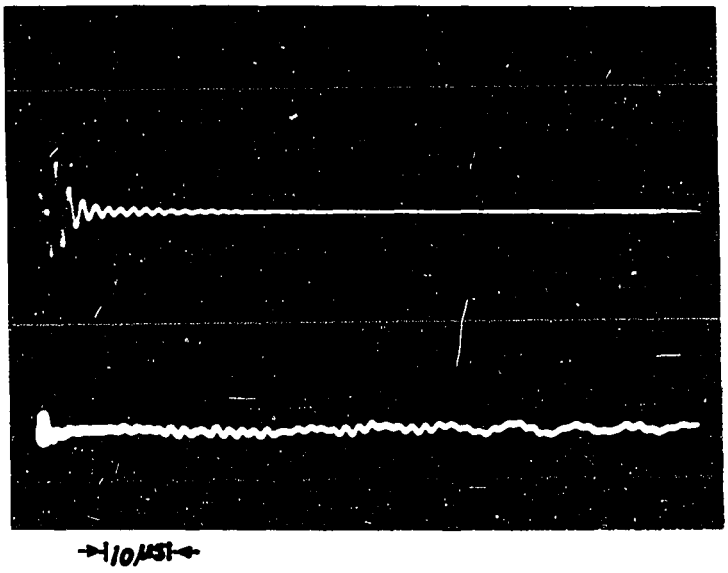

Fig. 46. Decrease in amplitude of waves with probes placed on the opposite sides of the crack.

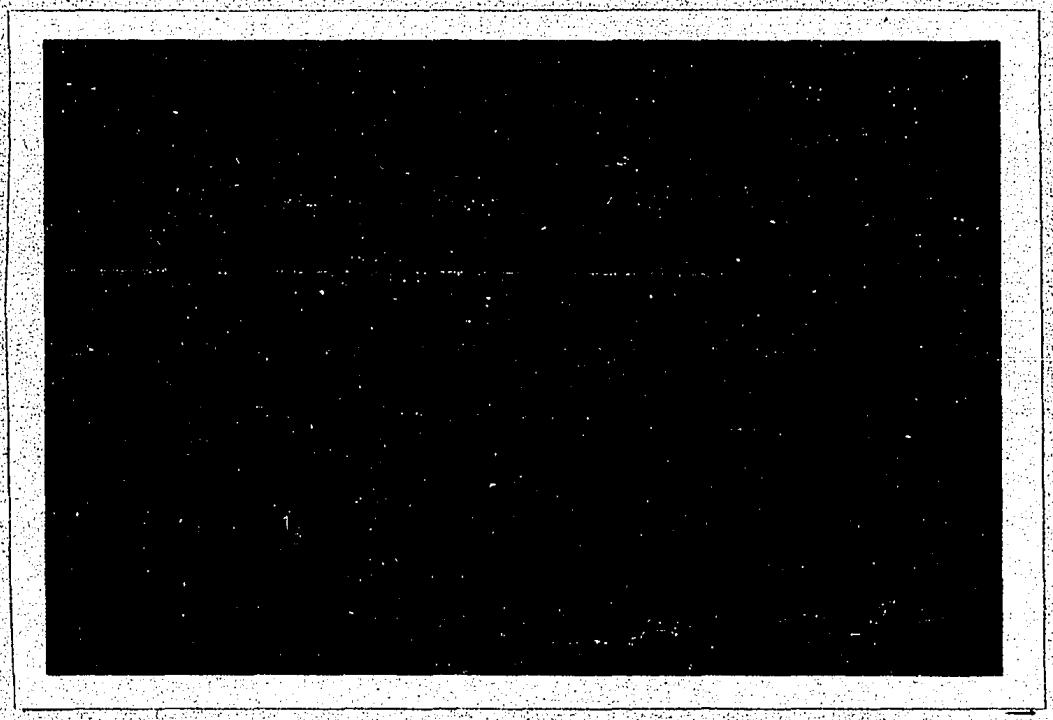

Fig. 47. Measurements of narrow cracks in the diorite block.

Fig. 47. Measurements of narrow cracks in the diorite block.

which has three parallel fractures. The three fractures are so narrow that they could not be measured by the thickness gauge. The transmitting and the receiving probes were placed on one face which is parallel to the three fractures and ultrasonic waves of frequency 450 kc/sec were transmitted through it. For the first position of the two probes, reflected waves from the fractures nearest and farthest from the rock face only were observed as shown in Fig. 48. When both probes were moved about 4 in. to one side, reflected waves from the fractures nearest and the middle were received (Fig. 49). With this arrangement the amplitude of the wave reflected from the middle fracture was so large that reflected waves from the farthest fracture could not be properly distinguished.

Fig. 48. Reflected waves from the nearest and the farthest fractures for the first position of the probes in the diorite.

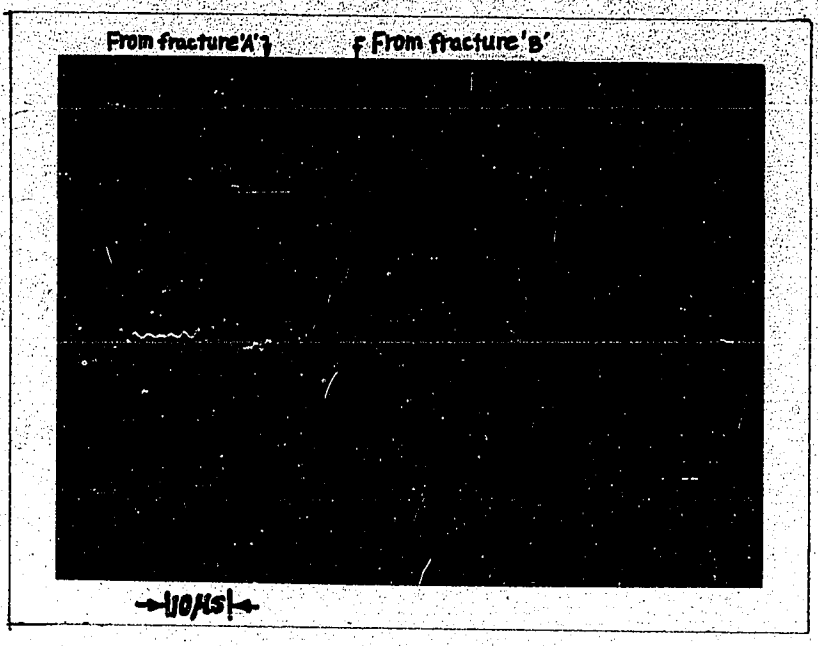

Fig. 49. Reflected waves from the nearest and the middle fractures for the second position of the probes in the diorite.

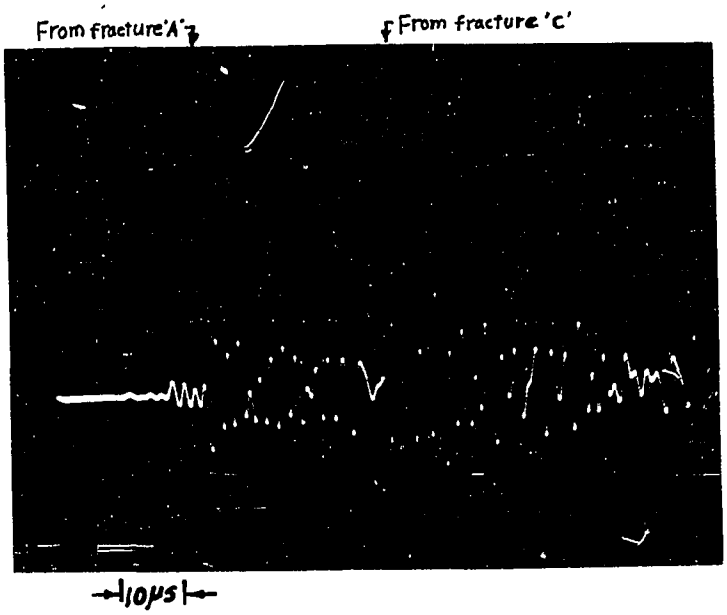

Fig. 48. Reflected waves from the nearest and the farthest fractures for the first position of the probes in the diorite.

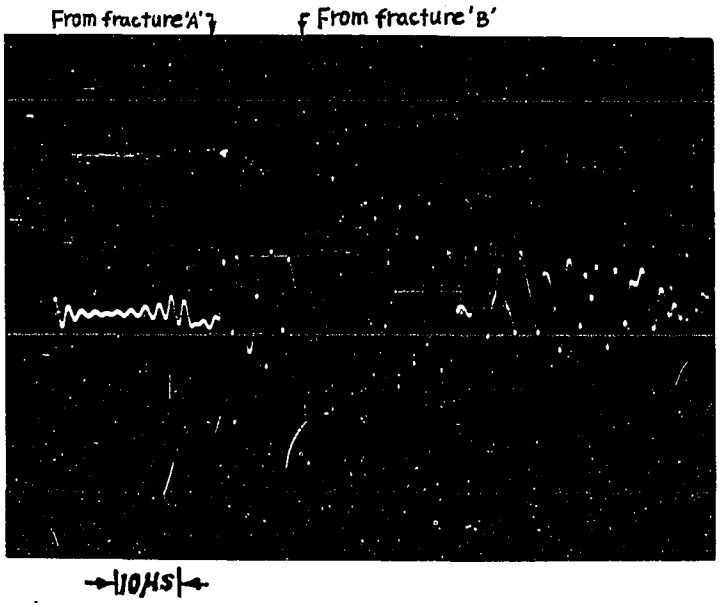

Fig. 49. Reflected waves from the nearest and the middle fractures for the second position of the probes in the diorite.

CHAPTER IV

DISCUSSION OF EXPERIMENTAL RESULTS

4.1 Velocity Measurement

It can be seen from Table 2, that using this equipment, the measured values of the velocities in different specimens when compared with those given by other authors agree well in most cases. Some discrepencies in the results are believed to be mainly due to the different properties of the specimens tested and possibly to a minor extent due to some unavoidable systematic errors in the instruments.

All velocity measurements were made using ultrasonic waves of frequency 450 kc/sec. Since the velocity of sound waves in solid is constant over a frequency range from 500 cps to 5000 kcps (1), the measured values can also be regarded as the seismic p-wave velocities in the specimens tested.

The velocities in five specimens of Trenton limestone were measured using the equipment. As shown in Fig.23, four of the five specimens, with an average velocity of 6642 m/sec, have their velocities very close to each other, but the velocity in the fifth specimen was found to have a significantly lower value of 6350 m/sec. This specimen was observed to have a quartzite dike in the core as shown in Fig. 50. The decrease in the velocity in the specimen might be attributed to the lower velocity of the quartzite dike in this specimen ($V_q \simeq$ 5000 m/sec). It, therefore, follows that the measurement of

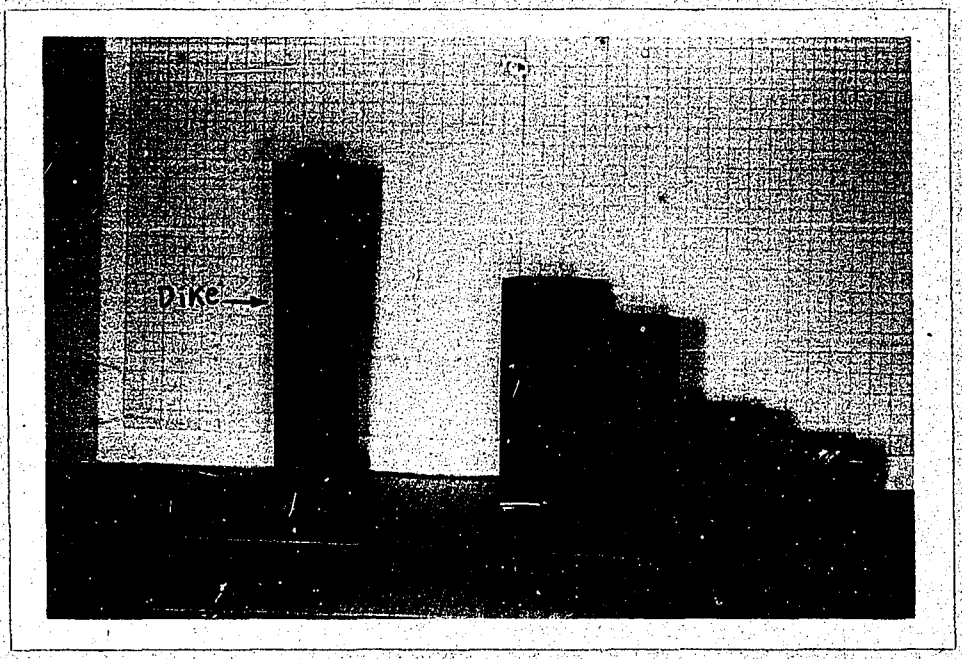

Fig. 50. Specimens of Trenton limestone showing A quartzite dike in the longest one.

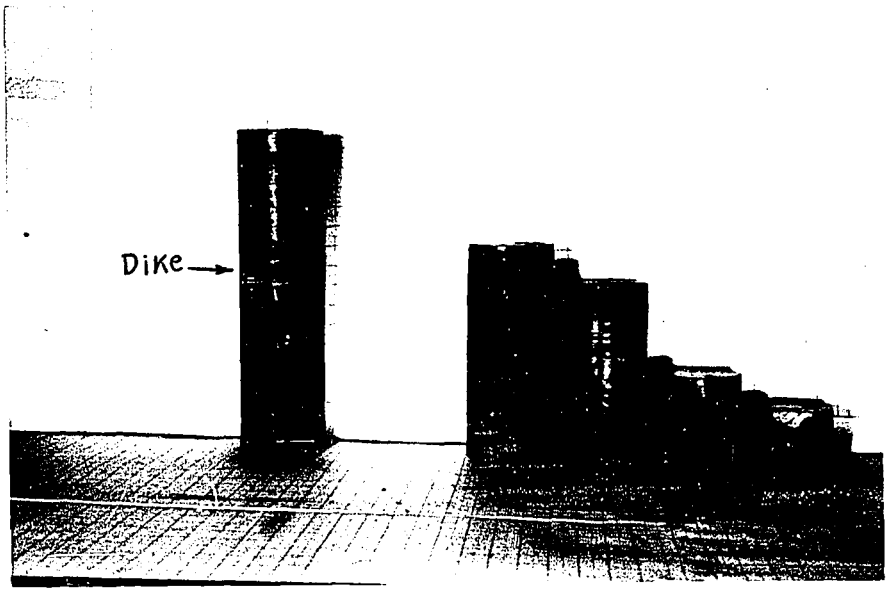

Fig. 50. Specimens of Trenton limestone showing A quartzite dike in the longest one.

ultrasonic p-wave velocity can be used to predict the presence of discontinuities in the specimen or can give a measure of the relative purity in the tested samples.

It was previously stated that in measuring the ultrasonic p-wave velocity in a specimen, the total delay time of 3 μsec (due to the transition layers in the probe and some time delay caused by the electronic instruments) should be substracted from the apparent travel time to give the true time for calculating the velocity in the specimen. The total delay time, however, is not a constant at all time, and it changes with the triggering level in the oscilloscope. In order to obtain reliable results, at least two specimens of the same material are required. From the time-distance graph for these specimens, a straight line is drawn; the straight line gives the reciprocal of the average velocity in the medium.

4.2 Measurement of Attenuation Constant

The measured values of the attenuation constants of epoxy resin, motar, Trenton limestone and paraffin were found to be 0.025 néper/cm, 0.09 néper/cm, 0.107 néper/cm and 0.19 néper/cm respectively. Although the measured values could not be compared with those given by other authors, they appear to be reasonable. For example the attenuation in paraffin should be much higher than that of epoxy resin, because of the high absorption of sound energy in paraffin while epoxy resin has an excellent elasticity.

Because of uncertain coupling effects within the probes and specimens, the measured values of the attenuation constant give only a general idea about the attenuation of seismic waves in the different materials.

4.3. Measurement of Fractures in Solids

In the estimation of depths to the fractures from the rock surface, the measured values were systematically higher than the actual values. The main reasons for this discrepency may be due to following reasons.

1) The estimated values are based on the simplifying assumption that the wave transmitted from the transmitting probe retraces the same path after being reflected from the discontinuity. Since the diameter of the two probes used in the experiment are 1.4 in., the paths of the transmitted and the reflected waves, in fact, is a conical one.

2) The wave reflected from fracture and observed on the oscilloscope gives the resultant effect of many waves. From the observed reflected wave, therefore, it can not be said which of the waves was reflected from a specified point on the fracture plane.

3) Other possible sources of error are the values of the ultrasonic p-wave velocity in various samples, the accuracy of the sweep rate of the oscilloscope, and the parallex error.

It can be seen in Fig.31that, in addition to the three large pulses reflected from the drill hole, the plane

fracture and the bottom of the specimen of epoxy resin, there are some small pulses between the transmitting pulse at the extreme left and the reflected pulse. Since the epoxy resin specimen was prepared layer by layer, these small pulses are believed to be the reflections from the interfaces between two consecutive layers. Due to incomplete binding between the upper and the lower layer, there is a difference in the acoustic impedances on the interface between two consecutive layers, so that waves may be reflected back from these interfaces. These small reflected waves were not observed in the specimen of paraffin shown in Fig. 33. This may be due to the fact that this specimen of paraffin, unlike the previous one, was molded at one time so that there is no layering.

4.4 Determination of Geometry of Fracture Planes

After initial difficulties in using paraffin and epoxy resin the subsequent experiments with water was found to give satisfactory results.

The experimental results show that the various measured values of the p-wave velocity in water, and of the immersed aluminum plate such as the strike direction, the apparent dip angle, the true dip angle and the vertical depth are fairly close to the actual values. It is believed that more accurate results could be obtained if a bigger tank was available. Since the faces of the two probes used are relatively large, very accurate results for the travel time of the reflected waves are not possible

If the probes were made smaller better results might be predicted.

It is often found that large fractures in rocks have plane surfaces. It may be possible that the geometry of the fracture plane can be determined by using this seismic technique. The rock surfaces, however, are rarely very flat. This is likely to lead to some difficulties in the actual measurements.

4.5 Measurement of Fractures in Rocks

It is seen from Fig.41, that the first reflected wave from the fracture plane in the diorite specimen has a travel time of 60.2 μsec. The second reflected wave from the same fracture plane has a travel time of 117.4 μsec. The first and second reflected waves each have a delay time of 3 μsec (as mentioned previously). Substracting the delay time from the observed travel times, the corrected travel times for the two groups of reflected waves are 57.2 μsec and 114.4 μsec, respectively. It is known that the second reflected wave with a travel time twice that of the first is due to double reflection from the fracture. Some care is, therefore, necessary in interpreting the reflected wave since, multiple reflections, as illustrated above, can easily mislead us into thinking that those are reflections from some deeper fractures.

This was also verified by observing the travel times of two successive reflections from the bottom of a water tank. The experiment was designed so that the travel time of the first reflected wave was at about 60.2 μsec. It was observed

that the second reflected waveshad a travel time of 117.4 μsec, just as obtained from the measurement on the diorite.

In the diorite block, at a depth about 5 cm from the rock face there is a thin quartzite dike(shown in Fig.39) of thickness approx. 0.01 in.. The dike plane is parallel to the fracture plane and no fissures are visible on the dike. However a reflected wave of low amplitude was observed from the dike with a travel time of 22 μsec(Fig. 41). It is believed that the reflected wave is due to the difference in the acoustic impedances between the country rock, diorite, and the quartzite dike. The low amplitude of the reflected wave can be attributed to rather small difference in the acoustic impedances between diorite and quartz.

In the diorite block, some minor fractures are visible below the fracture plane. Reflected waves were not observed from all these fractures. The absence of reflected waves may be due to the fact that most waves were reflected back from the fracture plane and little energy remained to reach any other fractures. This was later verified by measurement on a second block of diorite,having three parallel fractures so narrow that they could not be measured by the thickness gauge and were barely visible.(Fig. 47).

For the first position (see Fig. 47) of the two probes, reflected waves were observed as shown in Fig. 48. The reflected waves (marked A and C in Fig. 48) were due to reflections from the nearest (fracture A) and the farthest (fracture C) fractures.

Reflection from the middle fracture (fracture B) could not be observed because it is believed that for this position of the two probes the middle fracture was so small that all waves were transmitted through it to the third fracture. For the second position (see Fig. 47) of the two probes, reflected waves were observed from the nearest and the middle fractures, while no reflections were observed from the third fracture(Fig. 49). For this position of the probes the middle fracture is considerably larger so that almost all of the waves were reflected back from the middle fracture and very little transmitted wave energy reached the third fracture. Thus it appears that high frequency ultrasonic waves (450 kc) are more sensitive to thin cracks than low frequency (60 kc).

It is seen from Fig. 1 that when the transmitted ultrasonic waves are of low frequency, the ratio of reflected to incident energy decreases. Again this indicates that the sensitivity of the method for detection of narrow cracks varies directly with the frequency. This was also observed where 450 kc waves were reflected from the fracture in the diorite while the 60 kc wave passed through the fracture and was reflected back from the bottom of the rock (Fig.42). It was also found experimentally that ultrasonic waves of frequency 60 kc pass through a gap of thickness about 0.001 in. and generally have deeper penetration than waves of high frequency.

The plane cracks which are normal to the rock face or which make large angles with the rock face are hard to detect,

since the reflected wave can not easily reach the receiving probe. It was also observed that if the crack extends from the surface to the bottom, and if the probes are placed on opposite sides of the crack, then there is no reflected wave and hence no information about the crack can be obtained (see Fig.46).

CHAPTER V

CONCLUSIONS

The main object of this work was to study the application of ultrasonic waves in detecting fractures in rocks. Ultrasonic equipment was constructed to carry out the various experiments in rocks and other materials.

The experimental results may be summarized as follow:

1. The ultrasonic equipment can be used not only for the detection of fractures in rocks but also for three dimensional seismic model studies. It was also found that the equipment is capable of measuring the velocity of ultrasonic p-wave in solids fairly accurately.
2. The intensity of a sound wave decreases with the distance from the source. It is observed from the experiment that for plane sound waves, as produced by the transmitting probe, the relationship between the intensity of sound wave and distance is an exponential one.

In the measurement of the attenuation constant of sound waves in solids, the coupling between the probe and the specimen has to be identical throughout a series of measurements in the same material. This condition is hard to maintain in practice. The measured values of the attenuation constant in solids, therefore, are not always accurate.

3. For detecting fractures in rocks by the reflection technique, the choice of frequency of the transmitted wave depends mainly on the widths and the sizes of fractures to be detected. When the frequency of the transmitted ultrasonic wave is the order of 450 kc, most waves are reflected back from narrow cracks or small joints and very few pass through the cracks, the thickness of which can not be measured by the thickness gauge and can only be visualized. Hence, although high frequency ultrasonic waves are ideal for detecting small fractures in rocks they are unable to detect the presence of a second crack that may exist beyond the first. The maximum depth to which a fracture in rocks can be detected with high frequency depends upon the homogeneity of rock but it is usually small and in our experiment this depth is of the order of one foot or so.
4. When the transmitted ultrasonic wave has frequency in the range of 60 kc, it was observed that most waves pass through small gaps which are usually present in rock masses. With the low frequency ultrasonic wave, a reflected wave was observed from the bottom of the rock which is at a depth of about three feet. It can, therefore, be concluded that the ultrasonic waves in the low frequency range are suitable for detecting large fractures and for detecting fractures at large depths.

5. Although the ultrasonic equipment built for the experiments worked very satisfactorily, a more compact and portable set-up is desirable for the detection of fractures in rocks in the field. In addition, a better display for the resolution of pulses reflected from the fractures is needed if the equipment is to be developed for practical use.

BIBLIOGRAPHY

1. Lutsch, A. "The Experimental determination of the extent and degree of fracture of rock faces by means of an ultrasonic pulse reflection method," J. of The South Africa Inst. of Mining and Met., Vol. 59, No. 8, 1959.

2. Canadian Mining Journal, June, 1966, p.71.

3. Szendrei, M. E. and Lochner, J. P. A. "The determination of the extent of fracture of rock faces by sonic means," J, of The South Africa Inst. of Mining And Met., Vol. 59, No. 4, 1958.

4. Mongan, C. E. and Miller, T. C. "Use of sonic techniques in exploring coalmine roof strata," International Symposium on Mining Research, Univ. of Missouri, Vol. 2, 1962, p.669.

5. Larocque, G. E. "A sonic system for the determination of in situ dynamic properties and for the outlining of fracture zones," Mine Branch Technical Bulletin TB 75, 1965.

6. Rayleigh, J. "Theory of Sound" Dover Publications, 1945.

7. Tranóczy, T. Proc. of the second conference on ultrasonics, Warsaw, 1956.

8. Szilárd, J. "Ultrasound penetration through very thin gas layers embedded in solid bodies," Proc. of the fourth international conference on Non-Destructive testing, London, 1964.

9. Banks, B. et al., "Ultrasonic Flaw Detection in Metals," Iliffe Books Ltd., London, 1962, p.96.

10. Goldman, R. "Ultrasonic Technology," Reinhold Pub. Co., New York, 1962.

11. Birch, F. et al., "Handbook of Physical Constants," Geol. Sci. of Amer., Special paper, No. 36. 1942.

12. M. I. T. "Principles of Radar," 2nd ed., McGraw-Hill, 1946, ch. 2-70.

13. Mason, W. P. "Physical acoustics and the properties of solids," Princeton, Van Nostrand, 1958.

14. King, M. S. "Wave velocities in rocks as a function of overburden pressure and pore fluids sa saturants," Geophysics, V. 31, 1966, p.50-73.

15. Carlin, B. "Ultrasonic," McGraw-Hill, 1949.

16. Molotova, L.V. and Vassilev, Y. I., "Velocity ratio of longitudinal and transverse waves in rocks II." Bull. (IZV.) Acad. Sci. USSR, Geophys. Ser., 1960, p.731-743.

17. Wood, A. B. "A textbook of Sound," G. Bell and Sons, London, 1930, p.504.

18. Hughes, D. S. et al., "Transmission of elastic pulses in metal rods," Physical Rev., V. 75, No. 10, p.1552-1556.

19. Hogarth, C. A. and Blitz, J. "Techniques of Non-Destructive Testing," Butterworths, London, 1960.

20. Green, C. H. "Velocity determination by means of reflection profiles," Vol. 3, 1938, p.295-305.

21. Eve, A. S. and Keys, D. A. "Applied Geophysics," 5th ed., Cambridge Univ. Press, 1956.

APPENDICES

Appendix A — Tables of Measurement Results

TABLE A-1

Velocity and Attenuation Measurements in Epoxy Resin.

Code No.	Length		Amplitude		Travel time
	in.	cm	A(mv/cm)	LnA	μsec
E-1	1.035	2.628	17.5	2.86	14
E-2	1.530	3.886	17.0	2.83	19
E-3	1.775	4.508	16.5	2.80	21.2
E-4	2.025	5.143	15.0	2.70	23.7
E-5	2.522	6.406	16.0	2.77	28.8
E-6	3.018	7.666	15.0	2.70	34.0
E-7	3.534	8.976	16.0	2.77	38.8

TABLE A-2

Velocity and Attenuation Measurements in Mortar.

Code No.	Length		Amplitude		Travel time
	in.	cm	A(mv/cm)	LnA	μsec
M-1	2.495	6.337	13	2.56	19.0
M-2	2.969	7.541	12	2.48	23.2
M-3	3.425	8.699	10	2.30	26.0
M-4	5.206	13.223	6.25	1.83	37.2
M-5	6.634	16.850	6.00	1.79	47.0
M-6	11.750	29.845	1.00	0.00	85.6(discarded)

TABLE A-3

Velocity and Attenuation Measurements in Trenton Limestone.

Code No.	Length		Amplitude		Travel time
	in.	cm	A(mv/cm)	LnA	μsec
L-1	1.372	3.485	28	3.33	8.4
L-2	2.126	5.402	30	3.40	11.2
L-3	4.285	10.883	14	2.64	19.6
L-4	5.176	13.147	8	2.08	22.7
L-5	7.850	19.939	6	1.80	34.4

TABLE A-4

Velocity and Attenuation Measurements in Paraffin.

Code No.	Length		Amplitude		Travel time
	in.	cm	A(mv/cm)	LnA	μsec
P-1	1.446	3.673	190	5.24	19.2
P-2	2.525	6.413	150	5.00	32.8
P-3	3.316	8.423	100	4.60	41.6
P-4	4.317	10.965	60	4.10	52.6
P-5	4.555	11.397	40	3.68	56.8
P-6	4.725	12.001	23	3.175	58.8
P-7	5.200	13.208	15	2.70	63.8
P-8	7.500	19.050	5	1.61	90.0
P-9	9.775	24.828	2.4	0.875	116.8

Appendix B — General Efficiency of Coupling Transducers to Rock Faces

The efficiency of coupling transducers to rock faces depends upon several factors, such as, the transmitting and the receiving sensitivity of the transducer material, the acoustic impedance matching between the transducer and the rock, the smoothness of the rock faces and the frequency of the transmitted signal. In the experiments on fracture detection in rocks, the rock faces were coated with a layer of vaseline for easy transmission of energy between the probes and the rock face. In our experiments it was observed that in all cases only a small fraction of the transmitted energy reached the receiving probe. That the energy of the received signal depends to a large extent on the smoothness of the rock face was proved by an experiment in which one face of a 2 in. slab of Trenton limestone was polished by the portable grinder and the opposite side by the grinding table using 240 mesh carborundum. With a transmitted signal of 800 v and the probes placed on the face polished by the portable grinder the amplitude of the received signal was 90 mv and when the probes were placed on the opposite side polished by the grinder table, the amplitude of the received signal increased to 180 mv. This shows that polishing by the grinder table produces better coupling between the transducer probes and the rock face than the 240 mesh carborundum.